Synthesis & spectroscopic characterization of novel coordination complexes containing N- and O- donor ligands

THESIS

SUBMITTED FOR THE AWARD OF THE DEGREE OF

Doctor of Philosophy
In
Chemistry

BY

MO ISTIKHAR ALAM ANSARI

UNDER THE SUPERVISION OF
PROF. ZAFAR AHMAD SIDDIQI

DEPARTMENT OF CHEMISTRY
ALIGARH MUSLIM UNIVERSITY
ALIGARH (INDIA)
2016

CANDIDATE'S DECLARATION

I, **Mo Istikhar Alam Ansari,** Department of **Chemistry** certify that the work embodied in this Ph.D thesis is my own bonafide work carried out by me under the supervision of **Prof. Zafar Ahmad Siddiqi** at Aligarh Muslim University, Aligarh. The matter embodied in this Ph.D. thesis has not been submitted for the award of any other degree.

I declare that I have faithfully acknowledged, given credit to and referred to the research workers wherever their works have been cited in the text and the body of the thesis. I further certify that I have not willfully lifted up some other's work, para, text, data, result, etc. reported in the journals, books, magazines, reports, dissertations, thesis, etc., or available at web-sites and included them in this Ph.D. thesis and cited as my own work.

Date: ..... **(Signature of the candidate)**

MO ISTIKHAR ALAM ANSARI
(Name of the candidate)

Certificate from the Supervisor

This is to certify that the above statement made by the candidate is correct to the best of my knowledge.

Signature of the Supervisor
Name & Designation: Prof. Zafar A. Siddiqi, BSR Faculty Fellow
Department: CHEMISTRY

(Signature of the Chairman of the Department with seal)

COURSE/ COMPREHENSIVE EXAMINATION/ PRE-SUBMISSION SEMINAR COMPLETION CERTIFICATE

This is to certify that Mr. **Mo Istikhar Alam Ansari,** Department of **Chemistry** has satisfactorily completed the course work/comprehensive examination and pre-submission seminar requirement which is part of his Ph.D. programme.

Date: ……. **(Signature of the Chairman of the Department)**

COPYRIGHT TRANSFER CERTIFICATE

Title of the Thesis: **Synthesis & spectroscopic characterization of novel coordination complexes containing N- and O- donor ligands:**

Candidate's Name: **MO ISTIKHAR ALAM ANSARI**

Copyright Transfer

The undersigned hereby assigns to the Aligarh Muslim University, Aligarh, copyright that may exist in and for the above thesis submitted for the award of Ph.D. degree.

(Signature of the Candidate)

Dedicated

to

My Parents

DEPARTMENT OF CHEMISTRY
ALIGARH MUSLIM UNIVERSITY
ALIGARH—202 002

Phones { Ext. (0571) 703515
Int. 317, 318

Dated.....

Certificate

Certified that the work embodied in this thesis entitled, **"Synthesis & spectroscopic characterization of novel coordination complexes containing N- and O- donor ligands"** is the result of original research carried out under my supervision by Mr. Mo Istikhar Alam Ansari and is suitable for submission for the award of Ph.D. degree of Aligarh Muslim University, Aligarh, India.

Prof. (Rtd.) Zafar Ahmad Siddiqi
U.G.C. BSR Faculty Fellow,
Ph.D., AvH fellow (Germany),
STA fellow (Japan),
Member N.Y.A.A.Sc. (USA) & A.A.A.Sc. (USA)

ACKNOWLEDGEMENTS

First of all, I thank Almighty for giving me the courage and ability to start and finish this thesis.

There are a number of people who have helped me during the course of my research, however, it is impossible to record all of them here. I hope that they accept my sincere thanks and appreciation. I find myself deeply indebted to some people so I have to mention their names.

I would like to express my deepest sense of gratitude and thanks to my supervisor, Prof. (Rtd.) Zafar Ahmad Siddiqi, who gave me the freedom to explore on my own, and at the same time the guidance to recover when my steps faltered. His encouragement, valuable advice, constructive comments and suggestions for the improvement of the thesis have all been of inestimable value for the preparation of the thesis in its present form. I am greatly indebted to him.

My special thanks and appreciation goes to UGC, New Delhi for granting me a scholarship to carry on my higher studies. I am also grateful to the Chairman, Department of Chemistry, A.M.U., Aligarh for providing the necessary research facilities.

Dr. M. Khalid and Dr. M. Shahid, have always been there to listen and give advice. I am deeply grateful to them for the long discussions that helped me sort out the technical details of my work. I am also thankful to them for encouraging the use of correct grammar and consistent notation in my writings and for carefully reading and commenting on countless revisions of this thesis.

Special thanks are due to my colleagues Farasha, Mukul and Ashafaq for encouragement and practical advice.

I appreciate the support and love by my father Mr. Istiyak who have always encouraged and guided me and never tried to limit my aspiration. I thank my entire family for always being there for me. Knowing that they always held me in their thoughts and prayers gave me strength to go on.

I would be failing in my duty if do not express sincere thanks to all my friends specially Faizan, Shahzade, Zafar, Usman, Faiyaz Dr. Faizan, Mohsin, Arshad and Zuber.

Last but not the least, my greatest debt of gratitude and appreciation is to my mother Mrs. Rukhsana and loving sisters Iram, Shayma and Hina who have been a constant source of inspiration behind my achievements.

(MO ISTIKHAR ALAM ANSARI)

Contents

Chapter 1

An overview of the coordination chemistry of N- and O- donor ligands

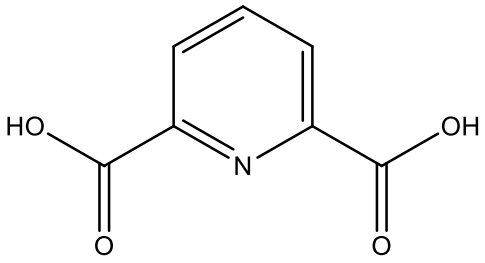

Pyridine-2,6-dicarboxylic acid (H_2pda)

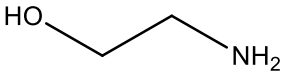

Monoethanolamine (Hmea)

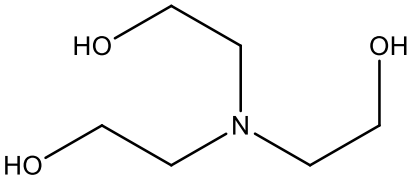

Triethanolamine (H_3tea)

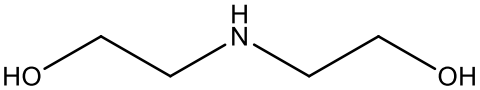

Diethanolamine (H_2dea)

Introduction

The designing of transition metal complexes has been an area of great interest owing to their fascinating structures and functional applications as magnetic, electronic, optical, catalytic and fluorescent materials [1,2]. Although a large number of transition metal complexes of chelating carboxylic acids and polyamines had been reported, relatively few complexes of chelating aminoalcohols and carboxylic acids have been isolated. To some extent, this situation is understandable since an alcohol group is normally a poorer coordinating agent than carboxylic acid or amine group. There is evidence that, in the presence of excess carboxylic or aminoalcohol groups, many metal ions form complexes in which the carboxylic and/ or amine group is coordinated. The aminoalcohols are, however, generally more acidic than the diamines. However, the deprotonation of aminoalcohols or carboxylic acids, result in the formation of aminoalkoxides or carboxylate anions, which exhibit increased chelating tendency such that it may often form additional bonds involving other metal ion(s) resulting in the formation of oxygen-bridged polynuclear complexes. The additional bonding by alkoxide/oxide group involves the hydrogen of a coordinated alcohol/carboxylate group, leading to hydrogen-bonded O–H–O bridged polynuclear complexes. The polynuclear complexes formed by either of the two ways are interesting because of their coordination geometries and the unusual magnetic interactions between the neighboring paramagnetic metal ions. Although, these interactions may often lead direct metal-metal bonding in some cases, but in most of the cases indirect interactions through the bridging ligating groups are definitely observed [1,2].

Aminoalcohol and carboxylic acid ligands are apparently ideal for the formation of polymeric compounds due to the bridging capability [3] of the oxygen donor atoms present in the ligands, however, according to the litreture, no extended structures based on exofunctional diethanolamine or similar amino alcohols and pyridine–2,6–dicarboxylic acid have been well documented. The diethanolamine (H_2dea) and its ionized analogs (i.e., $Hdea^-$ and dea^{2-}) may adopt a chelating mode to bind metal ions forming a five-membered chelate ring [4]. Extended structures if formed are usually based on hydrogen bonding that involve hydroxyl and amine groups of the ligand and pyridine–2,6–dicarboxylic acid (H_2pda) or its anion ($Hpda^-$).

Extended structures if formed are usually based on H- bonding that involves hydroxyl and amine groups of the ligand [4].

In synthetic point of view in coordination chemistry, one of the most important advantage of functionalized carboxylate ligands e.g. pyridine–2,6–dicarboxylic acid (H_2pda), iminodiacetic acid (H_2imda), adipic acid (H_2ada), oxydiacetic acid (H_2oda) or nitrilotriacetic acid (H_3nta) [5–12] is the presence of tridentate [N,O,O] or [O,O,O] coordination mode. The rigidity or flexibility of these ligands makes them useful in synthesizing a large number of beautiful networks with unique topology. The carboxylate groups present in different orientations in the ligand moiety facilitate the construction of such molecular assemblies, which may adopt a one-dimensional (1D) long chain [4,10,13], two-dimensional (2D) sheet [4] or three-dimensional (3D) supramolecular [4,14] networks.

The carboxylate ligands usually adopt diverse binding modes as terminal monodentate, symmetrical bidentate chelating to one metal center or bridging bidentate in a syn-syn, syn-anti and anti-anti configurations to bind two or more metal centers.

Chemistry of pyridine–2,6–dicarboxylic acid (H_2pda) ligand

A large numbers of MOFs containing carboxylate ligands have been prepared and almost all of them are in polymeric forms [15–17]. Pyridine–2,6–dicarboxylic acid (H_2pda) and its substituted analogs are of great interest to bioinorganic and medicinal chemistry as they are present in many natural products, such as vitamins and coenzymes. Metal complexes of pyridine–2,6–dicarboxylic acid (H_2pda) ligand have been exploited as interesting model systems and rigid angle (120°) between the central pyridine ring and two carboxylate groups energetically provides various coordination motifs to form both discrete and consecutive metal complexes under appropriate synthetic conditions[18–21] .

There are a number of reports dealing with the fascinating chemistry of H_2pda e.g. a dinuclear $[Cu(dipic)(\mu\text{-dipic})Cu(H_2O)_5]\cdot 2H_2O$ complex was synthesized by Mirzaei and Hosseini, before past two decades by using the reaction of pyridine–2,6–dicarboxylic acid with copper(II) nitrate in distilled water at 75 °C. The two H_2pda ligands are deprotonated in the

form of pda^{2-} coordinated to metal ion (**Fig. 1**) [22]. Both the pda^{2-} ligands are coordinated in a tridentate [N,O,O] manner to one copper atom. One of the two pda^{2-} groups also acts as a bridging ligand to the pentaaqua-Cu(II) unit. Both Cu(II) ions exhibit distorted octahedral geometry with Cu(1) coordinated by six oxygen atoms, five from coordinated water molecules and one from a carboxyl group of pda^{2-} of which the other oxygen atom is linked to Cu(2). Cu(2) is coordinated with four oxygen atoms of four carboxyl groups and two nitrogen atoms which are all from pda^{2-} ligand. Cu–O bond lengths are at the range expected, however it should be noted that coordination of O(8) atom to Cu(1) results in a slight lengthening of the Cu(2)–O(7) bond (2.213(1) Å) as compared with the three others (Cu(2)–O(1) = 2.170(1) Å, Cu(2)–O(3) = 2.113 (1) Å, Cu(2)–O(5) = 2.178(1) Å). Hydrogen bonds between coordinated water molecules and the carboxylate oxygen atoms of the pda^{2-} ligands link the dinuclear copper molecules to form a supramolecular 1D chain (**Fig. 2**) [23].

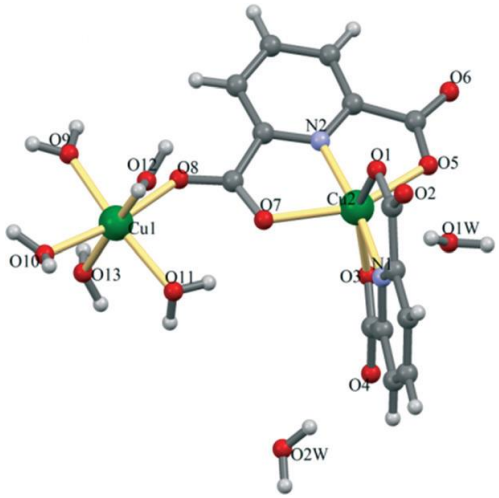

Fig. 1. Molecular structure of the $[Cu(dipic)(\mu\text{-dipic})Cu(H_2O)_5]\cdot 2H_2O$ with indication of the atom numbering scheme.

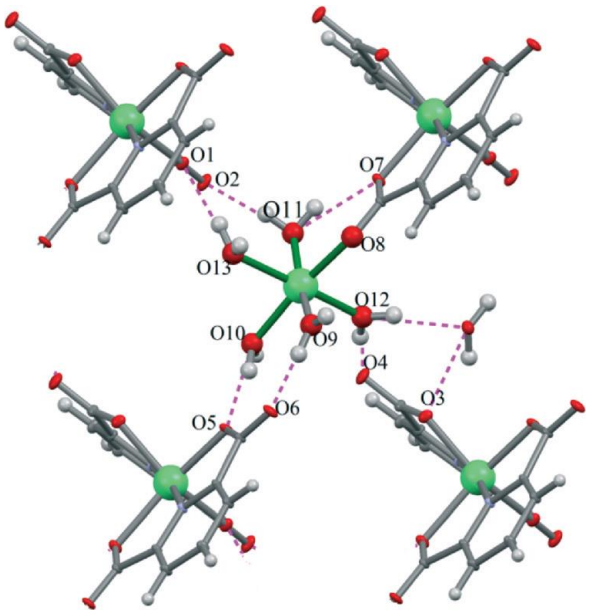

Fig. 2. O–H···O hydrogen bonds (pink-dashed lines) link the dinuclear copper molecules form a 1D chain.

Trinuclear copper complex was also synthesized by pyridine–2,6–dicarboxylic acid and copper(II) acetate in the presence of ethylenediamine. The stiochiometry and bonding features were ascertained by spectroscopic and single crystal X-ray crystallography.

The trinuclear complex shows monoclinic $P2_1/n$ space group and its molecular structure including the atom labeling scheme is given in **Fig. 3**. The molecular structure diagram shows that the compound is a trinuclear complex with two different types of metal centers, Cu1 and Cu2 metal ions (**Fig. 3**). Both Cu1 atoms are hexa-coordinated to four oxygen and two nitrogen atoms of two pyridine–2,6–dicarboxylic acid ligands (H_2pda). The aromatic rings are almost perpendicular to each other resulting in a distorted octahedral coordination sphere around Cu1. The coordination number for Cu2 is also six since it is coordinated to two ethylenediamine groups and two oxygen atoms of H_2pda ligands. Therefore, the structure can be defined as two Cu1 complexes that are acting as monodentate ligands for Cu2 in axial positions. Moreover, there are two uncoordinated water and one diprotonated ethylenediamine molecules in the repeating unit that act as counter ions.

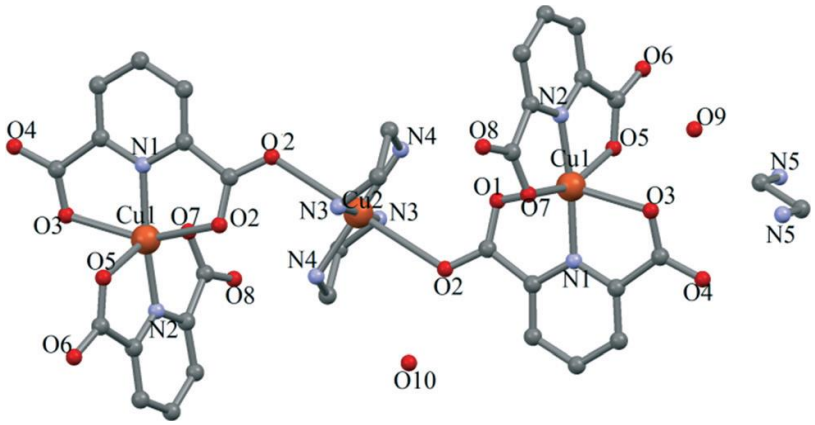

Fig. 3. Molecular structure of Cu_3 complex with indication of the atom numbering scheme.

Furthermore, π–π interactions with inter-centroid distance of 3.507 Å between the pyridine rings are crucial for the formation of the final 3D architecture, as can be observed in **fig. 4**. Interestingly, each trinuclear complex establishes four equivalent stacking interactions with four neighbouring complexes using the pyridine rings [24].

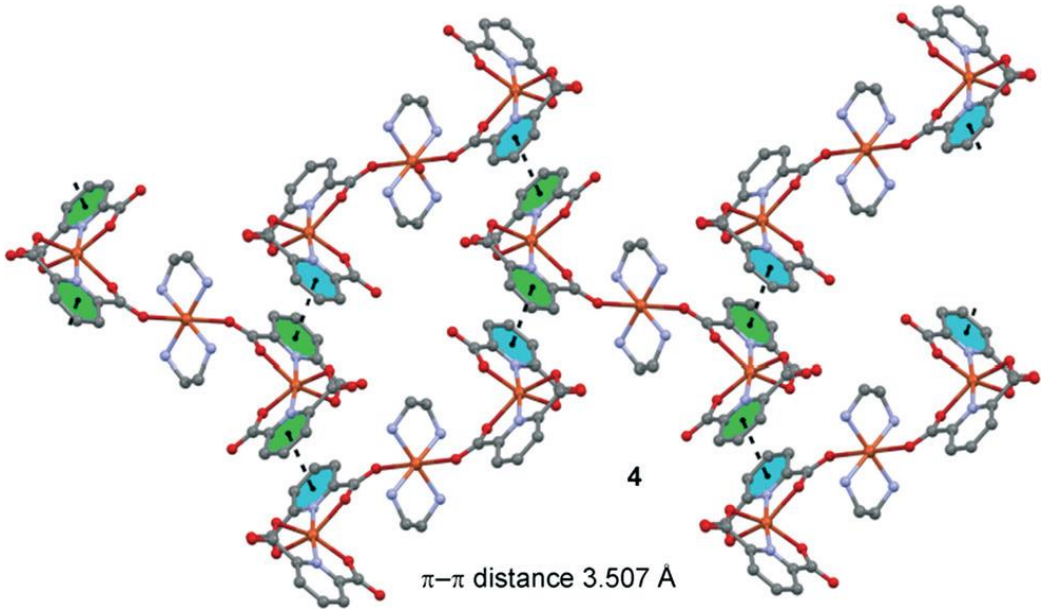

Fig. 4. Representation of π–π interactions. Hydrogen atoms are omitted for clarity.

Chemistry of aminoalcohol ligands

Alkoxide-bridged complex formed by the reaction of cobalt(II) salts and 2-aminoalcohols (abbreviated meaH), first reported by Heiber and Levy [25,26] in 1932, is the earliest well-characterized complex of this type. A series of the complexes were reported, and the cation was formulated as a cobalt(II) species, $[Co_3(meaH)_2(H_2O)^2]^{2+}$, involving edge-sharing octahedron. Potentiometric studies on aqueous solutions of stoichiometric mixtures of cobalt (II) salts and etanolamine indicated that the formula of the complex species should be $[Co_3(mea)_6]^{2+}$ with one cobalt(II) and two cobalt(III) ions [25]. The structural studies of the complex confirmed a face-sharing arrangement with octahedral coordination of the terminal cobalt(III) ions [28]. However, the central cobalt(II) was found to be six coordinated with an almost perfect trigonal prismatic arrangement of alkoxide oxygens (Fig. 5). The cobalt (III)-oxygen distances ranged from 1.885 to 1.975Å, the cobalt(II)-oxygen distances ranged from 2.005 to 2.104 Å, and the cobalt(III)-cobalt(II) distance was 2.597 Å.

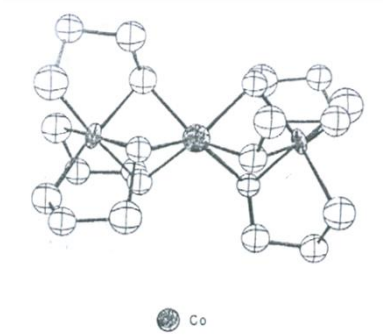

Fig. 5. Structure of the tri nuclear cobalt (II)-cobalt(III) complexes of 2-aminoethanol.

By the use of the oxidizing agent, potassium persulphate, the central cobalt was oxidized to cobalt(III), forming the salts which contain the complex $[Co_3(mea)_6]^{3+}$ cation. Complexes of the type $[M\{Co(mea)_3\}_2]^{2+}$ have also been prepared [25] by the reaction of zinc(II), copper(II), nickel(II), and magnesium(II) salts with the neutral cobalt(II) compound, $[Co(mea)_3]3H_2O$. The Structural investigations have not been determined for any of these complexes, and the coordination arrangements at the central metal ions are, thus not known. Similar attempts by workers to prepare trinuclear species from the use of the paramagnetic $[Cr(mea)_3]3H_2O$ compound have not yet been successful [27].

A dimeric cobalt complex, $[Co_2(mea)_3(H_2O)_3]^{2+}$, contain cobalt(II) and cobalt(III), having the assumed octahedral coordination of both metal ions, has also been reported in literature [7]. The proposed structure contained a tris-Co(III)-chelate having face-sharing of the alkoxide oxygens with a cobalt(II) ion [28].

Hetrometallic copper complexes had also been prepared as alkoxo-bridged copper(II) species as nodes, and anionic cyano-complexes as linkers: $[\{Cu_2(pa)_2\}\{M(CN)_2\}_2]$ (M= Ag, **1**; Au, **2**), $[\{Cu_4(mea)_4\}\{Au(CN)_2\}4\cdot H_2O]$ **3** and $[\{Cu_2(pa)_2\}\{Ni(CN)_4\}]$ **4** (pa = deprotonated propanolamine; mea = deprotonated monoethanolamine). Crystal structure of **1** consists of 2D layers formed by connecting the $[Cu_2(pa)_2]^{2+}$ centrosymmetric nodes through linear $[Au(CN)_2]^-$ linkers. The coordination geometry of the copper(II) ions is distorted square-pyramidal. The basal positions are occupied by two oxygen atoms arising from the alkoxo bridges, one nitrogen from the amino group, and one nitrogen from the spacer $[Au(CN)_2]^-$. The Cu–N distances (Cu(1)–N(2) 1.984(8), Cu(1)–N(3) 2.027(9)Å) are slightly longer than the Cu–O ones (Cu(1) –O(1) 1.938(6), Cu(1)–O(1)2 1.952(7)Å). The apical position is occupied by the nitrogen atom arising from another spacer molecule [Cu(1)–N(1) 2.298(10)Å]. Each binuclear node interacts through four $[M(CN)_2]^{2-}$ linkers with four other binuclear nodes. Infinite 2D chicken-wire sheets are formed (**Fig. 6**). The packing of the layers in the crystal is driven by the strong aurophilic interactions (Au···Au = 3.069Å) established between the gold atoms from different layers [29].

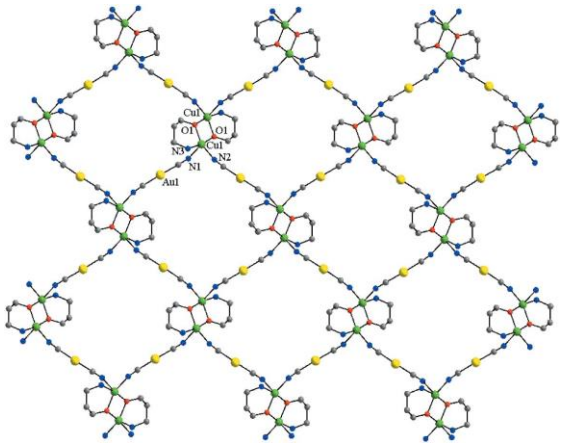

Fig. 6. View of a layer in 2, along with the atom numbering scheme. Cu–green, Au–yellow, N–blue, O–red and C–grey.

3D coordination polymers based on the same type of binuclear nodes can be obtained by increasing the number of cyano groups in the linker. Indeed, the assembly of $[Cu_2(pa)_2]^{2+}$ and $[Ni(CN)_4]^{2-}$ ions affords a 3D coordination polymer, $[\{Cu_2(pa)_2\}\{Ni(CN)_4\}]$ **4** (**Fig. 7**) [29 e].

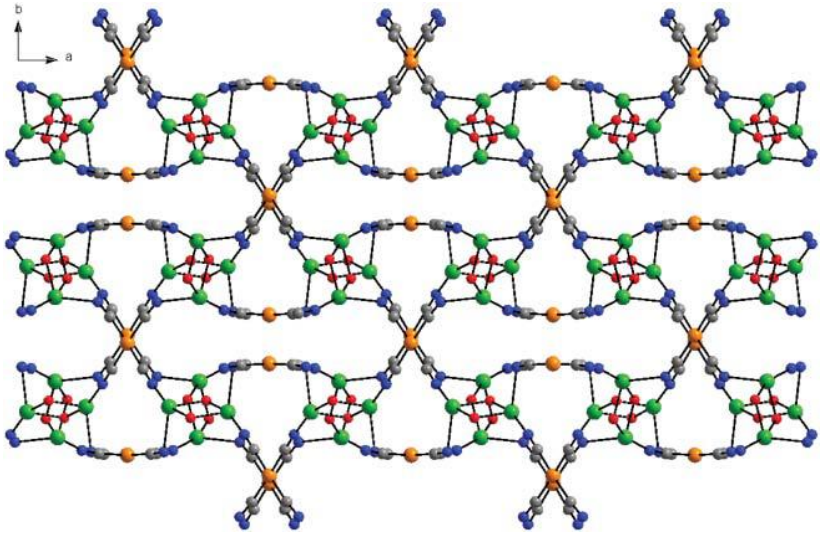

Fig. 7. The 3-D architecture of compound 4. Cu – green; Ni – orange; N – blue; O – red; and C – grey.

An interesting case is the one observed with the Cu(II)–monoethanolamine–$[Au(CN)_2]^{2-}$ system, when the heterometallic complex $[\{Cu_4(mea)_4\}\{Au(CN)_2\}_4\cdot H_2O]$ **3** is obtained.

Compound **3** is constructed from tetranuclear $\{Cu_4(mea)_4\}$ nodes connected through $[Au(CN)_2]^{2-}$ spacers. It is already known that $\{Cu^{II}_4O_4\}$ heterocubane cores can be assembled with monoethanolamine derivatives [30]. The pseudotetrahedral disposition of the copper ions within the node as well as the linearity of the spacer, $[Au(CN)_2]^{2-}$, fulfils the necessary condition for the construction of a diamondoid topology (**Fig. 8**). The $\{Cu^{II}_4O_4\}$ heterocubane moiety can act as a tetrahedral synthon (**Fig. 8a**).

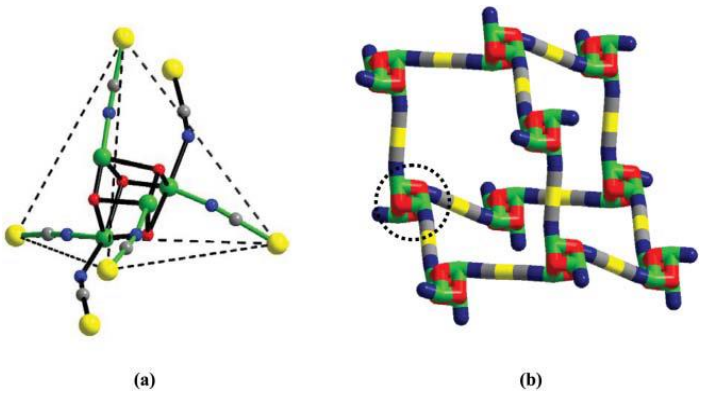

Fig. 8 (**a**) The tetrahedral synthon in compound **3**. (**b**) Illustration of an adamantane-like unit in the structure of **3**; one tetranuclear node is highlighted. For clarity, the carbon atoms from organic ligands as well as water molecules have been removed. Cu – green; N – blue; O – red; Au – yellow; and C – grey.

As expected, a 3D diamondoid net is assembled. The analysis of the packing diagram reveals a four-fold interpenetration of the diamondoid networks (**Fig. 8a**). Again, the aurophilic interactions intervene in sustaining the supramolecular architecture. Apart from the $[Au(CN)_2]^{2-}$ groups acting as linkers, there are two $[Au(CN)_2]^{2-}$ groups per tetranuclear cluster, which act as terminal ligands. The interpenetrating diamondoid nets are connected through aurophilic interactions established between the dangling $[Au(CN)_2]^{2-}$ ligands from adjacent nets. Infinite chains of gold atoms are thus formed (**Fig. 8b**). This is a unique case of fourfold interpenetrating nets that are interconnected through aurophilic interactions. The cryomagnetic investigation of 3 revealed a gradual increase, followed by a decrease of the $\chi_m T$ product as the temperature is lowered [29].

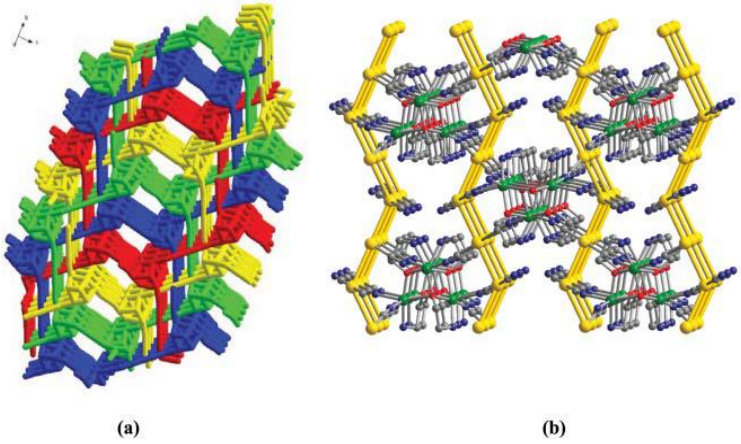

Fig. 8. Packing diagram for compound **3**, showing (**a**) the four-fold interpenetration; (**b**) the aurophilic interactions connecting the interpenetrating nets.

Mixed valent complexes of cobalt have also been resulted [30,31] from the reaction of cobalt(II) salts with 2,2'-dihydroxydiethylamine, abbreviated H_2dea. Both edge-sharing [30] and face-sharing [31] dimeric structures have been proposed for compounds of the types $Co_2(dea)_2X{\cdot}4H_2O$ and $Co_2(H_2dea)(dea)_2X{\cdot}H_2O$ (where X represents Cl, Br, or I). Due to the limited number of the lattice water molecules, a more complex structure was suggested for $Co_2(dea)_2(ClO_4){\cdot}2H_2O$.

A trans-facial arrangement of ligands was assumed for these Co(III) complexes. For the mixed-valence compounds, dinuclear structures involving edge-sharing octahedra were proposed. The structural and magnetochemical features of Co(II) [32] as well as Co(III) [33] based ligand bridged extended polymeric cubane motifs are well studied. However, studies on discrete mixed valent (Co_2^{II}–Co_2^{III}) anion bridged complexes are not so common [34].

Mixed valence (Co_2^{II}–Co_2^{III}) defect dicubane clusters are also obtained from the reaction of cobalt(II) salts with α-diimine chelator i.e. 2,2′-bipyridine or 1,10-phenanthroline, to obtain the final product $[Co_4(\mu_3\text{-}OH)_2(\mu_2\text{-}dea)_2(bipy)_4]4Cl{\cdot}8H_2O$ (**1**) and $[Co_4(\mu_3\text{-}OH)_2(\mu_2\text{-}dea)_2(phen)_4]4Cl{\cdot}8H_2O$ (**2**) (H_2dea = diethanolamine) in good yield. The change in oxidation state of cobalt from Co(II) to Co(III) may be due to the presence of abundant atmospheric oxygen molecules. The molecular unit of the complexes contains four cobalt ions arranged in a manner to form a defect dicubane core [35]. Each cobalt has a six coordinate but distorted octahedral environment. The dicubane Co_4 cores are illustrated in the inset of **Fig. 10**.

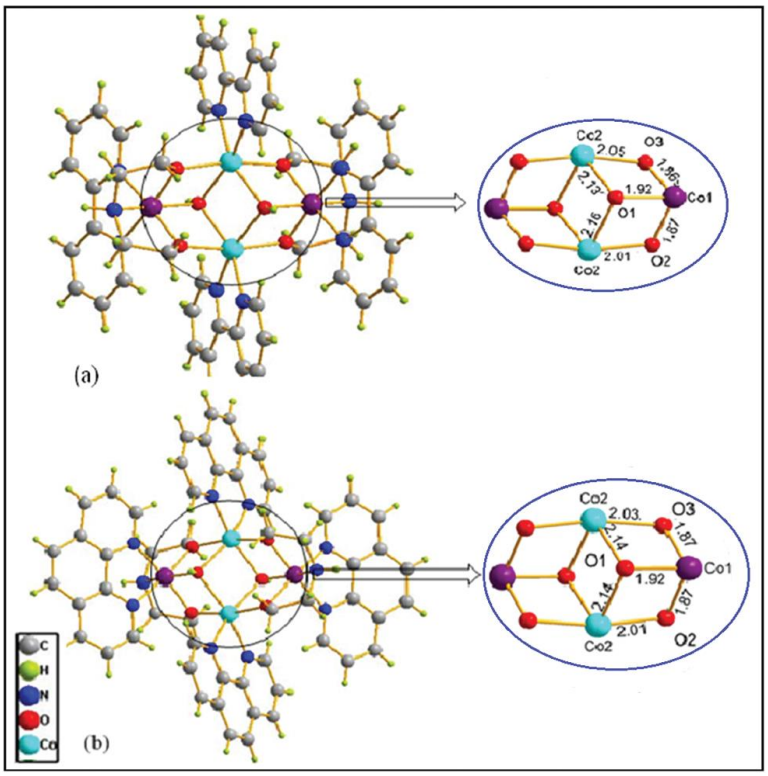

Fig. 10. Molecular structure of 1 with its cubane core and (b) molecular structure of 2 with its cubane core (the related atoms of the cubane are omitted for clarity. Green color is for Co(II) and purple for Co(III)).

Furthermore, each cobalt are effectively surrounded by one α-diimine (phen or bipy) chelator in addition to two dea^{2-} bridging moieties shared between the Co_4 units of the dicubane. The dea^{2-} anion here supports a strong alkoxo bridging (Co–O–Co). The α-diimine chelators provide two N-sites chelated to each cobalt atom. However, the secondary amine (NH) functions of the two dea^{2-} moieties is apparently coordinated to only two cobalt atoms (listed as Co1) of the Co_4 dicubane. The observed shorter bond lengths Co1–N1 and Co1–N2 are close to that reported [36] for N-coordination to a trivalent (CoIII) ion whereas the longer bond lengths (Co2–N3 and Co2–N4 ~2.14 Å) are comparable to the corresponding divalent Co^{II} oxidation state [36,37]. The tetranuclear discrete molecular unit is, therefore, an example of mixed valence hydroxo-bridged defect dicubane cluster having the actual stoichiometry as $[Co_2^{II}–Co_2^{III}(\mu_3\text{-}OH)_2(\mu_2\text{-}dea)_2(L–L)_4]4Cl\cdot 8H_2O$. The dicubane core in the present case contains two high-spin highly paramagnetic $Co^{II}(t_{2g}^5e_g^2$ configuration) centres and the remaining two cobalt atoms in low spin diamagnetic Co^{III} (t_2g^6 configuration).

Ni(II) complexes of aminoalcohols were also reported [25] in some of the early work, and at least one compound of 2, 2'-dihydroxydiethylamine, $Ni_2(Hdea)$ $(H_2Deta)_2Cl_3.2H_2O$, appeared to be polynuclear. No further work has been reported on that compound, till a dimeric complex of Ni(II) with N, N-bis-(2-diethylaminoethyl)-2-hydroxyethylamine has been reported [25]. The X-ray Crystallographic studies show that the Ni(II) ions are five coordinate with distorted trigonal-pipyramidal coordination such that the four membered nickel-oxygen ring is exactly planar, (**Fig. 11**) and the Ni···Ni distance is 3.09 Å. The compound is reported to have a reflectance spectrum diagnostic of five-coordinate high-spin Ni(II).

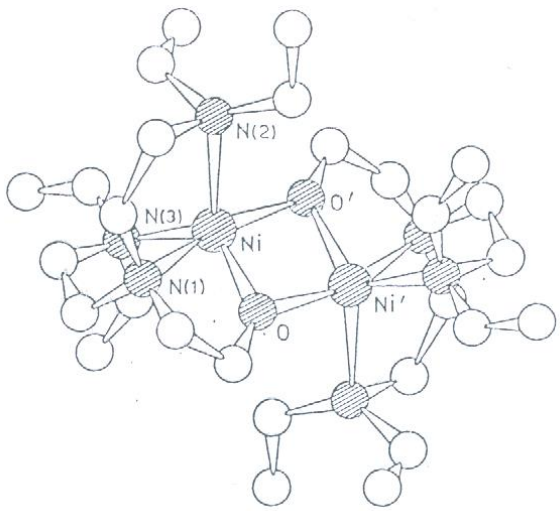

Fig. 11. Structure of the dimeric complex of Ni(II) with N,N-bis-(diethylaminoethyl)-2-hydroxyethylamine [38].

There are other reports of polynuclear complexes of Cu(II) with a number of substituted 2-aminoethanols. These compounds, which have the empirical formula $Cu(OCH_2CH_2NR_2)X$, have been investigated by several workers [39-42]. Uhlig and co-workers [41] divided the compounds into three categories on the basis of magnetic properties and the extent of molecular association. Compounds in the first group were described as dimeric species with four-coordinate Cu(II) ions, and they exhibited room temp magnetic moments, between 0.60 to 1.23 B.M., that were greatly reduced from the expected spin-only value of 1.73 B.M., for one unpaired electron. The second group of compounds showed higher degrees of association, approaching tetrameric values in concentrated solution, and exhibited normal magnetic

moments around 1.9 B.M. at room temperature and compounds in the third group exhibited intermediate moments and also appeared to be tetrameric.

The structure of a compound with properties similar to those of compounds of the above stated first type has been reported. The structure of $Cu(OCH_2CH_2NH_2)Br$ revealed planar four-coordinate Cu(II) ions bridged by alkoxide groups into dimeric units with a planar four-membered copper-oxygen ring. The Cu···Cu distance was 3.03 Å. Although crystal structures have not been reported for aminoalcohol compounds of the two tetrameric types. The structures determined for the two tetrameric iminoalcohol complexes [43], include one with a normal moment and one with a reduced moment at room temperature. It is highly probable that the aminoalcohol tetramers have similar structures.

The next homologue of 3-amino-1-propanol, also from analogous complex $Cu(OCH_2CH_2CH_2NH_2)$ (H_3CCO_2) [44], which was found to have an extremely low room temperature magnetic moment, 0.41 B.M. The crystallographic investigations confirm formation of planar four membered ring with a square-planar coordination around Cu(II) ions involving monodentatae acetate group and alkoxide groups (of the propanolamine) bridging the Cu(II) ions to result in a dimeric structure [44], (**Fig. 12**). The Cu···Cu distance here is 3.012 Å.

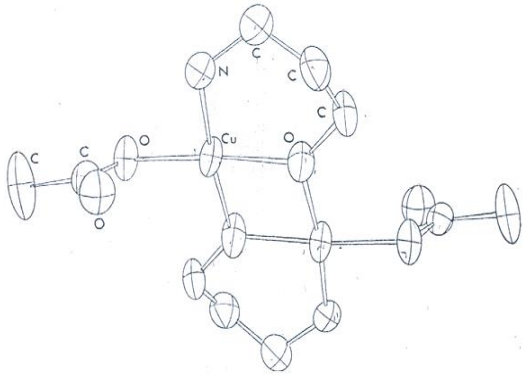

Fig. 12. The structure of a copper (II) complex of 3-amino-1-propanol, $[Cu(OCH_2CH_2CH_2NH_2)(H_3CCO)]_2$.

A series of complexes of 2-(β-hydroxyethyl)-pyridine, abbreviated EpH, with the formula Cu(Ep)X (X = Cl, Br, NO_3^-, NO_2^-,) are also reported [45] in the literature. These

complexes in general have moments in the range 0.44 to 0.91 B.M. A dimeric structure was then proposed for these complexes too.

Three novel complexes of Cu(II) were also investigated viz. $[Cu_2(H_2tea)_2$-(o-methoxybenzoate$)_2]$ (**1**) $[Cu_2(H_2tea)_2$(m-methoxybenzoate$)_2]\cdot 2H_2O$ (**2**) and $[Cu_2(H_2tea)_2$(p-methoxybenzoate$)_2]\cdot 2H_2O$ (**3**) (where H_2tea = mono-deprotonated triethanolamine). These were synthesized by addition of triethanolamine (H_3tea) to the hydrated Cu(o-,m-,p-methoxybenzoates$)_2$. The reported [46] complexes had been characterized by elemental analyses, spectroscopic techniques (electronic and FT-IR), magnetic moment determination, molar conductance studies, TGA, and single crystal X-ray determination.

The author indicate that while the complex **2** and **3** consist of two co crystallized water molecules in the molecular unit, the complex **1** does not posses but all are iso structure. In all cases, the benzoate molecule is linked to the Cu atom as an anxillary ligand by only one oxygen. In **1**, the mono deprotonated (H_2tea^-) ligand acts as a tridentate ligand, one OH group being 5 Å away from the metal, while the H_2tea^- deprotonated oxygen bridges two centrosymmetrically related Cu atoms with a Cu–O–Cu angle of 99.9(1)° and the Cu–Cu distance of 2.9456(7) Å.

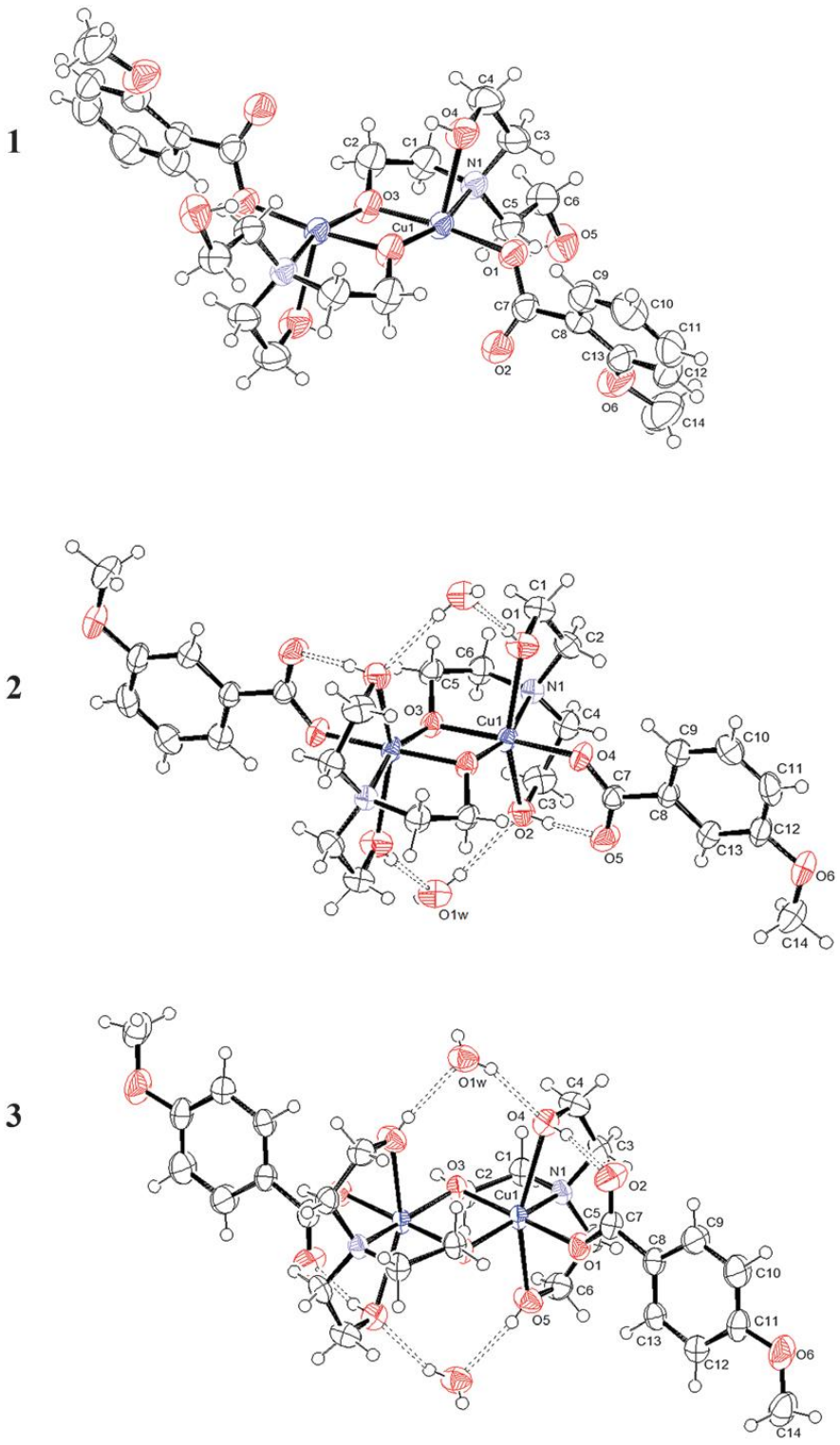

Fig. 13. ORTEP-III view and the atom numbering scheme for the complexes (1–3). Thermal ellipsoids are drawn at the 50% probability level. Hydrogen bonds are drawn as dashed lines [46].

The resulting coordination around each copper atom is square pyramidal, with the central Cu cation lying 0.03 Å above the mean-square plane formed by N1, O1, O3, and O3. The angle formed by this plane and the apical Cu–O4 line is 170.82°. Conversely, in **2** and **3** the H_2tea^- ligand acts as a tetradentate ligand through the nitrogen atom and the three oxygen atoms, the non-protonated one forming a bridge between two centrosymmetrically related hexacoordinated Cu(II) atoms, giving rise to distorted octahedral coordination. The Cu–O–Cu angle and the Cu–Cu distance are very similar in the two structures, being 97.51(6)1, 97.03(5)1 and 2.9212(2), 2.9158(2) Å in **2** and **3**, respectively (**Fig. 13**) [46].

The synthesis of hetronuclear clusters containing $\{Co^{III}_2Dy^{III}_2\}$ stoichiometry is reported using polyethanolamine derivatives [47] as main binding ligand have been found to posses interesting butterfly type of structure (**Fig. 14**) and display single molecule magnetic behaviours but with subtly different dynamic magnetic properties. $[Dy^{III}_2Co^{III}_2(OMe)_2(teaH)_2(O_2CPh)_4(MeOH)_4](NO_3)_2\cdot MeOH\cdot H_2O$ (**1**) and $[Dy^{III}_2Co^{III}_2(OMe)_2(dea)_2(O_2CPh)_4(MeOH)_4](NO_3)_2$ (**2**) (H_3tea= triethanolamine and H_2dea= triethanolamine) are heterometallic 3d/4f clusters but magnetically can be considered as dinuclear Dy^{III} units, due to the low spin Co^{III} d^6 ions [47]. Complex **1** (**Fig. 14**) crystallizes in the tetragonal space group $I4_1/a$ with the asymmetric unit consisting of two similar but unique heterometallic tetranuclear complexes. Overall both clusters consist of two Co^{III} and two Dy^{III} ions, with the metallic core best described as a planar butterfly motif, with the Dy^{III} ions occupying the body positions and the Co^{III} ions the outer wing-tips. However, the difference found between the two compounds is minor, with slightly different coordination environments found around the Dy^{III} ions, via the terminal ligands. Compound **2** crystallizes in the monoclinic space group $P2_1/n$, with the asymmetric unit containing half the cluster, which lies upon an inversion center and a nitrate counter ion. The complex is exclusively cationic, as observed with **1**, with two MeOH ligands terminally coordinating to each Dy^{III} ion, with two nitrate counter ions found in the crystal lattice. The only overall difference is the two doubly deprotonated dea^{2-} ligands that are now present, both of which display the $\mu_3:\eta^2:\eta^2:\eta^1$ bonding mode. The two Co^{III} ions are six coordinate with octahedral geometries, with an average $Co-L_{N,O}$ bond length of 1.926 Å. The two Dy^{III} ions are eight coordinate with distorted square antiprismatic geometries, and have an average Dy−O bond length of 2.370 Å. The

closest intermolecular Dy···Dy distance is 7.99 Å. Both complex displayed a unique anisotropy barrier, with values ranging from 50 to 70 cm^{-1}. Previous studies had revealed that the slow relaxation of the magnetization was of single ion in origin. The variation in barrier height was thus determined to be a consequence of the unique coordination and geometric environments observed around the Dy^{III} ions of both complex [47].

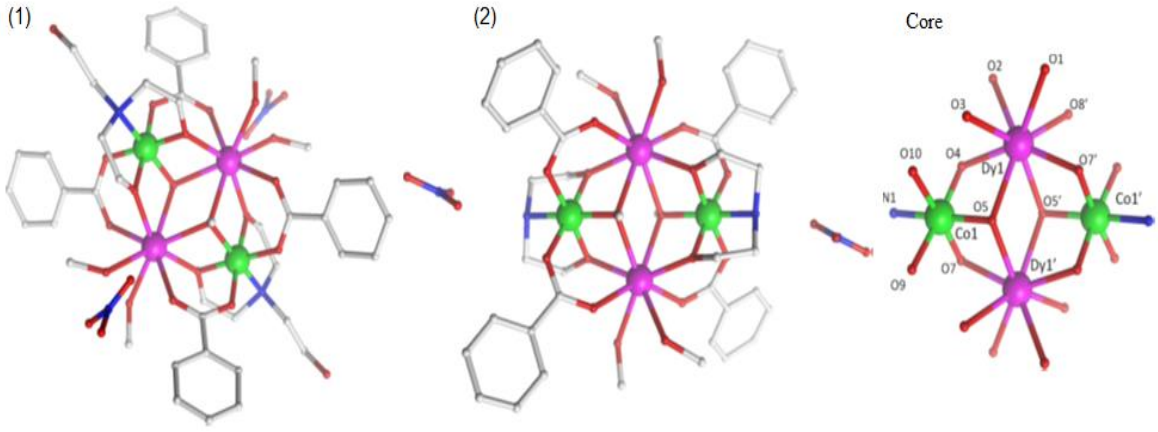

Fig. 14. The structure of 1 (left), 2 (middle) and labeled core structure (right) in the crystal. Disordered and H atoms are omitted for clarity. Color scheme; Co^{III}, green; Dy^{III}, purple; O, red; N, blue; C, light gray.

Chemistry of amino alcohol ligands in constructing hetropolynuclear clusters is also interesting and reported in literature. A novel heterometallic tetranuclear complex $[Cr_3Cd(NCS)_4(H_2tea)(Htea)_3]\cdot 3CH_3OH$ (**1**) has been reported using cadmium oxide, Reinecke's salt, ammonium thiocyanate and a methanol solution of triethanolamine (H_3tea) in air. Crystallographic investigations revealed that the molecular structure of the complex is based on an uncommon asymmetric $\{Cr_3Cd(\mu_3\text{-}O)_2(\mu\text{-}O)_4\}$ core with firstly observed terminal coordination of the NCS-groups in such molecular structure type. A network of O–H···O hydrogen bonds as well as S···S interactions link the molecules into a two-dimensional supramolecular network. Single crystal X-ray analysis shows that the molecular structure of complex **1** is based on an asymmetric tetranuclear core $\{Cr_3Cd(\mu_3\text{-}O)_2(\mu\text{-}O)_4\}$ what could be described as two incomplete cube arrays, fused via common face (**Fig. 15**) [48]. The alkoxy O atoms of the triethanolamine bridge the Cr and Cd centers, whereby two μ_3 [O(4), O(6)] and four μ_2 bridge atoms [O(2), O(3), O(7), O(10)] exist. The main structural features of the core

were first discovered in the structure of titanium methoxide, $Ti_4(OMe)_{16}$ [49] and widely described for many tetranuclear alkoxide aggregates [50]. Albeit, in the former, a rather rare asymmetric organization of the metal centers was reported [48]. An example of this type of organization with an asymmetric $\{M_4(\mu_3\text{-}X)_2(\mu\text{-}X)_4\}$ core, according to the CSD [51] was found only in three complexes: $[Mn_3Ti(\mu_3\text{-}OCH_2CH_2OCH_3)_2\text{-}(m\text{-}OCH_2CH_2OCH_3)_3(\mu\text{-}Cl)Cl_2(OiPr)_2]$, $[Mg_3Cu(HMQCA)_4\text{-}(H_2O)_4](H_2O)_4$ and $[Mg_3Cu(HMQCA)_4(H_2O)_3(DMSO)]\text{-}(H_2O)_7(DMSO)_2$ (where HMQCA is a quinoline-based progenitor) [52] The Complex contains three crystallographically independent chromium(III) atoms, Cr(1), Cr(2) and Cr(3), each of them has a distorted octahedral environment with N_2O_4, NO_5 and N_3O_3 donor sets, respectively.

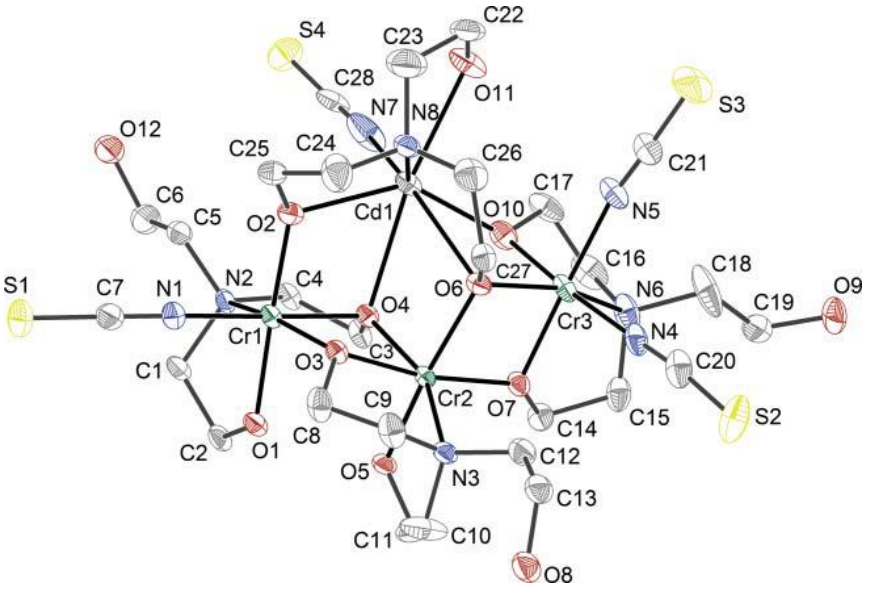

Fig. 15. Molecular structure of 1, showing the atom numbering, with 40% probability displacement ellipsoids. H atoms and methanol molecules are omitted for clarity, and only one of the two sets of disordered atoms O(9) and S(2) are shown.

The Cr–O(N) bond lengths are in the range 1.907(2)–2.153(3) Å and the O–Cr–$O(N)_{trans}$ angles vary from 158.64(9) to 178.34(11)°. For each Cr(III) atom the coordination sphere is formed differently, for Cr(1)— by one NCS-group and $Htea^{2-}$ ligands, for Cr(3)—by two NCS groups and $Htea^{2-}$ ligands, and for Cr(2)—by triethanolamine ligands only. The presence of a Cd(II) atom, which allows a wide range of geometries and coordination numbers

could cause its essential deformation of the tetranuclear core which can also explain the different coordination of the aminoalcohol to the Cr(III) atoms. The aminoalcohol should be a ligand that determines the structure of the molecular core, while the role of the other ligands lies mainly in the compensation of the charge (for charged ligands) or occupying vacant coordination sites (for neutral ligands).

Polynuclear transition metal complexes with paramagnetic ions are of great interest in molecular magnetism, especially because they are good candidates for investigating slow relaxation of the magnetization phenomena (single molecule magnet behaviour, SMM) [53]. In numerous polynuclear complexes, the exchange interactions are mediated by bridging HO^-, O_2^-, RO^-, and RCO_2^- ligands, or a combination of two or more of these groups [54]. In comparison with the rich cluster chemistry generated by manganese, iron and vanadium, in various oxidation states, the number of hydroxo- and/or alkoxo-bridged cobalt clusters is more limited [55]. Since Co(III) is diamagnetic, the interesting magnetic properties of mixed-valence cobalt clusters arise from Co(II), which is a paramagnetic ion with a strong Ising-type anisotropy. In a few cases, the SMM behaviour was observed [56]. Several synthetic approaches leading to homometallic polynuclear complexes were established, but the structure and the topology of the resulting systems cannot be easily predicted. An efficient synthetic procedure consists in the slow oxidation of divalent transition metal ions [Mn(II) and Co(II)] in the presence of organic acids and other potential ligands. Very useful ligands in obtaining high-nuclearity clusters are the amino-alcohols (e.g. monoethanolamine, diethanolamine, triethanolamine) because of their versatile bridging modes [57]. Recently, a heptanuclear complex, $[Co^{II}_4Co^{III}_3(dea)_6(CH_3COO)_3](ClO_4)_{0.75}(CH_3COO)_{1.25}0.5H_2O$ (H_2dea = diethanolamine), with the seven cobalt ions held together by alkoxo bridges arising from bis-deprotonated diethanolamine molecules is reported [58] (**Fig. 16**). In order to emphasize the role played by the carboxylato ligands on the aggregation of such clusters, the acetate ion was replaced with pivalate affording a new heterovalent Co^{II}–Co^{III} hexanuclear, $[Co_4^{II}Co_2^{III}(dea)_2(Hdea)_4)(piv)_4](ClO_4)_2H_2O$ cluster (**Fig. 17**).

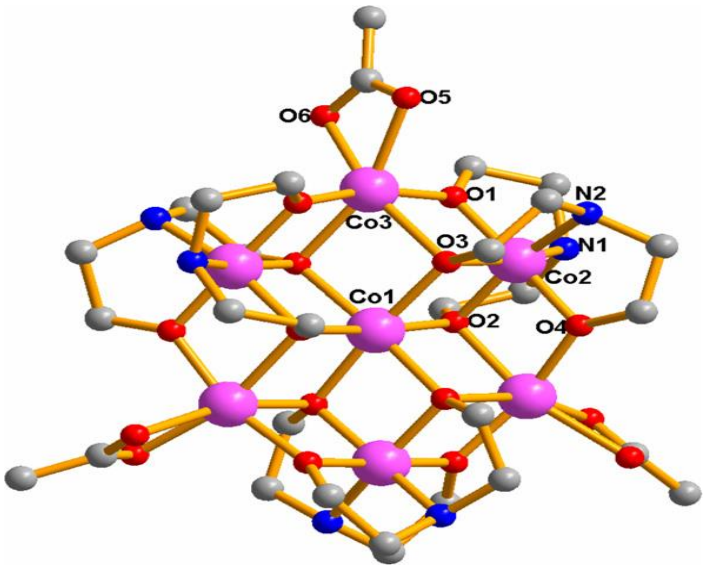

Fig. 16 (a). Perspective view of the heptanuclear cation in crystal structure of $[Co^{II}_4Co^{III}_3(dea)_6(CH_3COO)_3](ClO_4)0.75(CH_3COO)_{1.25}0.5H_2O$.

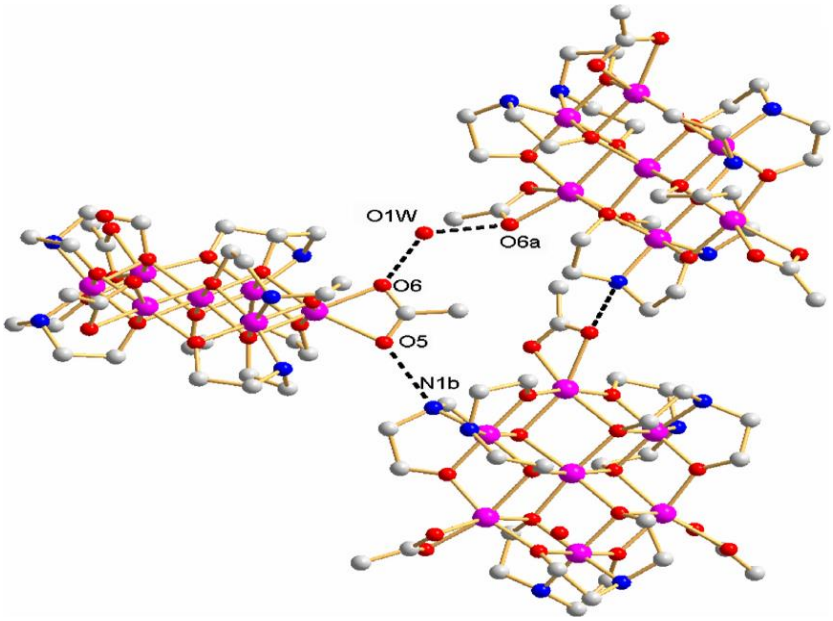

Fig. 16 (b). Packing diagram of $[Co^{II}_4Co^{III}_3(dea)_6(CH_3COO)_3](ClO_4)_{0.75}(CH_3COO)_{1.25}0.5H_2O$ showing the hydrogen bonds interactions established between the heptanuclear cationic clusters

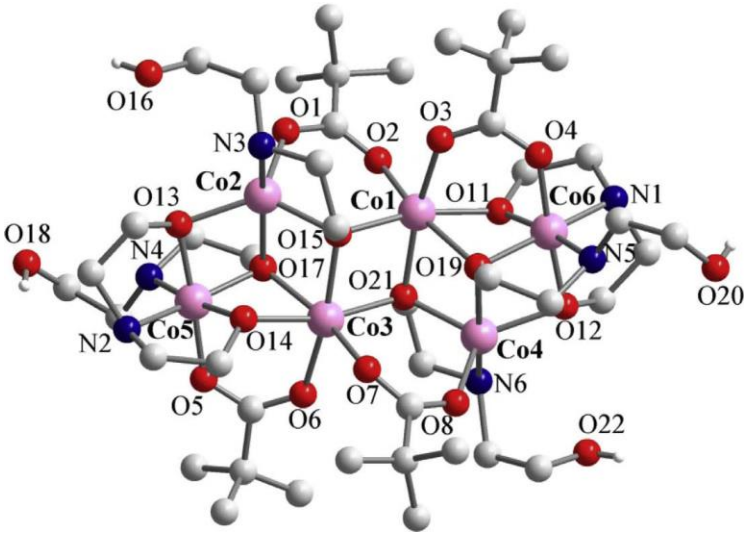

Fig. 17. Perspective view of the hexanuclear cation, $[Co_4^{II}Co_2^{III}(dea)_2(Hdea)_4)(piv)_4]^{2+}$.

The mixed valent Co^{II}/Co^{III} complex, $[\{Co^{II}Co^{III}(mea)_3\}_2(bpe)_3](ClO_4)_4\cdot 1.5CH_3OH\cdot 1.5H_2O$ (**Fig. 18**), where [Hmea = monoethanolamine and bpe = 1,2-bis(4-pyridyl)ethane], is reported to have ‘‘Chinese lantern”-like shaped cations, formed by connecting two $\{Co^{II}Co^{III}(mea)_3\}$ moieties with three flexible bpe ligands. The coordination sphere of the outer cobalt(III) ions is built by three amino groups arising from the mea- ligands, and by three bridging alkoxo-oxygen atoms whereas that of the inner cobalt(II) ions is constituted by the three alkoxo oxygen atoms and by three nitrogen atoms from three bpe ligands.

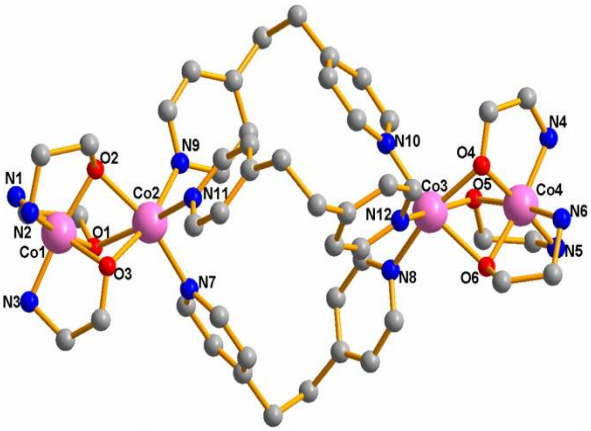

Fig. 18. Perspective view of the two crystallographically independent tetranuclear cations in $[\{Co^{II}Co^{III}(mea)_3\}_2(bpe)_3](ClO_4)_4\ 1.5CH_3OH1.5H_2O$.

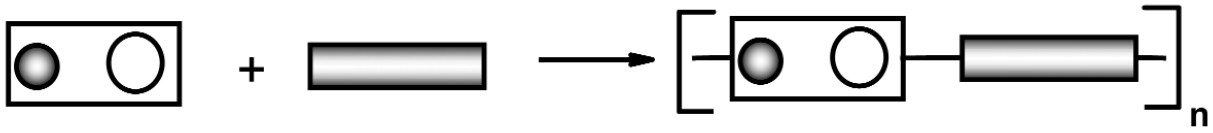

Fig. 19. The building block approach.

Oligonuclear complexes as well as coordination polymers with various topologies can be obtained by using homo- or heterobinuclear complexes as starting materials."The building block approach", which consist of anionic complex with potentially bridging ligands (linkers), which may interact with a wide variety of assembling cations (connectors) (**Fig. 19**). These building blocks are stable complexes, where the metal ions are held together by compartmental ligands, or alkoxo-bridged Cu(II) species. The binuclear nodes can be connected through appropriate exo-dentate ligands, or through metal-containing anions (e.g., $[M(CN)_6]^{3-}$, M = Cr^{III}, Fe^{III} and Co^{III}). A rich variety of 3d-3d and 3d-4f heterometallic complexes, with interesting architectures and topologies of the spin carriers, has been obtained. A particular case is the one concerning the 3d-4f binuclear nodes. Following this strategy, we were able to obtain coordination polymers containing three different spin carriers (2p-3d-4f; 3d-3d'-4f).

The following types of cationic species are employed as connectors: (i) alkoxo-bridged Cu(II) species; (ii) binuclear Cu(II) species with end-off compartmental Schiff-base ligands; (iii) binuclear Cu(II) complexes with macrocyclic Robson ligands; (iv) heterobinuclear 3d-4f species with side-off Schiff-base ligands (**Fig. 20**).

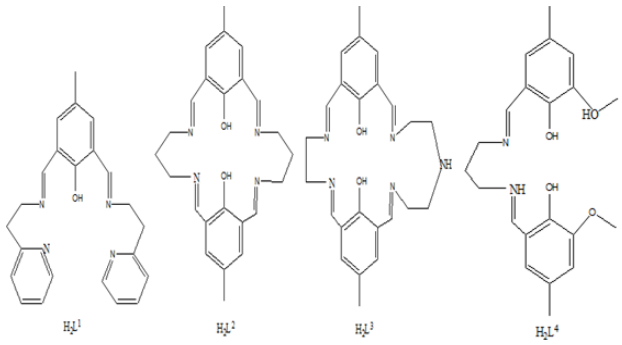

Fig. 20. Various Ligands which can be used as linkers.

Various ligands can be used as linkers: neutral organic molecules, anionic organic species, and anionic complexes with potentially bridging ligands. This approach broadens the synthetic concept proposed by Cotton, Lin, and Murillo [60], which is based on binuclear metal–metal bonded cationic entities as building units.

References

[1] (a) O. Kahn, Molecular Magnetism, VCH, New York. (1993) 131. (b) J.S. Miller, A.J. Epstein, Angew. Chem., Int. Ed. Engl., 33 (1994) 385. (c) J. Ribas, A. Escuer, M. Monfort, R. Vicente, R. Cortes, L. Lezama, T. Rojo, Coord. Chem. Rev., 193 (1999) 1027. (d) G. Christou, D. Gatteschi, D.N. Hendrickson and R. Sessoli, MRS Bull., 25 (2000) 66. (e) L.K. Thompson, Coord. Chem. Rev., 233 (2002) 19. (f) M.M. Turnbull, T. Sugimoto, L.K. Thompson, Molecule- Based Magnetic Materials—Theory, Techniques and Applications, ACS, Washington, 644 (1996). (g) K.G. Alley, G. Poneti, J.B. Aitken, R.K. Hocking, B. Moubaraki, K.S. Murray, B.F. Abrahams, H.H. Harris, L. Sorace, C. Boskovic, Inorg. Chem., 51 (2012) 3944.

[2] (a) R.E.P. Winpenny, in Comprehensive Coordination Chemistry, ed. J.A. McCleverty, T.J. Meyer, Pergamon Press, Oxford, 2004, ch. 7.3, vol. 7, p. 125; (b) R.E.P. Winpenny, Adv. Inorg. Chem., 52 (2001) 1.

[3] (a) L.Q. Chen, S.R. Breeze, R.J. Rousseau, S.N. Wang, L.K. Thompson, Inorg. Chem., 34 (1995) 454. (b) S.R. Breeze, S.N. Wang, Inorg. Chem., 33 (1994) 5113. (c) S.N. Wang, S.J. Trepanier, M.J. Wagner, Inorg. Chem., 32 (1993) 833. (d) S. Myllyviita, R. Sillanpaa, J.J.A. Kolnaar, J. Reedijk, J. Chem. Soc., Dalton Trans. (1995) 2209. (e) S. Myllyviita, R. Sillanpaa, J. Chem. Soc., Dalton Trans. (1994) 2125. (f) A.V. Sienkiewicz, V.N. Kokozay, Polyhedron, 13 (1994) 1439.

[4] (a) A. Karadag, V.T. Yilmaz, C. Thoene, Polyhedron, 20 (2001) 635. (b) J. Madarasz, P. Bombicz, M. Czugler, G. Pokol, Polyhedron, 19 (2000) 457. (c) V.T. Yilmaz, Y. Topcu, F. Yilmaz, C. Thoene, Polyhedron, 20 (2001) 3209. (d) V.T. Yilmaz, A. Karadag, C. Thoene, R. Herbst- Irmer, Acta Cryst., C 56 (2000) 948. (e) J.A. Bertrand, E. Fujita, D.G. VanDerveer, Inorg. Chem., 18 (1979) 230. (f) R.W. Saalfrank, I. Bernt, F. Hampel, Angew. Chem. Int. Ed. Engl., 40 (2001) 1700. (g) E.A. Vinogradova, V.N. Kokozay, O.Yu. Vassilyeva, B.W. Skelton, Acta Cryst. E, 59 (2003) 148. (h) O. Andac, Y. Topcu, V.T. Yilmaz, W.T.A. Harrison, Acta Cryst. C, 58 (2000) 14.

[5] M.-Q. Cheng, L.-F. Ma, L.-Y. Wang, Z. Kristallogr., 221 (2006) 369.

[6] M.P. Brandi-Blanco, J.M. Gonzalez-Perez, D.C. Lazarte, R. Carballo, A. Castinereiras, J. Niclos-Gutierrez, Inorg. Chem. Commun., 6 (2003) 270.

[7] Z.A. Siddiqi, M. Shahid, Mohd. Khalid, S. Kumar, Eur. J. Med. Chem., 44 (2009) 2517.

[8] A.C. Gozalez-Baro, E.E. Castellano, O.E. Piro, B.S. Parajon-Costa, Polyhedron, 24 (2005) 49.

[9] B. Setlow, P. Setlow, Appl. Environ. Microbiol, 59 (1993) 640.

[10] Z.A. Siddiqi, M. Khalid, S. Kumar, M. Shahid, S. Noor, Eur. J. Med. Chem., 45 (2010) 264.

[11] C.D. Nicola, A. Galindo, J.V. Hanna, F. Marchetti, C. Pettinari, R. Pettinari, E. Rivarola, B.W. Skelton, A.H. White, Inorg. Chem., 44 (2005) 3094.

[12] B. Barja, R. Baggio, M.T. Garland, P.F. Aramendia, O. Pena, M. Perec, Inorg. Chim. Acta, 346 (2003) 187.

[13] L. Carlucci, G. Ciani, D.M. Proserpio, Coord. Chem. Rev., 246 (2003) 247.

[14] Z.A. Siddiqi, M. Shahid, S. Kumar, M. Khalid, S. Noor, J. Organomet. Chem., 694 (2009) 3768.

[15] P. Laine, A. Gourdon, J.-P. Launay, J.-P. Tuchagues, Inorg. Chem., 34 (1995) 5150.

[16] P. Laine, A. Gourdon, J.-P. Launay, Inorg. Chem., 34 (1995) 5138.

[17] M. Biagini-Cingi, A. Chiesi Villa, C. Guastini, M. Nardelli, Gazz. Chim. Ital., 101 (1971) 825.

[18] H. Watanabe, M. Nakai, K. Komazawa, H. Sakurai, J. Med. Chem., 37 (1994) 876.

[19] H. Sakurai, K. Tsuchiya, M. Nukatsuka, J. Kawada, S. Ishikawa, H. Yoshida, M. Komatsu, J. Clin. Biochem. Nutr, 8 (1990) 193.

[20] K. Kawabe, M. Tadokoro, Y. Kojima, Y. Fujisawa, H. Sakurai, Chem. Lett. (1998) 9.

[21] J. Li, G. Elberg, D.C. Crans, Y. Shechter, Biochemistry, 35 (1996) 8314.

[22] M Mirzaei, H. E.-Hosseini, A. Bauzá, S. Zarghami, P. Ballester, Joel T. Maguee, A. Frontera, CrystEngComm, 16 (2014) 6149.

[23] (a) M.M. Habeeb, R.M. Alghanmi, J. Chem. Eng. Data, 55 (2010) 930. (b) S. Jin, L. Liu, D. Wang, J. Guo, J. Mol. Struct., 59 (2011) 1005.

[24] (a) G.A. Jeffrey, An Introduction to Hydrogen Bonding, Oxford University Press, Oxford, 1997. (b) G.R. Desiraju, T. Steiner, The Weak Hydrogen Bond in Structural Chemistry

and Biology, Oxford University Press, Oxford, 1999. (c) C.A. Hunter, J.K.M. Sanders, J. Am. Chem. Soc., 112 (1990) 5525. (d) S.K. Burley, G.A. Petsko, Science, 23 (1985) 229.

[25] (a) W. Hieber, E. Levy, Ann., 500 (1932) 14. (b) W. Hieber, E. Levy, Z. Anorg. Chem., 219 (1934) 225.

[26] V.V. Udovenko, A.N. Gerasenkova, Russ. J. Inorg. Chem., 11 (1966) 1105.

[27] J.A. Bertrand Kelly, E.G. Vassian, J. Am. Chem. Soc., 91 (1969) 2394.

[28] V.V. Udovenko, A.N. Gerasenkova, Russ. J. Inorg. Chem., 12 (1967) 654.

[29] (a) M. Andruh, Pure Appl. Chem., 77 (2005) 1685. (b) M.J. Katz, C.J. Shorrock, R.J. Batchelor, D.B. Leznoff, Inorg. Chem., 45 (2006) 1757. (c) G. Marin, V. Tudor, V. Ch. Kravtsov, M. Schmidtmann, Y.A. Simonov, A. Muller, M. Andruh, Cryst. Growth Des, 5 (2005) 279. (d) V. Tudor, V. Kravtsov, Y.A. Simonov, J. Lipkowski, M. Brezeanu, Inorg. Chim. Acta, 35 (2003) 353. (e) C. Paraschiv, M. Andruh, S. Ferlay, M. Wais Hosseini, N. Kyritsakas, J.-M. Planeix, N. Stanica, Dalton Trans. (2005) 1195.

[30] V.N. Evreev, G.A. Kotlyor, Russ. J. Inorg. Chem., 15 (1970) 1121.

[31] V.N. Evreev, V.A. Golub, Russ. J. Inorg. Chem., 18 (1973) 387.

[32] (a) Y. Chen, Q. Liu, Y. Deng, H. Zhu, C. Chen, H. Fan, D. Liao, E. Gao, Inorg. Chem., 49 (2001) 37245. (b) D. Foguet-Albiol, K.A. Abboud, G. Christou, Chem. Commun. (2005) 4282. (c) R.T.W. Scott, S. Parsons, M. Murugesu, W. Wernsdorfer, G. Christou, E.K. Brechin, Chem. Commun. (2005) 2083. (d) E.K. Brechin, Chem. Commun. (2005) 5141. (e) S.K. Langle, K.J. Berry, B. Moubaraki, K.S. Murray, J. Chem. Soc., Dalton Trans. (2009) 973.

[33] (a) E.C. Yang, D.N. Hendrickson, W. Wernsdorfer, M. Nakano, L.N. Zakharov, R.D. Sommer, A. L. Rheingold, M. Ledezma-Gairaud, G. Christou, J. Appl. Phys., 91 (2002) 7382. (b) M. Murrie, S.J. Teat, H. Stoeckli-Evans, H.U. Güdel, Angew. Chem., Int. Ed., 42 (2003) 4653. (c) S.J. Langley, M. Helliwell, R. Sessoli, P. Rosa, W. Wernsdorfer, R.E.P. Winpenny, Chem. Commun. (2005) 5029. (d) M.-H. Zheng, M.-X. Yao, H. Liang, W.-X. Zhang, X.-M. Chen, Angew. Chem., Int. Ed., 46 (2007) 1832. (e) S.J. Langley, M. Helliwell, R. Sessoli, S.J. Teat, R.E. P. Winpenny, Inorg. Chem., 47 (2008) 497. (f) S.J. Langley, M. Helliwell, R. Sessoli, S.J. Teat, R.E.P. Winpenny, Dalton Trans. (2009) 3102.

[34] G.I. Chillas, M. Stylianou, M. Kubicki, T. Vaimakis, P. Kögerler, A.D. Keramidas, T. Kabanos, Inorg. Chem., 47 (2008) 4451.

[35] (a) Z.A. Siddiqi, A. Siddique, M. Shahid, M. Khalid, P.K. Sharma, Anjuli, M. Ahmad, S. Kumar, Y.L, A.K. Powell, Dalton Trans., 42 (2013) 9513. (b) P. King, R. Clérac, W. Wernsdorfer, C.E. Anson, A.K. Powell, Dalton Trans. (2004) 2670.

[36] Y.A. Mikhailenko, E.V. Peresypkina, A.V. Virovets, T.G. Cherkasova, Russ. J. Inorg. Chem., 54 (2009) 568.

[37] A. Baysal, M. Aydemir, F. Durap, S. Ozkar, L.T. Yildirim, Inorg. Chim. Acta, 371 (2011) 107.

[38] P. Dapporto, L. Sacconi, Chem. Commun. (1969) 329.

[39] F. Hein, W. Ludwig, Z. Anorg. Allgem. Chem., 341 (1965) 61.

[40] A. Pajunen, M. Lehtonen, Suom. Kemi B, 44 (1971) 200.

[41] E. Uhlig, K. Steiger, Z. Anorg. Allegem. Chem., 346 (1966) 21.

[42] E. Uhlig, K. Steiger, Z. Anorg. Allegem. Chem., 360 (1968) 39.

[43] J.A. Bertrand, J. A. Kelley, Inorg. Chim. Acta, 4 (1970) 203.

[44] J.A. Bertrand, Etsuko Fugita, D.G. Vanderveer Inorg. Chem., 18 (1979) 230.

[45] E. Uhlig, H. Raimann, K. Staiger, Z. Anorg. Allgem. Chem., 35 (1967) 296.

[46] (a) R.P. Sharma, A. Saini, P. Venugopalan, V. Ferretti, F. Spizzo, C. Angelib, C.J. Calzadoe, New J. Chem., 38 (2014) 574. (b) Z. Boulsourani, V. Tangoulis, C.P. Raptopoulou, V. Psycharisb, C. Dendrinou-Samara, Dalton Trans., 40 (2011) 7946. (c) K.R. Gruenwald, A.M. Kirillov, M. Haukka, J. Sanchiz, A.J.L. Pombeiro, Dalton Trans. (2009) 2109

[47] (a) S.K. Langley, N.F. Chilton, L. Ungur, B. Moubaraki, L.F. Chibotaru, K.S. Murray, Inorg. Chem., 51 (2012) 11873. (b) S.K. Langley, L. Ungur, N.F. Chilton, B. Moubaraki, L.F. Chibotaru, K.S. Murray, Inorg. Chem., 53 (2014) 4303.

[48] V.V. Semenaka, O.V. Nesterova, V.N. Kokozay, V.V. Dyakonenko, O.V. Shishkin, R. Boca, J. Jezierskae, Dalton Trans., 39 (2010) 1734.

[49] K. Watenpaugh, C.N. Caughlan, Chem. Commun. (1967) 76.

[50] (a) V.G. Kessler, Chem. Commun. (2003) 1213. (b) K.G. Caulton, L.G. Hubert-Pfalzgraf, Chem. Rev., 90 (1990) 969. (c) L.G. Hubert- Pfalzgraf, Coord. Chem. Rev., 967 (1998) 178.

[51] (a) There are 7 structures of heterometallic Cd/Cr complexes in the Cambridge Structural Database (CSD), version 5.30 (May 2009). (b) F.H. Allen, Acta Crystallogr., Sect. B: Struct. Sci., 58 (2002) 380.

[52] (a) L.B. Jerzykiewicz, J. Utko, L. John, M. Duczmal, P. Sobota, Inorg. Chem., 46 (2007) 9024. (b) B. Courcot, D. Firley, B. Fraisse, P. Becker, J.-M. Gillet, P. Pattison, D. Chernyshov, M. Sghaier, F. Zouhiri, D. Desmaele, J. d'Angelo, F. Bonhomme, S. Geiger, N.E. Ghermani, J. Phys. Chem. B, 111 (2007) 6042. (c) J. Tao, X.-M. Chen, R.-B. Huang, L.-S. Zhenga, J. Solid State Chem., 170 (2003) 130. (d) F. Li, Z.Ma, Y.-L.Wang, R. Cao, W.-H. Bi, X. Li, Cryst. Eng. Comm, 7 (2005) 569. (e) A. Gulino, P. Dapporto, P. Rossi, I. Fragala, Chem. Mater., 14 (2002) 4955. (f) B. Barszcz, A. Jabłonrska-Wawrzycka, K. Stadnicka, S.A. Hodorowicz, Inorg. Chem. Commun., 8 (2005) 951.

[53] (a) R. Sessoli, D. Gatteschi, A. Caneschi, M.A. Novak, Nature, 365 (1993) 141. (b) D. Gatteschi, Adv. Mater., 6 (1994) 635. (c) R. Sessoli, D. Gatteschi, Angew. Chem., Int. Ed., 42 (2003) 268.

[54] G. Aromi, E.K. Brechin, Struct. Bonding, 122 (2006) 1.

[55] (a) E.K. Brechin, S.G. Harris, A. Harrison, S. Parsons, A.G. Whitaker, R.E.P. Winpenny, Chem. Commun. (1997) 653. (b) M. Mikuriya, N. Nagao, K. Kondo, Chem. Lett. (2000) 516. (c) B. Chiari, A. Cinti, O. Crispu, F. Demartin, A. Pasini, O. Piovesana, J. Chem. Soc., Dalton Trans. (2001) 3611. (d) E.K. Brechin, A. Graham, P.E.Y. Milne, M. Murrie, S. Parsons, R.E.P. Winpenny, Philos. Trans. R. Soc. London, Ser. A, 357 (1999) 3119. (e) G.S. Papaefstathiou, A. Escuer, C.P. Raptopoulou, A. Terzis, S.P. Perlepes, R. Vicente, Eur. J. Inorg. Chem., 357 (2001) 1567. (f) V.A. Milway, L.K. Thompson, D.O. Miller, Chem. Commun. (2004) 1790. (g) Z. Serna, M.K. Urtiaga, M.G. Barandika, S. Martin, L. Lezama, M.I. Arriortua, T. Rojo, Inorg. Chem., 40 (2001) 4550. (h) G.A. Seisenbaeva, M. Kritikos, V.G. Kessler, Polyhedron, 22 (2003) 2581. (i) M. Du, Y.-M. Guo, X.-H. Bu, J. Ribas, Eur. J. Inorg. Chem., (2004) 3228. (j) T.C. Stamatatos, S. Dyonissopoulou, G. Eftymiou, P. Kyritsis, C.P. Raptopoulou, A. Terzis, R. Vicente, A.

Escuer, S.P. Perlepes, Inorg. Chem., 44 (2005) 3374. (k) T. Komiyama, S. Igarashi, Y. Hoshino, Y. Yukawa, Chem. Lett. (2005) 300. (l) J.K. Beattie, T.W. Hambley, J.A. Klepetko, A.F. Masters, P. Turner, Polyhedron, 16 (1997) 2109. (m) L.F. Jones, P. Jensen, B. Moubaraki, J.D. Cashion, K.J. Berry, K.S. Murray, Dalton Trans. (2005) 3345.

[56] (a) E.-C. Yang, D.N. Hendrickson, W. Wernsdorfer, M. Nakano, L.N. Zakharov, R. Sommer, A.L. Rheingold, M. Ledezma-Gairaud, G. Christou, J. Appl. Phys., 91 (2002) 7382. (b) M. Murrie, S.J. Teat, H. Stoeckli-Evans, H.U. Güdel, Angew. Chem. Int. Ed., 42 (2003) 4653. (c) A. Ferguson, A. Parkin, J. Sanchez-Benitez, K. Kamenev, W. Wernsdorfer, M. Murrie, Chem. Commun. (2007) 3473. (d) M. Moragues-Canovas, C.E. Talbot-Eekelaers, L. Catala, F. Lloret, W. Wernsdorfer, E.K. Brechin, T. Mallah, Inorg. Chem., 45 (2006) 7038. (e) Y.-Z. Zhang, W. Wernsdorfer, F. Pan, Z.-M. Wang, S. Gao, Chem. Commun. (2007) 3302.

[57] (a) W. Plass, Eur. J. Inorg. Chem. (1998) 799. (b) Y. Chen, Q. Liu, Y. Deng, H. Zhu, C. Chen, H. Fan, D. Liao, E. Gao, Inorg. Chem., 40 (2001) 3725. (c) D. Foguet-Albiol, K.A. Abboud, G. Christou, Chem. Commun. (2005) 4282. (d) R.T.W. Scott, S. Parsons, M. Murugesu, W. Wernsdorfer, G. Christou, E.K. Brechin, Chem. Commun. (2005) 2083. (e) E.K. Brechin, Chem. Commun. (2005) 5141.

[58] V. Tudor, G. Marin, F. Lloret, V.Ch. Kravtsov, Y.A. Simonov, M. Julve, M. Andruh, Inorg. Chim. Acta, 361 (2008) 3446.

[59] F.A. Cotton, C. Lin, C.A. Murillo. Acc. Chem. Res., 34 (2001) 759.

Chapter 2

Novel Cu_3- and Zn_2-aminotriethanolate complexes anchored by carboxylate ancillary: crystallographic, Hirshfeld surface analyses, photoluminescence and catalytic properties

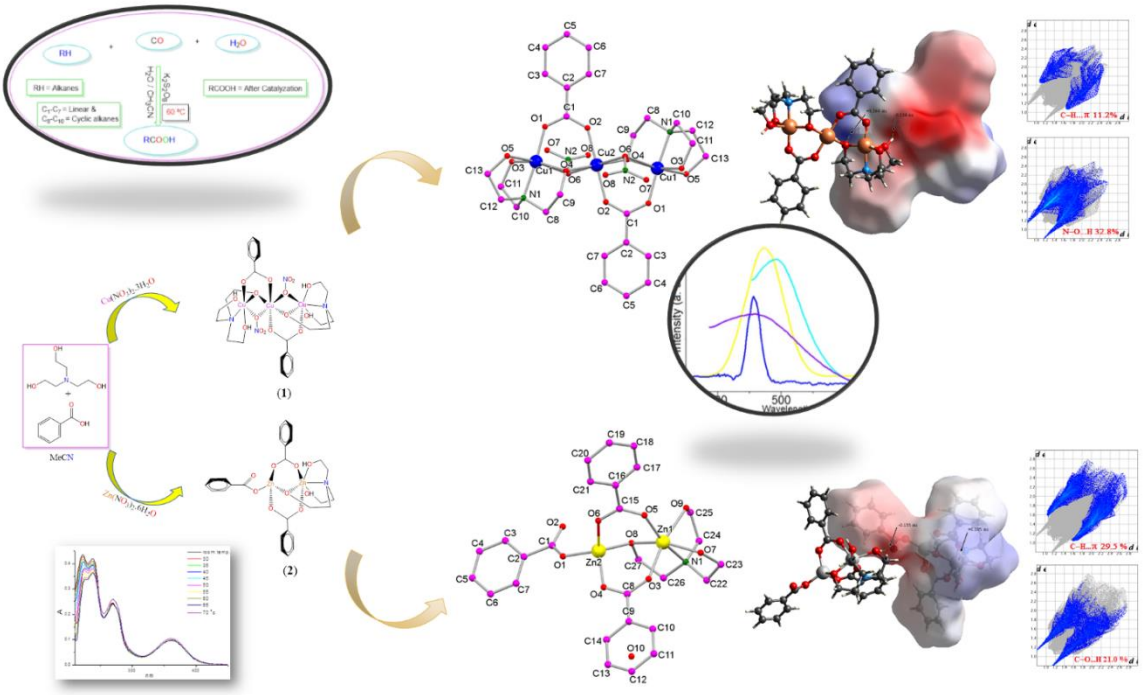

Introduction

The designing of polynuclear transition-metal complexes bearing unique structural features has become a challenge in the past decade due to their broad applications such as in catalysis, biochemistry, materials science and medicinal chemistry. The reason for the wide utility of the high nuclearity metal complexes is their complex molecular structures, topology and electronic versatility. Though several transition metal ions yield polynuclear clusters, special emphasis has always been given to the Cu(II) and Zn(II) chemistry [1].

The chemistry of polynuclear copper complexes is a topic of great scientific interest due to its relevance to many areas, including bioinorganic chemistry and materials science. Copper complexes have recently attracted increasing attention as alternative O_2 reduction catalysts. Among numerous copper-containing enzymes such as hemocyanin, cytochrome c oxidase, and, nitrous oxide reeducates, few molecular examples play a variety of critical roles in biology responsible for activation and transformation of small molecules [2]. Besides copper, the coordination chemistry of d^{10} systems like Zn(II) complexes has also attracted much attention owing to their versatile role in various metalloenzymes like carbonic anhydrase. Zn(II) complexes have been proven better enzymatic mimics in the recent years. Specially the polynuclear zinc complexes are explored as efficient catalysts e.g. zinc cluster is used in direct conversion of ester, carboxylic acids and lactones to oxazolines [3]. Simultaneously, Cu(II) catalysts have been reported in literature to catalyse a number of organic reactions [4]. In designing polynuclear clusters of Cu(II) and Zn(II) metal ions, it is important to select the ligands which decide the structural topology and nuclearity of the resulting clusters [4].

Flexible amino-polyalcohols are recognized as useful ligands in coordination chemistry and related areas, and have ability to show a variety of coordination modes being broadly used for the preparation of diverse materials with mono- and specially polynuclear metal complexes [5].

Amino-alcohol derivative ligands are useful in the synthesis of polynuclear coordination clusters by chelating to one metal centre and bridging other metal centres through the alkoxide arms. Furthermore, the introduction of the auxiliary ligands like carboxylic acid,

plays a key role in maintaining the structural topology and integrity of the cluster exhibiting unusual coordination modes (**Scheme 1**) [5,6].

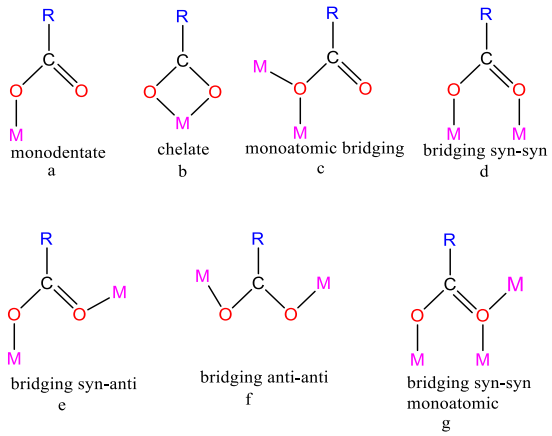

Scheme 1. Selected coordination modes of carboxylate (COO^{-}) group.

Triethanolamine (H_3tea) is an ideal amino alcohol ligand which acts as deprotonated multidentate in the area of clusters chemistry with its [N,O,O,O] donor sites. This ligand exhibits versatile bridging and chelating modes, as it can, in theory, bind to upto a number of metals at a time. Its flexibility in cluster science gives rise to various deprotonated forms as: H_3tea, H_2tea^{-}, $Htea^{2-}$ and tea^{3-}, which further provides numerous different types of bonding modes. The flexible nature of the H_3tea is what makes it so much promising and has thus far been known to display eight different modes of bonding (**Scheme 2**) [7].

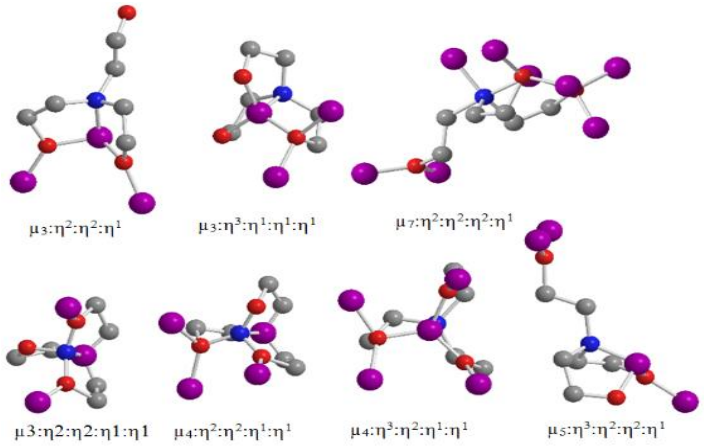

Scheme 2. Coordination modes of the ligand triethanolamine (H_3tea). Metals ions are purple, oxygen atoms red, nitrogen atom blue and carbon atoms grey. (H atoms are not shown for clarity).

For 3d metal ions these amino alcohols and carboxylate units can combine in more interesting ways and yield more elaborate products. When fully deprotonated (tea^{3-}), the tendency of the three alkoxide arms of the tri-anion generally directs the formation of dinuclear [M_2] and triangular [M_3] units where each arm of the ligand bridges produces edge of the triangle. In the presence of co-ligands such as carboxylates or β diketonates etc, these smaller units can combine to produce complexes whose structures range from 'simple' [M_2], [M_3] or [M_4] (centered) triangles to rod-like complexes describing '1-D' arrays of edge-sharing triangles; planar disc-like complexes describing 'two dimensional' arrays of edge-sharing triangles; and more complicated 'three dimensional' arrays commonly based on tetrahedra, octahedra and icosahedra. These ligands are excellent candidates for use in paramagnetic cluster synthesis as they have the ability to act as both terminal and bridging ligands. These coordination clusters self-assemble through syn syn carboxylate and / or nitrate bridges, often supported to form poly systems, 1D tapes, 2D sheets, and 3D networks which have been constructed through non-covalent interactions. Among others, carboxylic acids have been successfully used in crystal engineering to generate a variety of 3D bridged architectures [7].

In view of the above and due to our ongoing interest for new preparative routes to polynuclear complexes of various transition metal complexes, we chose to investigate the coordination chemistry of copper and zinc with triethanolamine (H_3tea) in the presence of benzoic acid as the ancillary ligand. This combination of aminoalcoholate and benzoate with Cu(II) and Zn(II) results in the trinuclear (Cu_3) and dinuclear (Zn_2) complexes which are further proven to be efficient catalysts for the conversion of alkanes to carboxylic acids.

Experimental

Materials and methods

All reagents of analytical grade were obtained from commercial sources and used without further purification. The infrared (IR) spectra of the compound were recorded within the range 4000–400 cm^{-1} using KBr pellets on Perkin Elmer Model spectrum GX spectrophotometer. Melting points were determined by open capillary method and are uncorrected. Electronic spectrum and molar conductivity of 10^{-3} M solution in MeOH was recorded on Perkin Elmer λ-850 UV-visible spectrophotometer at various temperatures with cu-vettes of 1 cm path length and Systronics-305 digital conductivity bridge, at room temperature respectively. The elemental C, H and N analyses were obtained from Micro-Analytical Laboratory of Central Drug Research Institute (CDRI), Lucknow, India. Fluorescence measurements were determined on Hitachi F-2700 spectrophotometer. Solid state fluorescence spectra were recorded on Jobin Yvon Horiba Fluorolog-3 spectro fluorimeter at room temperature. The EPR spectrum of the complexes was acquired on a Perkin-Elmer spectrometer using X-band frequency (9.1 GHz) at room temperature in solid. Thermal gravimetric analysis (TGA) data were recorded from room temperature up to 600 °C at a heating rate of 20 °C/min. The data were obtained using a Shimadzu TGA-50H instrument. Magnetic susceptibility was measured by magnetic susceptibility balance, Sherwood scientific Cambridge U. K. at room temperature. Cyclic voltammetry (CV) was performed on EG&G PAR 273 Potentiostat/Galvanostat an IBM PS2 computer with EG&G M270 software for data acquisition. The three-electrode cell configuration comprised of, a platinum sphere, a platinum plate and Ag(s)/$AgNO_3$ were used as working, auxiliary and reference electrodes, respectively. The supporting electrolyte used was $[^nBu_4N]ClO_4$. Platinum sphere electrode was sonicated for 2 min in dilute nitric acid, dilute hydrazine hydrate and then in double distilled water to remove the impurities. The solutions were deoxygenated by bubbling research grade nitrogen gas and an atmosphere of nitrogen was maintained over the solution during measurements.

Crystallographic data collection and refinements

Single crystal X-ray diffraction of the compounds (**1** and **2**) was performed at 100 K on a Bruker SMART APEX CCD diffractometer, X–ray data was collected using graphite monochromated Mo-Kα radiation (λ = 0.71073 Å). The linear absorption coefficients, scattering factors for the atoms, and the anomalous dispersion corrections were taken from the International Tables for X–ray Crystallography [8]. The data integration and reduction were processed with SAINT Software [9]. An empirical absorption correction was applied to the collected reflections with SADABS [10] and the space group was determined using XPREP [11]. The structures were solved by direct methods using SIR-97 [12] and refined on F^2 by full matrix least squares using the SHELXl-97 program package [13]. All non-hydrogen atoms were refined with anisotropic displacement parameters. A summary of the crystallographic data and the structure refinement for the complexes is given in Table 1. CCDC reference numbers for **1** and **2** are 1474749 and 1474750, respectively.

Table **1**. Crystal data with refinement parameters for complexes **1** and **2**.

Parameters	Complex **1**	Complex **2**
Empirical formula	$C_{26}H_{38}Cu_3N_4O_{16}$	$C_{27}H_{31}NO_{10}Zn_2$
Formula weight	849.22	660.27
Temp (K)	100(2)	296(2)
Crystal system	Monoclinic	Monoclinic
Space group	P 2_1/c	P 2_1/n
Unit cell dimensions		
a (Å)	8.1872(6)	14.49(2)
b (Å)	16.9482(13)	11.44(3)
c (Å)	11.7093(9)	18.17(2)
α (°)	90.00	90.00
β(°)	101.284(4)	109.49(5)
γ (°)	90.00	90.00
V (Å^3)	1593.4(2)	2839(14)
Z	2	4
ρ (calc) (g cm^{-3})	1.770	1.746
F (000)	866	1363.15
Index ranges	$-9 \leq h \leq 9$	$-17 \leq h \leq 17$
	$-20 \leq k \leq 19$	$-13 \leq k \leq 13$
	$-14 \leq l \leq 14$	$-22 \leq l \leq 22$
No of reflections collected	17858	4985
No. of independent reflection	2941	36277
GOF	1.035	0.8410
Final R indices [I > 2σ(I)]	R_1 = 0.0417	0.0789
	wR_2 = 0.843	0.0757
R indices all data	R_2 = 0.0310	0.0406
	wR_2 = 0.091	0.0876

Table **2**. Selected bonds length (Å) and bonds angle (°) of complex.

Complex (**1**)		Complex (**2**)	
Bond lengths			
Cu1−O1	1.911(2)	Zn1−O3	2.124(5)
Cu1−O4	1.959(2)	Zn1−O5	1.988(5)
Cu1−N1	2.019(2)	Zn1−N1	2.140(5)
Cu1−O3	2.067(2)	Zn1−O8	2.078(4)
Cu1−O5	2.239(3)	Zn1−O7	2.172(6)
Cu2−O4	1.938(2)	Zn2−O8	1.941(5)
Cu2−O2	1.994(2)	Zn2−O1	1.926(5)
Cu2−O2	1.9933(19)	Zn2 −O4	1.960(4)
Cu1−O1	1.9099(19)	Zn2−O6	1.959(6)
Bond angles			
O1 −Cu1−O4	97.42(9)	O5−Zn1−O3	97.11(11)
O1−Cu1−N1	173.90(10)	N1−Zn1−O3	97.10(12)
O4−Cu1−N1	88.63(9)	N1−Zn1−O5	165.68(12)
O1−Cu1−O3	90.53(10)	O8−Zn1−O3	92.65(10)
O4−Cu1−O3	157.57(10)	O8−Zn1−O5	95.60(10)
N1−Cu1−O3	83.57(9)	O8 −Zn1−N1	82.02(11)
O1−Cu1−O5	99.17(11)	O7 −Zn1−O3	81.56(11)
O4−Cu1−O5	99.77(10)	O7 −Zn1−O5	102.80(11)
N1−Cu1−O5	80.38(10)	O7 −Zn1−N1	81.02(12)
O3−Cu1−O5	99.61(11)	O7 −Zn1−O8	161.24(11)
O4−Cu2−O4	180.00(5)	O9 −Zn1−O3	167.84(12)
O4−Cu2−O2	91.82(9)	O9 −Zn1−O5	88.36(13)
O4−Cu2−O2	88.18(9)	O9 −Zn1−N1	78.02(14)
O4−Cu2−O2	88.18(9)	O9 −Zn1−O8	97.63(12)
O4−Cu2−O2	91.82(9)	O9−Zn1−O7	86.65(13)
O2−Cu2−O2	180.0	O4−Zn2−O1	99.85(11)
C1−O1−Cu1	127.3(2)	O6−Zn2−O1	112.45(13)
N1−C12−C13	112.8(2)	O6−Zn2−O4	111.85(12)
N1−C10−C11	109.7(2)	O8−Zn2−O1	120.92(11)
N1−C8−C9	109.4(2)	O8−Zn2−O4	107.99(11)
Cu1−Cu2−Cu1	180.0	O8−Zn2−O6	103.83(12)

Hirshfeld surface analysis

Hirshfeld surfaces mapped with various properties and 2D fingerprint plots were generated using Crystal Explorer 3.0 [14]. This have been proven to be a useful visualization tool for the analysis of intermolecular interactions in the crystal packing [15]. The Hirshfeld surface can be defined in a crystal as the region around a molecule where the ratio of the electron distribution of a sum of spherical atoms for the molecule (the promolecule) to the corresponding sum over the crystal (the procrystal) equals to 0.5. The shape and nature of the surface is directly influenced by the surrounding environment of the molecule in the crystal.

For each point on the Hirshfeld iso surface, two distances d_e, the distance from the point to the nearest nucleus external to the surface, and di, the distance to the nearest nucleus internal

to the surface, are defined. The normalized contact distance (d_{norm}) based on de and di is given by

$$d_{norm} = \frac{d_i - r_i^{vdW}}{r_i^{vdW}} + \frac{d_e - r_e^{vdW}}{r_e^{vdW}}$$

Where r_i^{vdW} and r_e^{vdW} being the van der Waals radii of the atoms. The value of d_{norm} may be negative or positive depending on the intermolecular contacts being shorter or longer than the van der Waals separations [16]. The parameter d_{norm} displays a surface with a red-white-blue colour scheme, where bright red spots highlight shorter contacts, white colour areas represent contacts around the van der Waals separation, and blue colour regions are devoid of close contacts.

The electrostatic potential (ESP) were mapped on the Hirshfeld surface [17] over the range −0.139 au (red), through 0 (white), to 0.225 au (blue) and −0.161 au (red), through 0 (white), to 0.208 au (blue) respectively, for **1** and **2**. For this purpose, ab initio wave functions were obtained at HF/STO-3G** using Crystal Explorer 3.0 software. Molecular geometries were taken directly from the relevant crystal structure with H atoms at their neutron distances. 3D-deformation density (DD) maps were also plotted for the molecule at the crystal geometry over the electron density iso-surface (the value is 0.008 e/au^3) using Crystal Explorer 3.0. For this purpose, ab initio wave functions were also obtained at HF/ STO-3G.

Catalytic activity

In a typical experiment, the reaction mixtures were prepared as follows: to 4.0 μmol of the copper promoter **1** or zinc promoter **2** contained in a 13.0 mL stainless steel autoclave, equipped with a Teflon-coated magnetic stirring bar, were added 1.00–1.50 mmol of $K_2S_2O_8$, 2.0 mL of H_2O, 4.0 mL of MeCN (typical total solvent volume was 6.0 mL) and 1.00 mmol of alkane (if liquid). Then the autoclave was closed and flushed with CO three times to remove the air, and finally pressurized with 0.75−1.0 atm of alkane (if gaseous) and 10−20 atm of CO. The reaction mixture was stirred for 6 h at 60 °C using a magnetic stirrer and an oil bath, whereupon it was cooled in an ice bath, degassed, opened and transferred to a flask. Diethyl

ether (9.0–11.0 mL) and 90 μL of cycloheptanone (GC internal standard) were added. The obtained mixture was vigorously stirred for 10 min, and the organic layer was analyzed by gas chromatography (internal standard method), revealing the formation of the corresponding monocarboxylic acids as the dominant products. In the reactions with cycloalkane substrates, cyclic ketones and alcohols were also formed as by-products of partial alkane oxidation, whereas in the transformations of linear alkanes the generation of the corresponding oxygenates was negligible (their overall yields were not exceeding 1.0%). Blank tests indicated that the hydrocarboxylations also proceed in the metal-free systems [18], although typically leading to 3-5 times inferior yields of carboxylic acids in comparison with the Cu_3/Zn_2-promoted transformations. Additional experiments were performed under the typical reaction conditions in the presence of the carbon-centred radical trap $CBrCl_3$, revealing the suppression of the formation of carboxylic acids. The acetonitrile solvent is nonreactive in the present systems, since no generation of acetic or propionic acids from MeCN was detected when the reactions were repeated in the absence of alkane. Furthermore, the alkane hydrocarboxylations do not proceed either in sole H_2O or MeCN solvent.

Synthesis

Synthesis of $[Cu_3(H_2tea)_2(ba)_2(NO_3)_2]$ (1)

A mixture of $Cu(NO_3)_2{\cdot}3H_2O$ (0.031 g, 0.13 mmol) and benzoic acid (Hba) (0.016 g, 0.13 mmol) in MeCN (20 mL) was stirred for 10 min at 80 °C producing a blue-green solution. A solution of H_3tea (0.298 g, 2 mmol) in CH_3CN (10 mL) was added dropwise to the above mixture. The reaction was then stirred for 5 h after addition of 10 drops of NEt_3. The resulting green solution was allowed to evaporate slowly. After being at room temperature, green block crystals of **1** were collected, which were suitable for X-ray crystallographic study in 70% yield based on the added amounts of metal salt. Elemental analysis: Calcd: for $C_{26}H_{34}Cu_3N_4O_{16}$ (M = 795): C, 36.74; N, 6.59; H, 4.00%. Found: C, 36.92; N, 6.78; H, 4.12%. Molar conductance, Λ_m (10^{-3} M, methanol): 35.0 $\Omega^{-1}cm^2mol^{-1}$. FT–IR (as KBr, ν/cm^{-1}): 1572/1386s $\nu_{as}/\nu_s(COO^-)$, 3400 (O–H), 945s (Cu–O–Cu).

Synthesis of $[Zn_2(H_2tea)_2(ba)_3]\cdot H_2O$ (2)

2 was synthesized by similar procedure to that used for **1** except that equal amount of $Zn(NO_3)_2\cdot 4H_2O$ was used in place of $Cu(NO_3)_2\cdot 3H_2O$. Yield: 65.0% based on the added amounts of metal salt. Elemental analysis: Calcd: for $C_{27}H_{31}NO_{10}Zn_2$ (M = 660): C, 49.10; N, 2.12; H, 4.69%. Found: C, 49.80; N, 2.20; H, 4.50%. Molar conductance, Λ_m (10^{-3} M, methanol): 50.0 $\Omega^{-1}cm^2mol^{-1}$. FT–IR (as KBr, ν/cm^{-1}): 1542/1390s $\nu_{as}/\nu_s(COO^-)$, 3450w (O–H), 940s (Zn–O–Zn).

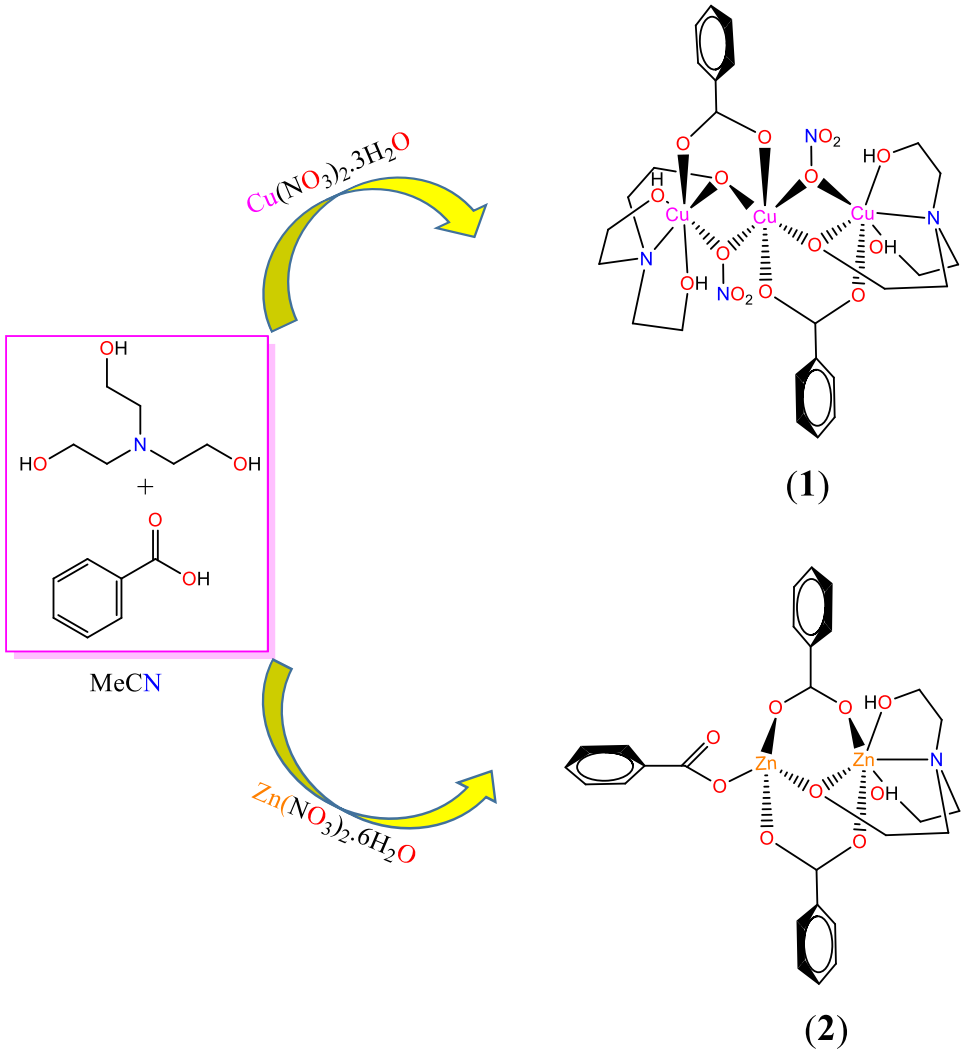

Scheme 3. Synthetic procedure for the complexes (**1** and **2**).

Results and discussion

The fascinating coordination chemistry of new trinuclear Cu(II)- and binuclear Zn(II)-triethanolamine complexes supported by aromatic carboxylate ancillary has been presented in **Scheme 3** and discussed here. The trinuclear **1** bears distorted octahedral geometry of around the Cu(II) metal ions while **2** has unusual geometry, as two zinc metal ions are present in different coordination environment. One of the Zn(II) adopts distorted tetrahedral and other Zn(II) has distorted octahedral geometry with same oxidation state i.e., +2. Both tetrahedral and octahedral Zn(II) ions are joined with the syn-syn ba^- and H_2tea^- bridges. General synthetic approach was employed in the formation of trinuclear **1** and dinuclear **2** complexes. The formation of **1** and **2** can be represented by equations (**i**) and (**ii**). The single crystal X-ray determination revealed that both the complexes consist of neutral trinuclear and neutral binuclear entities as $[Cu_3(H_2tea)_2(ba)_2(NO_3)_2]$ (**1**) and $[Zn_2(H_2tea)_2(ba)_3]\cdot H_2O$ (**2**). Molar conductivity measurements of the complexes reveal the non-electrolytic nature of **1** and **2** in CH_3CN solution, with molar conductivity values Λ_m 35 and 50 $\Omega^{-1}cm^2mol^{-1}$. The results agree with the non-ionic nature of the compounds in solution.

$$3Cu(NO_3)_2.3H_2O + 2H_3tea + 2Hba \xrightarrow[4Et_3N]{MeCN} [Cu_3(H_2tea)_2(ba)_2(NO_3)_2] + 4Et_3NH^+ + 3H_2O \quad (i)$$

$$2Zn(NO_3)_2.6H_2O + H_3tea + 3Hba \xrightarrow[4Et_3N]{MeCN} [Zn_2(H_2tea)(ba)_3(H_2O_2)] + 4Et_3NH^+ + 5H_2O \quad (ii)$$

FTIR Spectra

The FTIR spectra of newly synthesized complexes have been recorded in the region 4000−400 cm^{-1} (**Fig. 1**). The band at ~3400 cm^{-1} was assigned to OH(H_2O) stretching vibrations. Triethanolamine ion (H_2tea^-) molecules are investigated at three regions in both **1** and **2**: (a) medium band at 3400 cm^{-1} assignable to the stretching vibrations of OH groups; (b) at about 2944 cm^{-1} and 2904, due to the ν_{as}(C–H) and ν_s(C–H), respectively; and (c) three bands in the region of 1058 cm^{-1} are attributed to the ν(C–O) stretching vibrations [19]. The bands in the region 1607–1598 cm^1 are attributed to ν(C–C) of the aromatic moiety.

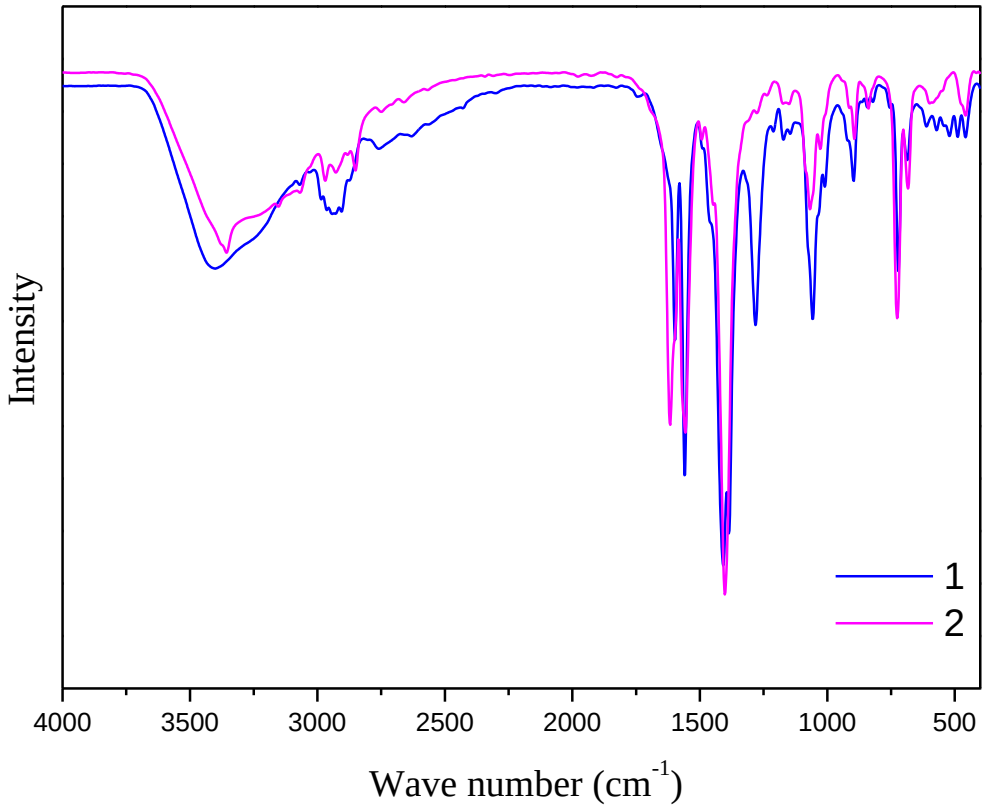

Fig. 1 FTIR spectra for the complexes (**1** and **2**).

The bands at 1572/1386 cm^{-1} in **1** and 1557/1398 cm^{-1} in **2** are characteristic of $\nu_{as}(COO)$ / $\nu_{s}(COO)$ vibrations of the carboxylic acid. In particular, taking into account that the carboxylates can coordinate to the metal ions in a bidentate or monodentate fashion (**Scheme 1**), on the basis of $\Delta\nu$ criterion [$\Delta\nu = \nu_{as}(COO) - \nu_{s}(COO)$], we can conclude that in **1** and **2**, one or both unsaturated carboxylates adopt bridging mono- or bidentate, coordination modes with Δ values observed at ~170 cm^{-1}, which is in the region close to that found in the precursor copper(II) acrylate a dinuclear $[Cu_2(CH_2{=}CHCOO)_4(H_2O)_2]$. The magnitudes of $\Delta\nu$ indicating that both the complexes are consist asymmetric bidentate mode (mode d) in addition to the anionic monodentate mode (mode a) in **2**, which is also confirmed from the X-ray crystallography of the complexes.

Absence of any sharp band at 1385 cm^{-1} confirmed that anion is not present in the **1** and **2**. It was further confirmed by the magnitude of molar conductance [19]. The presence of the

coordinated nitrates in **1** is ascertained by two bands; the asymmetric stretching vibration of nitrate $\nu_{as}(-ONO_2)$ at 1479 cm^{-1} and the symmetric stretching vibration, $\nu_{sym}(-ONO_2)$ at 1299 cm^{-1}. These vibrations do not occur in the ionic nitrates (NO_3^-) in lattice and the frequency difference $\Delta\nu(\nu_{as}-\nu_{sym})$ = 180 cm^{-1} is indicative of syn−syn bidentate coordination mode of the nitrate ions (**Scheme 4**), and is in line with already reported examples [20]. The band appearing at 945 cm^{-1} is characteristic of M–O–M bridging in both the complexes.

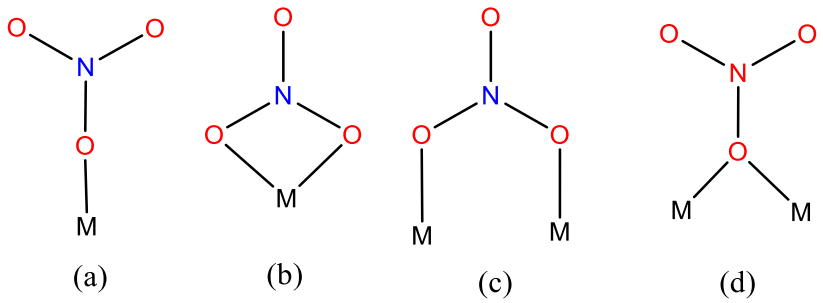

Scheme 4 Selected coordination modes of nitrate (NO_3^-) group.

The bands in 600–800 cm^{-1} region are associated with deformation modes of benzoate (ba^-) group. The medium to weak intensity bands at 873–950 cm^{-1} are attributed to the C–C vibrations. The strong to medium bands in the region 955–1253 cm^{-1} may be due to the C–O stretching vibrations of O–CH_2. The bands in the region 469–499 cm^{-1} and 575–570 cm^{-1} are ascribed to ν(M–N) and ν(M–O) vibrations, respectively.

Electronic and EPR Spectral Studies

The electronic spectra of **1** (d^9, trinuclear) and **2** (d^{10}, dinuclear) were recorded in 10^{-3} M methanol at various temperatures. Absorption spectra of the complexes exhibited (**Fig. 2**), well resolved absorption bands at 224, 240, 270 and 363 nm in **1** and 228, 242, 332 and 338 nm in **2**. The first three well resolved bands are assignable to intraligand transitions as n→π*, π→π* and CT in **1** and n→π*, π→π* transitions in **2**. The broad absorption bands below 400 nm are characteristic of the ligand-to-metal charge transfer (LMCT) (in **1**) and are consistent with the distorted octahedral geometry about the metal ions. Blue methanolic solution showed

a broad low intensity band at 660 nm **1** which can be assignable to d–d transitions band [21], while this type of band above 400 nm was absent in the Zn(II) **2**.

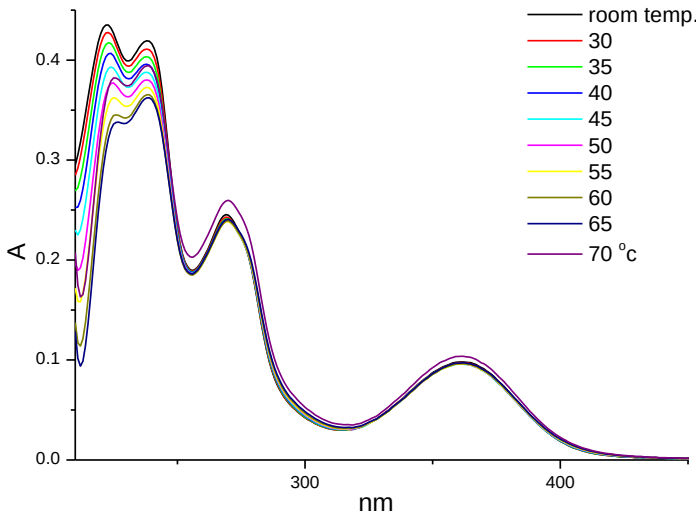

Fig. 2(a) Absorption spectra for **1**.

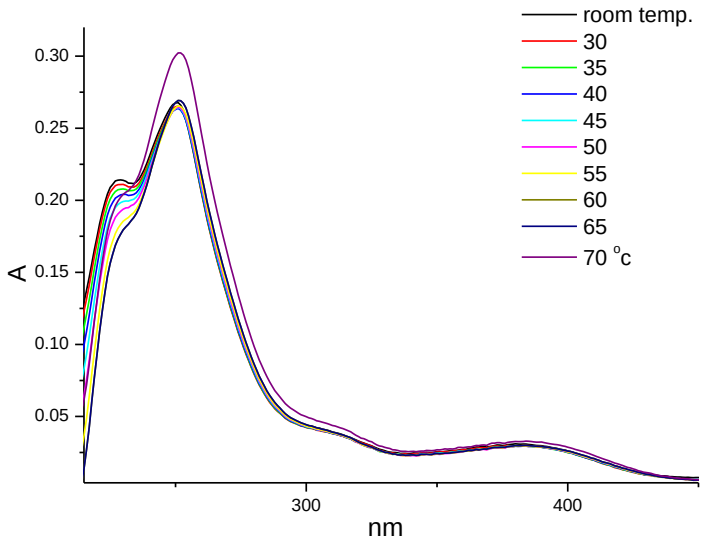

Fig. 2(b) Absorption spectra for **2**.

The EPR spectrum of **1** is consistent with the paramagnetic nature with the expected three lines at lower field. From the magnitude of g_1, g_2 and g_3, it is clear that $g_1 > (g_2 + g_3)/2$

which is characteristic of Cu(II) complex in $d_{x^2-y^2}$ ground state and elongation of the axial bonds [22]. The distorted octahedral geometry of **1** is consistent with the above data (**Fig. 3**).

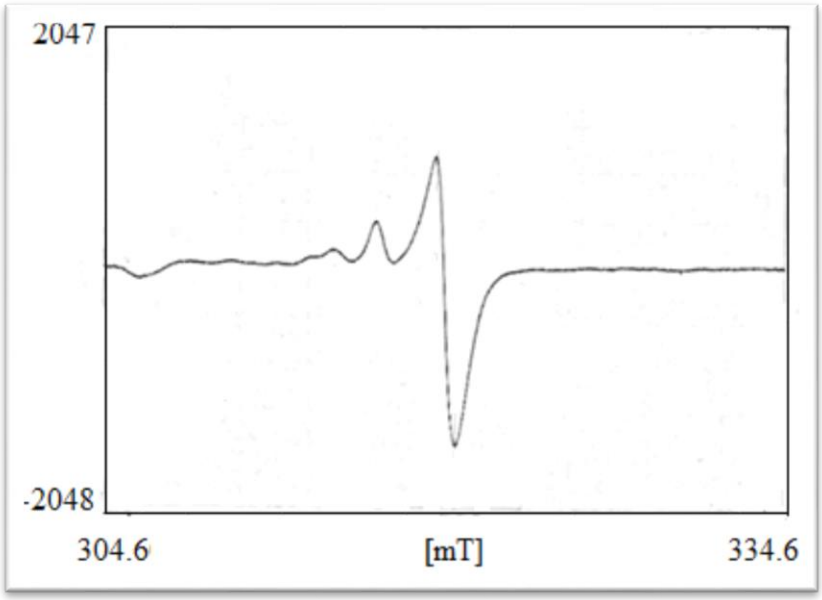

Fig. 3. EPR spectrum of **1**.

Crystal structure of 1

The single crystal X-ray determination results revealed that **1** consists of neutral trinuclear entity. Molecular structure of the complex is given as **Fig**. **4**. Selected bond distances and angles are listed in Table **1**. The trinuclear copper complex is monoclinic with space group P 2_1/c. In the trinuclear (Cu1–Cu2–Cu1) system, Cu2 ion is present in octahedral enviroment on the center of inversion with half a population so that a linear trinuclear copper entity is equivalently furnished. The central Cu2 ion is triply bridged to both of the terminal copper atoms (Cu1) through one alkoxide bridge of the single deprotonated triethanolamine (H_2tea^-) ion, one syn–syn oxide bridge from ($–ONO_2^-$), and a syn–syn carboxylato bridge provided from the deprotonated benzoic acid (ba^-). Both the central and terminal copper ions have same coordination (distorted octahedral) environments with CuO_6 and CuO_5N chromophores, respectively.

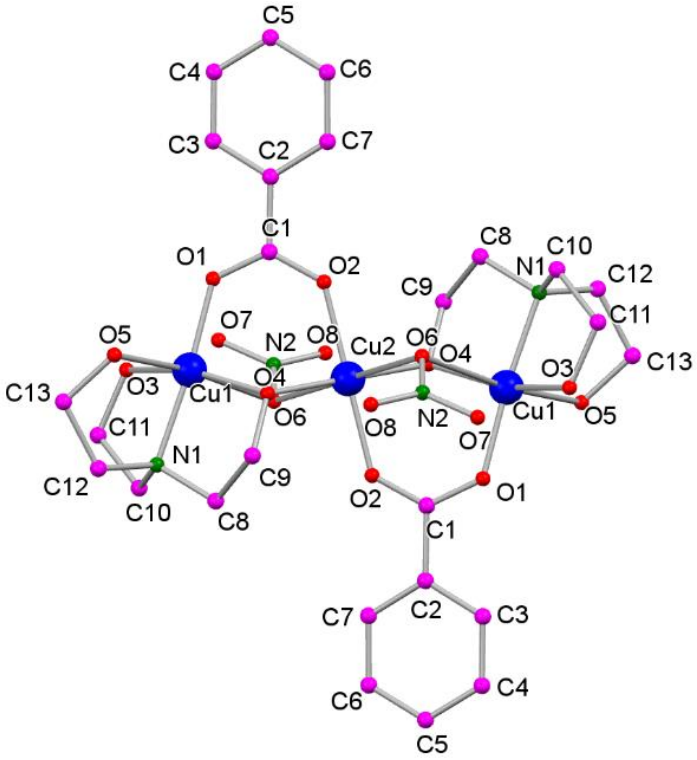

Fig. 4(a). Atomic labelling diagram for **1** (Hydrogen atoms are omitted for clarity).

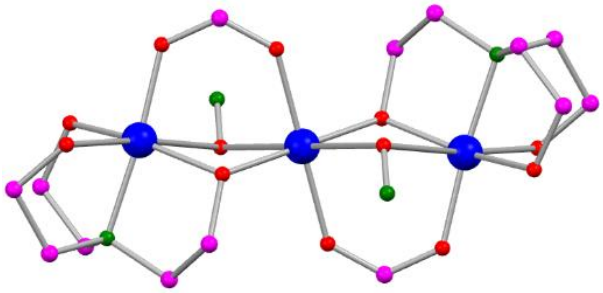

Fig. 4(b). Core diagram for **1** (Hydrogen atoms are omitted for clarity).

The equatorial plane of the central copper atom is formed by two oxygens provided from the carboxylate ligand (1.944(3) Å) and two oxygens from the oxide bridge of H_2tea^- (1.959(2) Å) while the apical positions are occupied by two oxygens from the oxide bridge of $–ONO_2^-$ (2.584(2) Å). The terminal copper ions contain the equatorial plane, from two oxygens provided by the carboxylate ligands (1.911(3) and 1.911(3) Å), the oxygen from the alkoxide bridge of $–ONO_2^-$ (2.750(3) Å), the oxygen from the oxide bridge of H_2tea^- (1.938 (3) and

1.959 Å) and the nitrogen atom of H_2tea^- (2.019(3) Å). The basal plane is composed the two free alkoxide oxygen atoms, defined as Cu–O(H), (Cu1– O2 = 1.912(2) and Cu1–O3 = 2.071(3) Å), while the apical positions are occupied by the nitrogen atom of H_2tea^- (Cu1–N = 2.008(3) Å) and the carboxylate oxygen (Cu1–O12 = 1.912(2) Å)(**Fig. 5**).

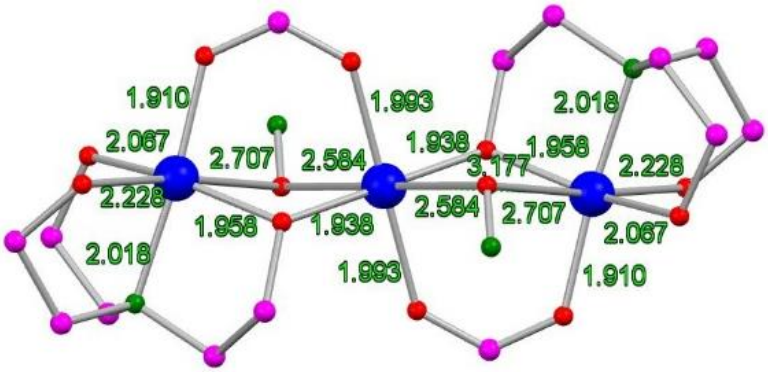

Fig. 5(a). Molecular core of **1** with bond lengths.

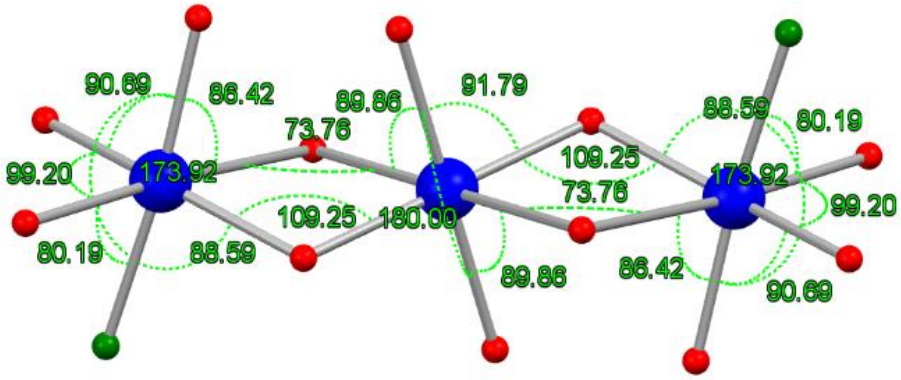

Fig. 5(b). Molecular core of **1** with bond angles.

The O−Cu−O angle around Cu2 center is 180°, indicating further an octahedral environment. The shortest length of Cu−O bond is assigned to deprotonated μ_2-alkoxo bridging intersections. The Cu···Cu distance within the trinuclear molecular unit is 3.177 Å.

Furthermore, the H-bonding and other non-covalent interactions are also present in the molecule, which contribute to the generation of supramolecular network. Two intramolecular and one intermolecular O−H···O hydrogen bonds are formed (**Table 3**). The intramolecular

interactions involve the alkoxo OH of the H_2tea^- ligand and the free nitrate oxygen (O−H···O = 1.883 Å) (**Fig. 6**).

Table 3. Distances and angles of non-covalent interaction in **1** and **2**.

D–H···A	d(D–H)	d(H···A)	d(D···A)	∟(DHA)
(**1**)				
O3–H3···O7	0.768	1.883	2.468	174.51
O5–H5···O4	0.729	2.160	2.806	147.31
C5–H5···O8	0.939	2.528	3.453	173.22
C–H···O	0.930	2.686	3.313	125
C12–H12···π	0.970	2.806	3.529	146.20
C12–H12···C7	0.970	2.810	3.657	131.85
C11–H8···C8	0.969	2.853	3.681	143.98
(**2**)				
O10–H10[a]···O2	0.765	2.066	2.810	164.24
O10–H10[b]···O8	0.801	2.003	2.766	158.89
O7–H7···O2	0.717	2.099	2.804	167.99
C10–H10…O8	0.930	2.436	3.321	159.22
C3–H3···O3	0.931	2.549	3.466	168.32
C–H··· π	0.930	2.890	3.652	140.12
C4–H4···C15	0.931	2.871	3.665	144.10
C7–H7···C19	0.930	2.803	3.650	151.91

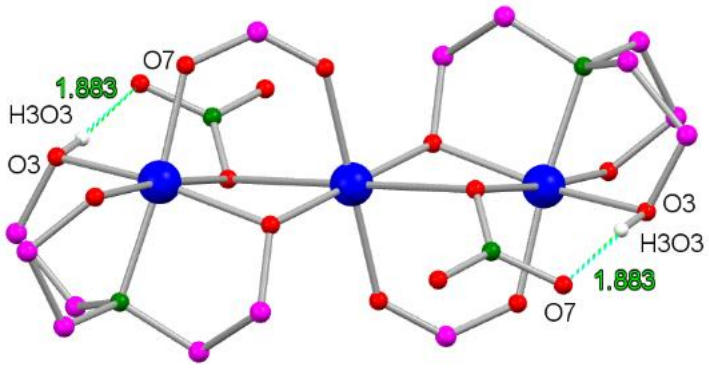

Fig. 6. Intramolecular O−H…O interactions in **1**.

The intermolecular O−H···O bonds are formed between two adjacent complex units, involving the alkoxo OH of the H_2tea^- ligand and the bridging oxygen (O−H···O = 2.806 Å) (**Fig. 7**).

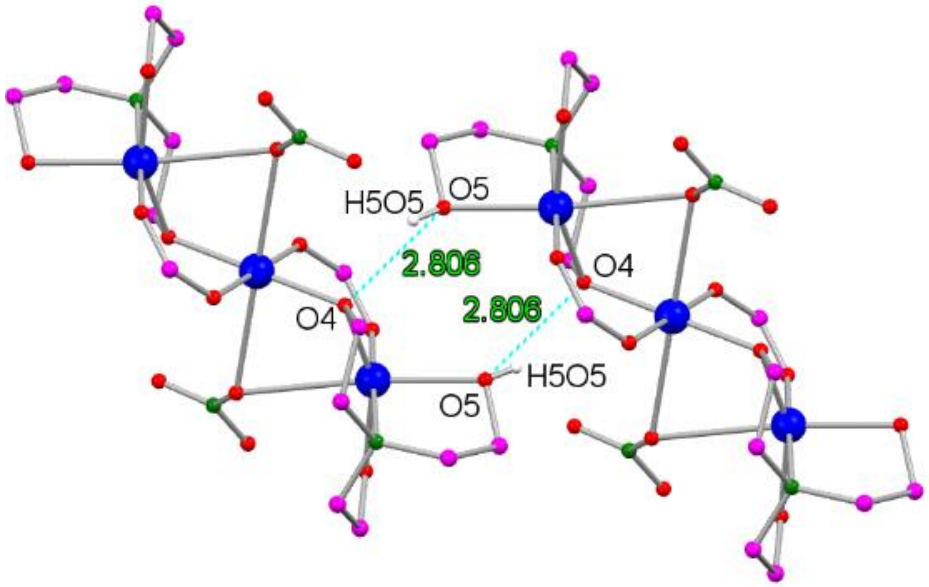

Fig. 7. Intermolecular O−H…O interactions in **1**.

A number of weak C−H···O interactions also contribute to the crystal robustness (**Table 3**) and (**Fig. 8**), while no π···π interactions between the aromatic rings were found. The C−H···π interactions are also formed within the range 2.806-2.810 Å (**Fig. 9**). The non-covalent

interactions result in a 1 D polymeric chain (**Fig. 10**). These supramolecular interactions have been verified further by Hirshfeld surface Analysis (vide infra) (**Fig. 11**).

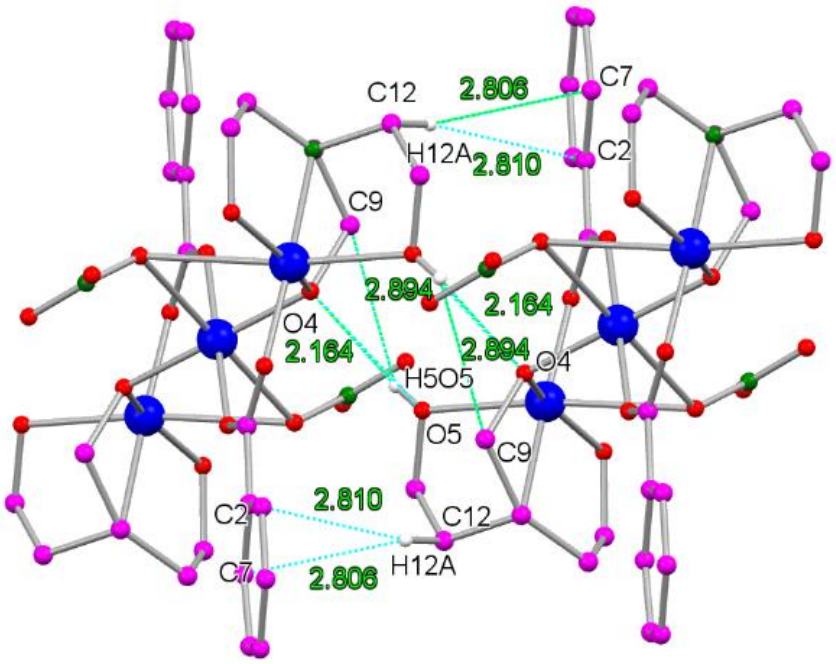

Fig. 8. C−H… π and O−H…O interactions in **1**.

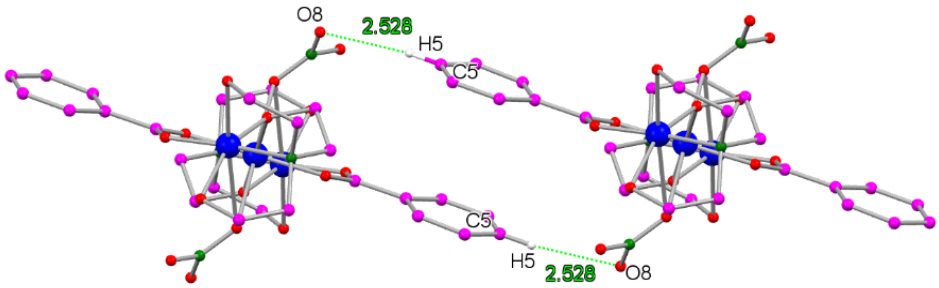

Fig. 9. C−H…C interactions in **1**.

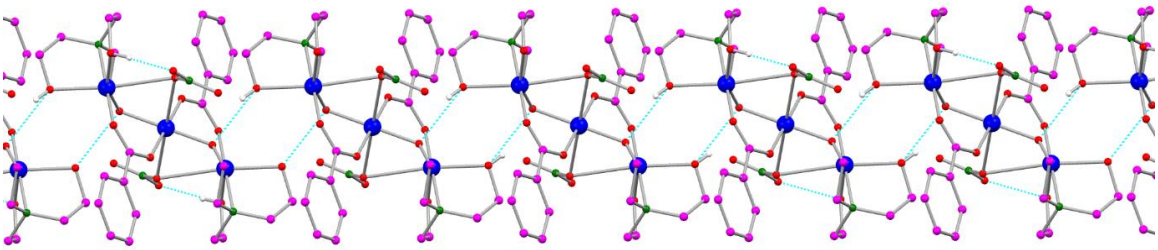

Fig. 10(a). 1 D polymer chain formed by non-covalent interactions in **1**.

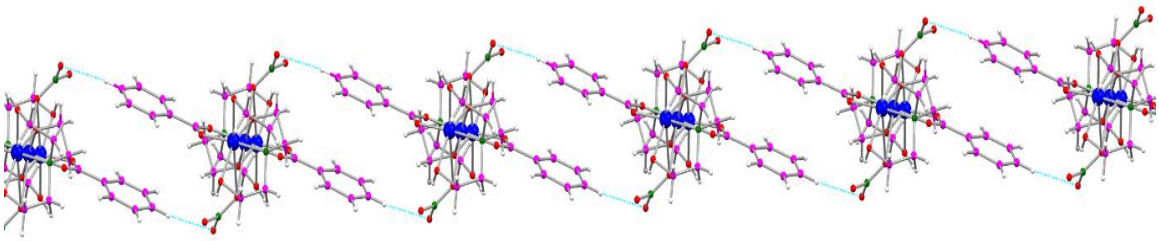

Fig. 10(b). 1 D polymer chain formed by non-covalent interactions in **1**.

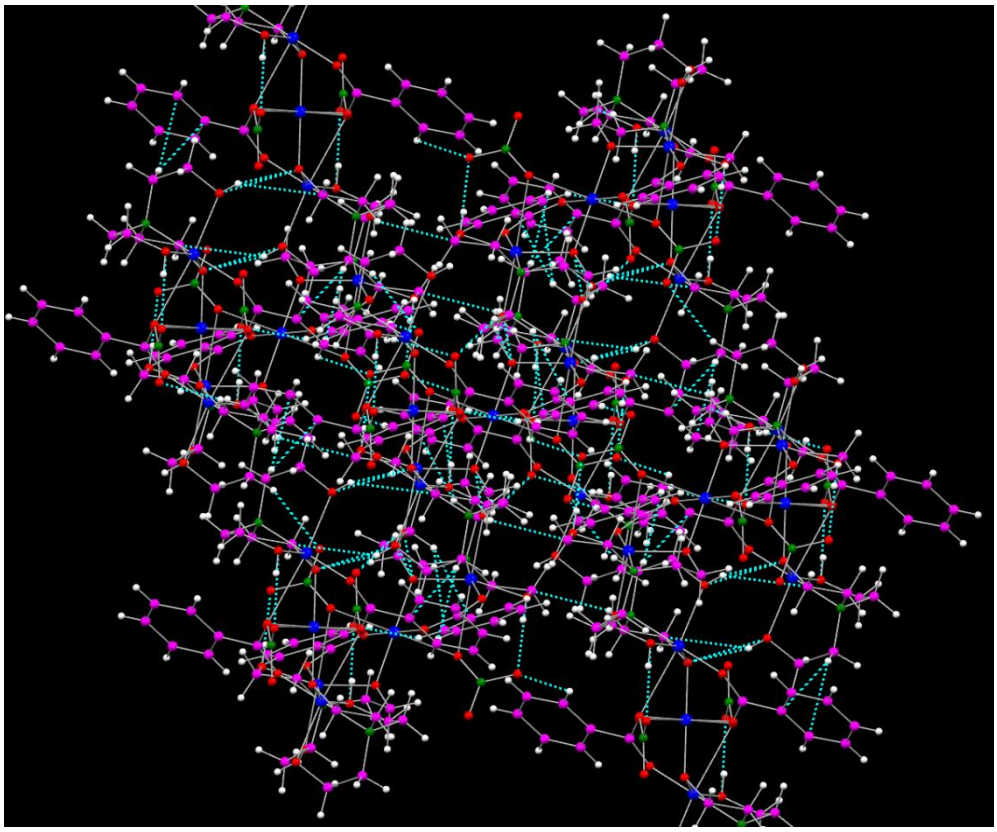

Fig. 11(a). 3 D supra molecular network of **1**.

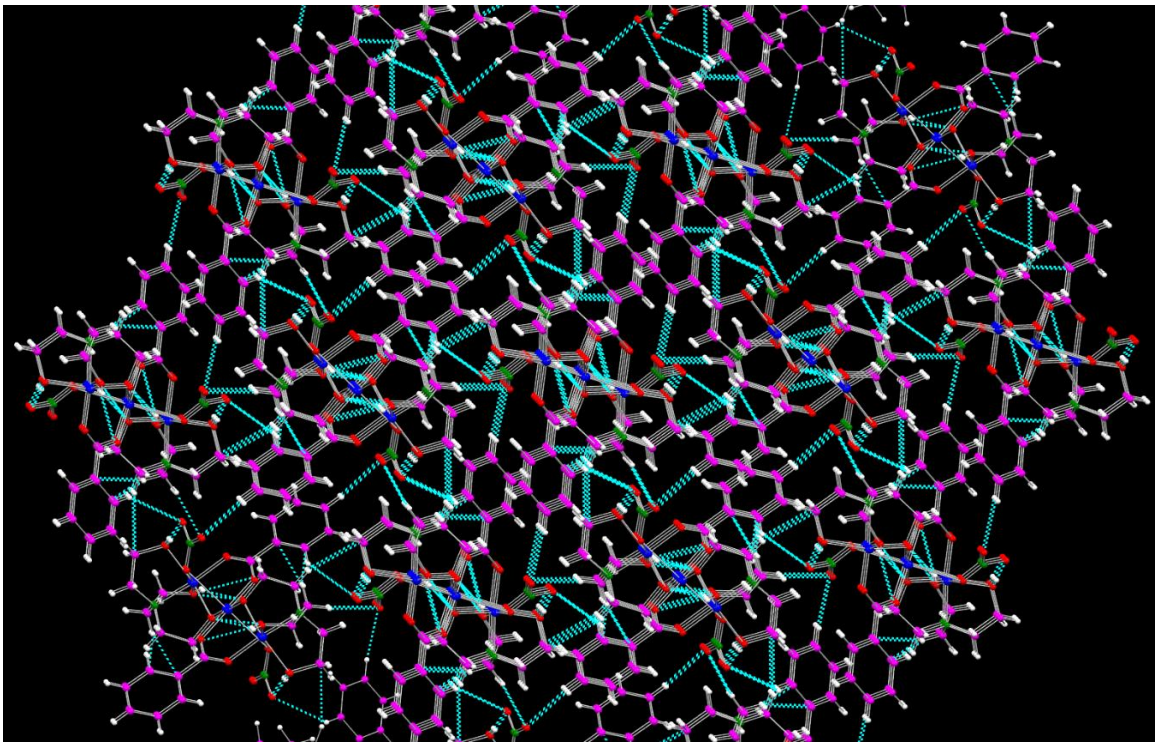

Fig. 11(b). 3 D supra molecular network of **1**.

Crystal structure of 2

The single crystal X-ray diffraction of **2** reveals that the binuclear zinc complex is monoclinic with same space group similar to that of **1**. It is interesting to note that two type of zinc atoms are present in the same molecule of the dinuclear unit with one of the zinc (Zn2) in tetrahedral and another zinc (Zn1) in octahedral environment. Such tetra and octahedral Zn(II) systems present in a complex, have not yet been reported so far and constitute unique bimetallic Zn system (**Fig. 12**).

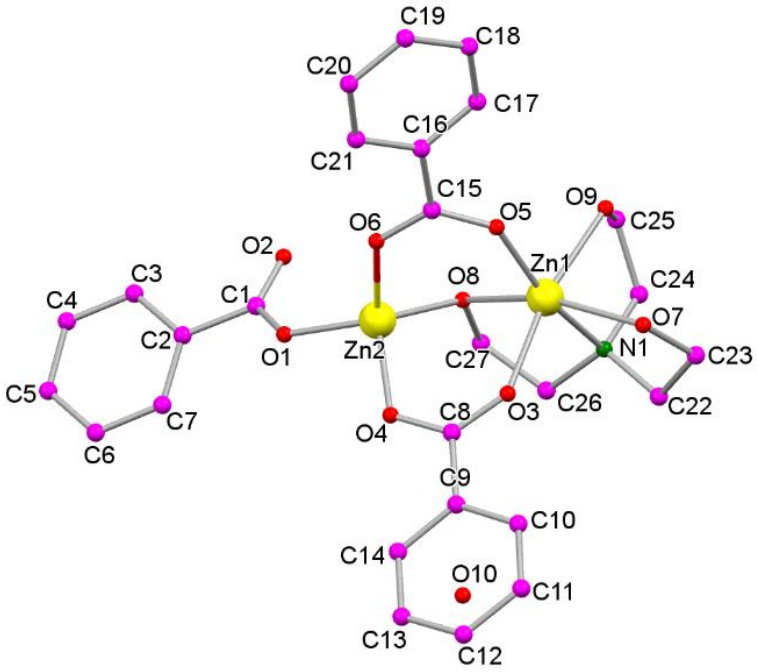

Fig. 12(a). Atomic labelling diagram for **2** (Hydrogen atoms and lattice molecule are omitted for clarity).

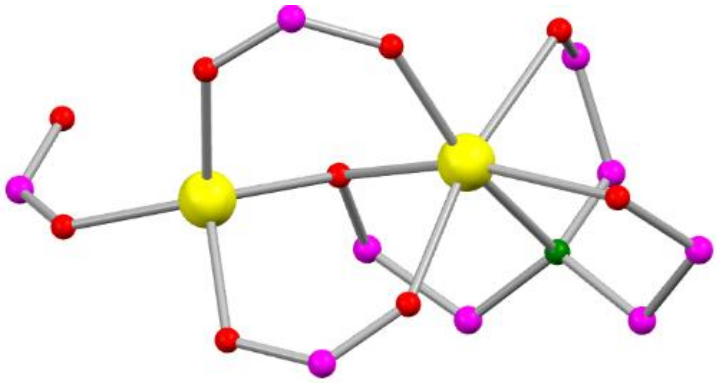

Fig. 12(b). Core diagram for **2** (Hydrogen atoms and lattice molecule are omitted for clarity).

The asymmetric unit of **2** consists of one single deprotonated H_2tea^-, two units of syn–syn carboxylate bridge provided from the deprotonated ba^-, one asymmetric monodentate coordination provided from ba^-, and one water molecule present in the lattice. The Zn1 center is distorted octahedral with ZnO_5N while Zn2 center has tetrahedral environment with ZnO4 chromophores. Three ba^- anions adopt two types of coordination modes (**Scheme 1**): (a) syn-syn bridging mode between two metal centers on (Zn1 and Zn2) and (b) monodentate mode

where it binds with Zn2 center only. The octahedral Zn1 binds with two alkoxide of the H_2tea^- arms with the distances Zn1−O7 = 2.173 and Zn1−O9 = 2.152 Å, two oxygen atoms provided from the carboxylate (ba^-) ligand attached to the metal ion with the distances Zn1−O3 =2.124 and Zn1−O5 = 1.988 Å, the oxygen from the oxide bridge of H_2tea^- (Zn1−O8 = 2.708 (3), Å) and the nitrogen atom of H_2tea^- (Zn1−N1 = 2.139 Å). The tetrahedral Zn2 binds with two oxygen atoms of corboxylato ligand (ba^-) with the metal oxygen bond distance Zn2−O4 = 1.960 and Zn2−O6 = 1.960 Å, one oxygen atom of corboxylate ligand in the asymmetric monodentate coordination manner (Zn2−O1= 1.926 Å) and one oxygen atom from the oxide bridge of H_2tea^- (Zn1−O8 = 2.708 (3), Å). The Zn···Zn distance within the dinuclear moeity is 3.142 Å (**Fig. 13**).

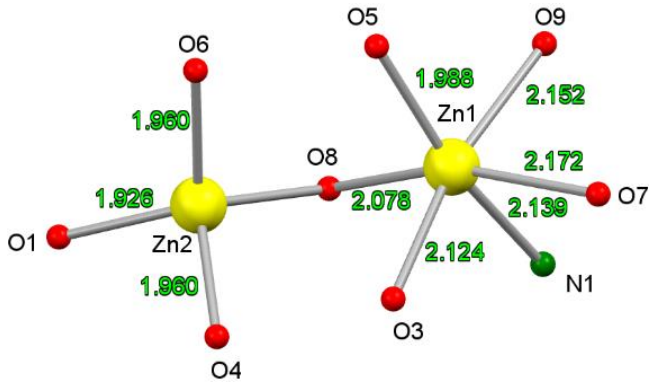

Fig. 13 (a): Molecular core of **2** with bond lengths.

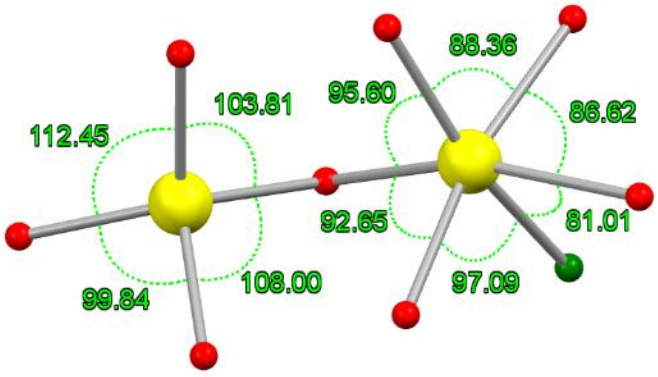

Fig. 13 (b): Molecular core of **2** with bond angles.

Due to the hydrogen bonding donor atoms present in the complex, structure shows intermolecular O−H···O hydrogen bonds (**Table 3**) formed between two adjacent moieties, the

intermolecular interactions involve the alkoxo (OH) group of the H_2tea^- ligand (first unit) and the oxygen atom of the asymmetric monodentade carboxylate ligand of the second unit of the complex with O−H···O distances to be 2.804 Å (**Fig. 14**). The other intermolecular O−H···O bonds are formed with the link of two adjacent units as shown in **Fig. 15**, i.e. between alkoxo (OH) group of the H_2tea^- ligand (first unit) and the water molecule (O−H···O = 2.640 Å). Two O−H···O bonds are also formed with the interaction of water molecule with the bridging carboxylate oxygen (O−H···O = 2.766 and 2.810 Å).

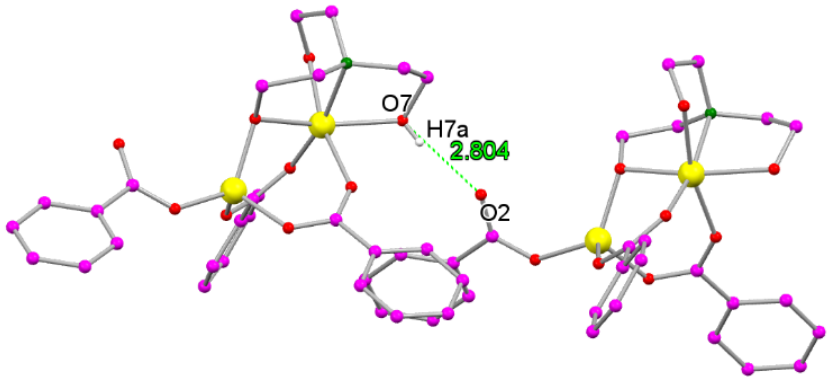

Fig. 14. Intramolecular O−H···O interactions in **2**.

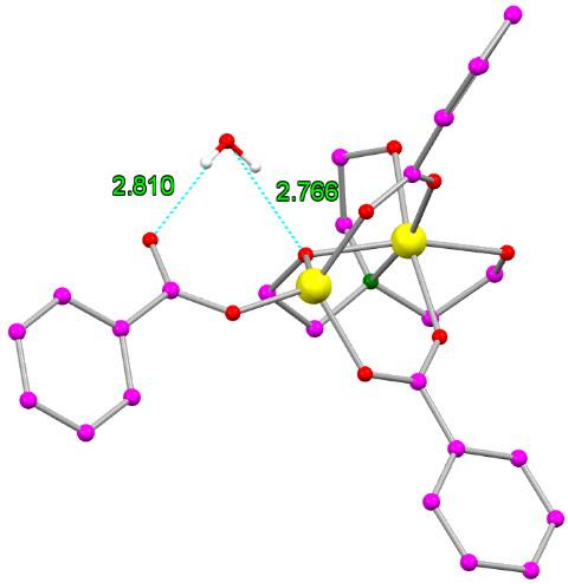

Fig. 15. Intermolecular O−H···O interactions in **2**.

Various weak interactions such as intramolecular C–H···O and intermolecular O–H···O, C–H···O, C–H···π contacts with the unusual new C–H···C contacts are observed in **2** to consolidated the crystal lattice. The presence of intermolecular C–H···C interactions add a new dimension to the crystallography, which may thus be considered to support the supramolecular network (**Figs. 16** and **17**).

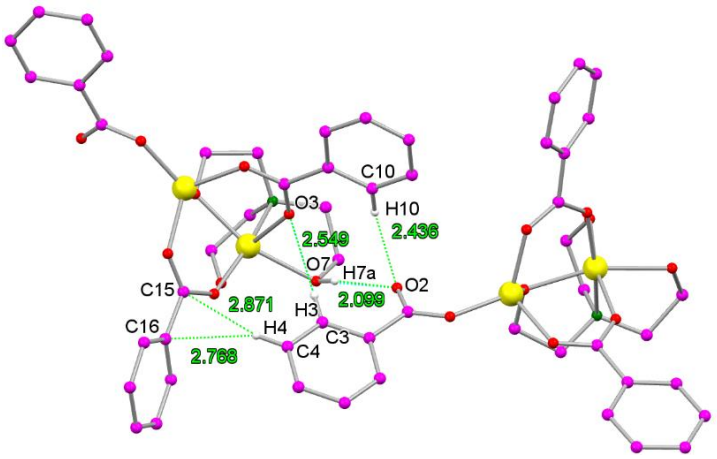

Fig. 16. C–H···C interactions in **2**.

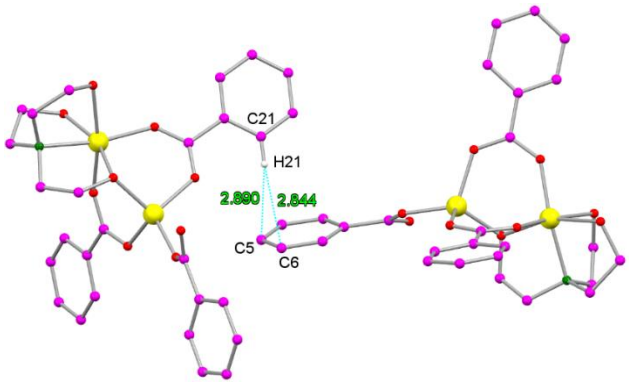

Fig. 17. C–H··· π interactions in **2**.

Theoretical calculations (vide infra) support this view. There are two kinds of C–H···C contacts between ba^{-} ligands of neighbouring units. Clearly, the C–H···C bridges are of bifurcated type since C–H moiety participating in this form of supramolecular interaction is connected to two benzoate ligand carbon atoms. One pair of C4(sp^3)–H4···C15(sp^3) (C···C = 2.871Å) and another pair of C7(sp^3)–H7···C19(sp^3) (C···C = 2.803Å) interactions exit in the molecular units of **2**.

It is noteworthy that reports on C–H···C contacts are rather scarce in published previous literature. Although such 'non-covalent interactions were identified early, studied theoretically, and established crystallographically, these interactions invoked in the description of supramolecular network of the crystal structures [23]. The crystallographic results just discussed suggest strongly that this form of non-covalent bonding constitutes an important feature of the 1D supramolecular structure of the present complexes (**Figs. 18** and **19**).

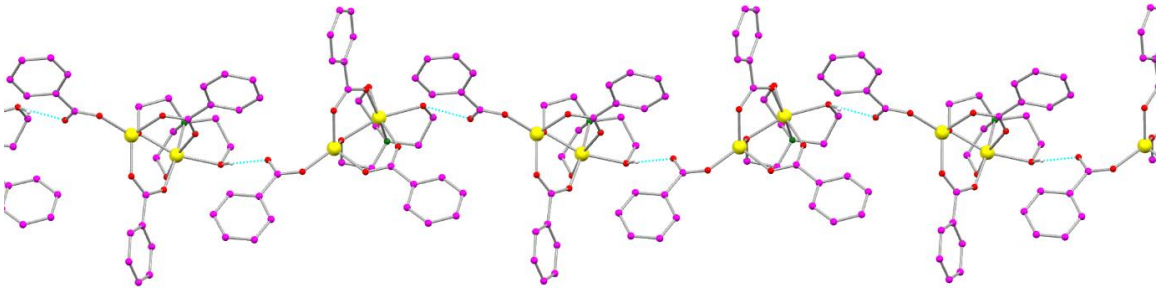

Fig. 18. 1 D polymer chain formed by non-covalent interactions in **2**.

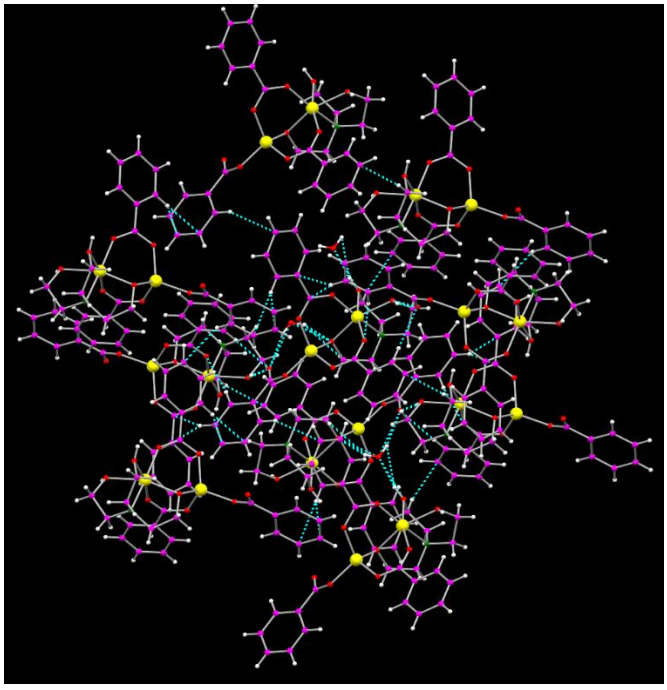

Fig. 19. 3 D supramolecular network of **2**.

Photoluminescence properties

Coordination complexes with d^9/d^{10} metal configurations and conjugated organic linkers have become attractive as luminescent materials because of their closed or nearly closed-shell ions. This led us to study fluorescence and solid-state photoluminescence properties of the two coordination complexes at room temperature (**Fig. 20**). **1** exhibits an emission maximum at 405 nm in solution and 410 nm in microcrystalline solid state upon excitation at 270 nm. However, **2** displays an emission maximum at 440 in solution and 490 nm in solid state upon excitation at 330 nm.

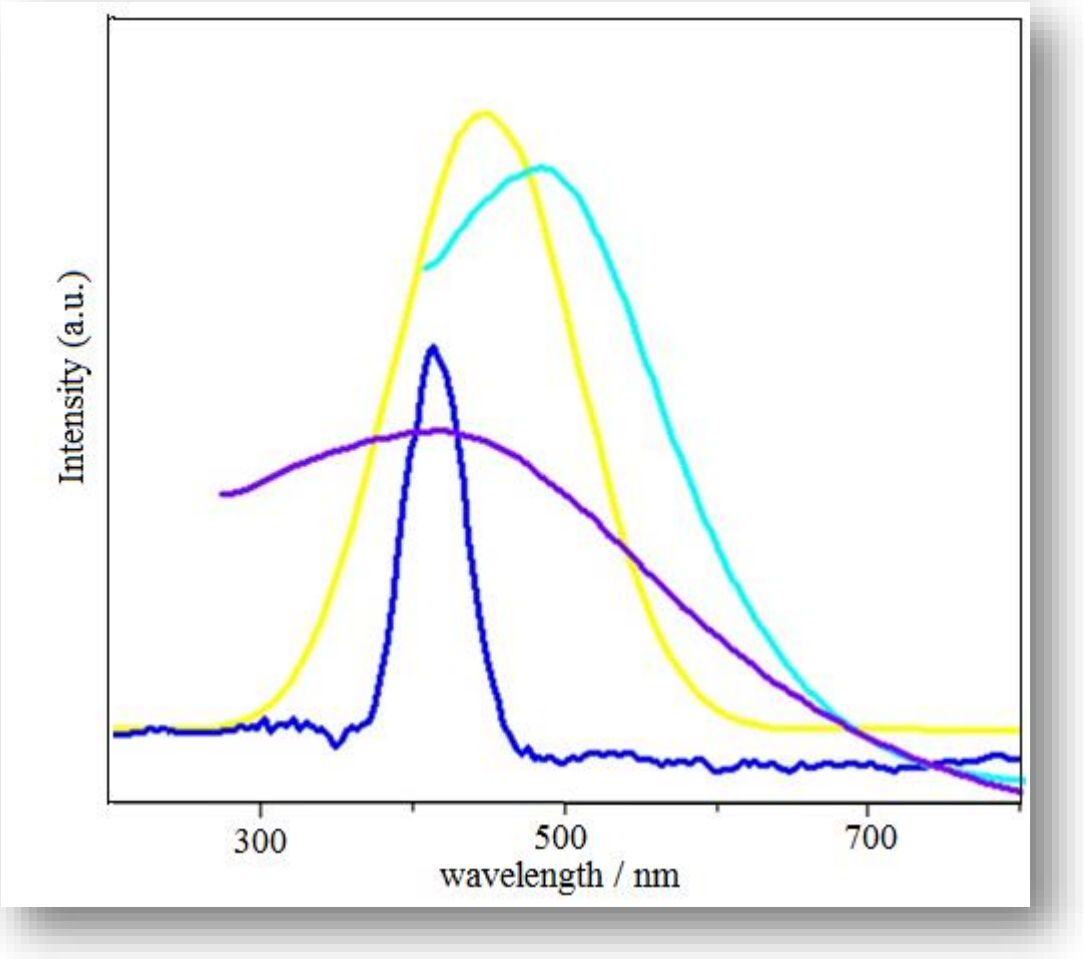

Fig. 20. Liquid and solid-state photoluminescence (PL) spectra for **1** and **2** recorded in 10^{-4} M MeOH. (Blue, yellow in liquid medium and violet, cyan in solid state).

From the photoluminescence spectra recorded in the solid state, it is clearly evident that in comparison to the solution phase, the emissions in the solid state are relatively red-shifted. This red shift in the solid-state emission spectra may be attributed to the presence of non-covalent interactions in the solid state, which are not significant in the solution state. The emission peaks at 410 nm for **1** and 490 nm for **2** may be attributed to the ligand-to-metal charge-transfer (LMCT) suggesting that the trinuclear (Cu_3) and dinuclear (Zn_2) complexes could potentially be used as luminescent materials [24].

Cyclic voltammetric studies

The electrochemical properties of the oxo and carboxylate bridged trinuclear Cu(II) and binuclear Zn(II) complexes have been studied at 27 °C. The cyclic voltammograms of **1** and **2** in the potential range +1.0 to –1.0 V with reference to Ag/AgCl electrode in the presence of tetrabutylammonium perchlorate were recorded to investigate the changes in oxidation states of metal ions in solution. Although the ligands involved are redox-inactive in the applied potential range, the electrochemical processes should arise from the metal-based redox reactions. The electrochemical redox properties of **1** and **2** are given as **Fig. 21** at 300 V/s scan rate. The voltammogram for the complexes shows a cathodic peak (E_P^c = 0.48 (**1**) or 0.58 V (**2**)) in the forward direction, which is coupled with anodic peak (E_P^a = 0.02 (**1**) or – 0.30 V (**2**)) in the reverse direction, forming a quasi-reversible redox couple at $E^0_{1/2}$ = 0.23 (**1**), – 0.44 V (**2**) (**Fig. 7**). The CV data indicated that there is a formation of quasi-reversible redox couple in solution state of both the complexes (**1** and **2**). An additional cathodic peak, E_P^c = – 0.18 V (**2**) is consistence with irreversible reaction in solution [25]. Moreover, the magnitude of $E^0_{1/2}$ < 1V is indicative of catalytic behavior of **1** and **2**.

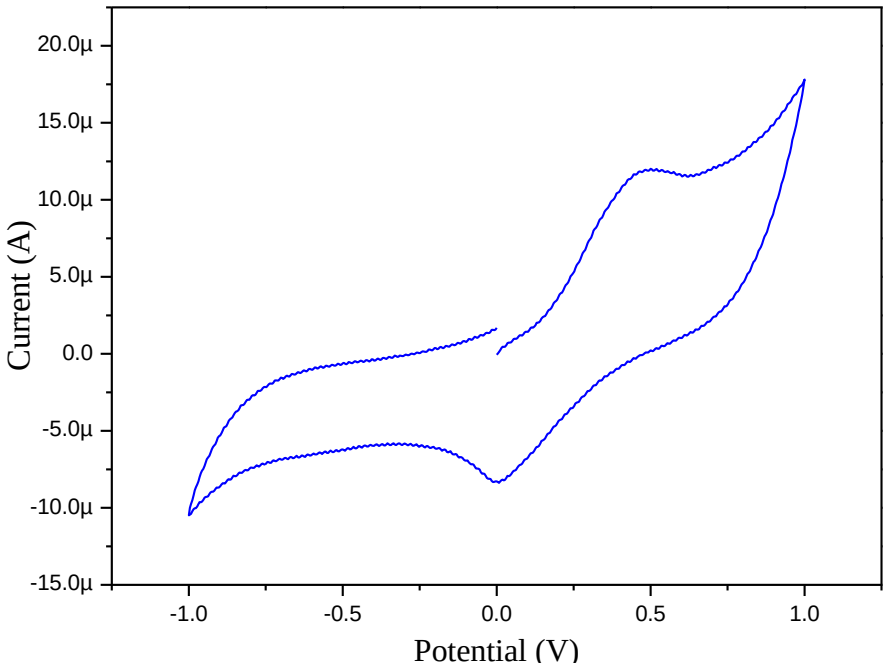

Fig. 21(a). Cyclic voltammogram for **1** recorded at 200 mV/s scan rate in MeOH solution.

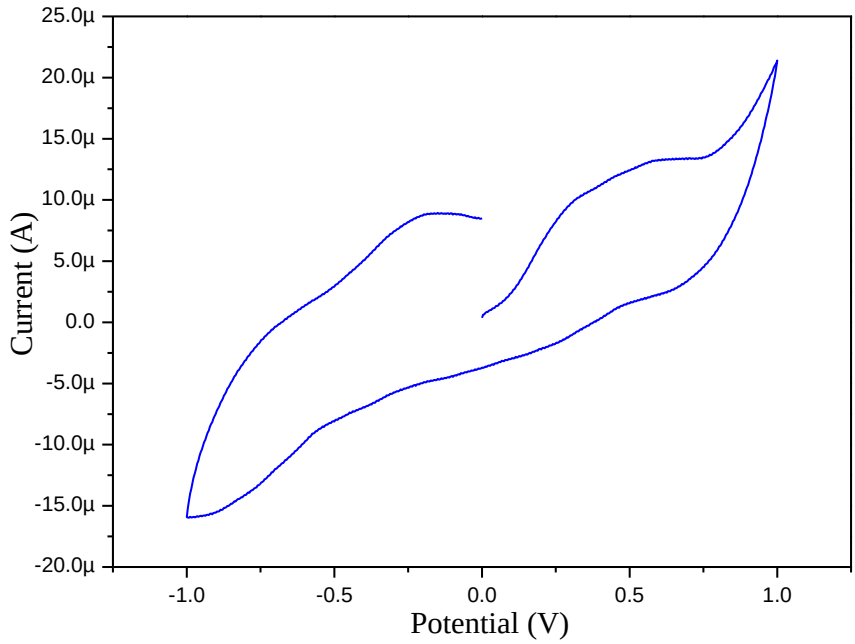

Fig. 21(b). Cyclic voltammogram for **2** recorded at 200 mV/s scan rate in MeOH solution.

Thermal Analysis (TGA)

To estimate the stability of the coordination compounds, thermogravimetric analyses (TGA) were carried out. The compounds were heated under an N_2 atmosphere in the temperature range 27-600 °C at a heating rate of 20 °C min^{-1}. Thermal stability of the complexes have provided enough information regarding stoichiometry. As shown in **Fig**. **22**, Analysis of trinuclear copper compound **1** indicates the stability of the compound up to 180 °C but binuclear zinc compound **2** shows the release of the water molecule up to 150 °C (found 3.2%, calculated 3.7%), present in the lattice. Further, as the temperature increases up to 300 °C, two nitrate, two H_2tea^- ligand eliminate (found 39%, calculated 38%) from the compound **1** but in the compound (**2**) one $Htae^-$, one ba^- ligands eliminate (found 45%, calculated 42%). Finally, decomposition of organic benzoic acid linkers above 350 °C taken place [26].

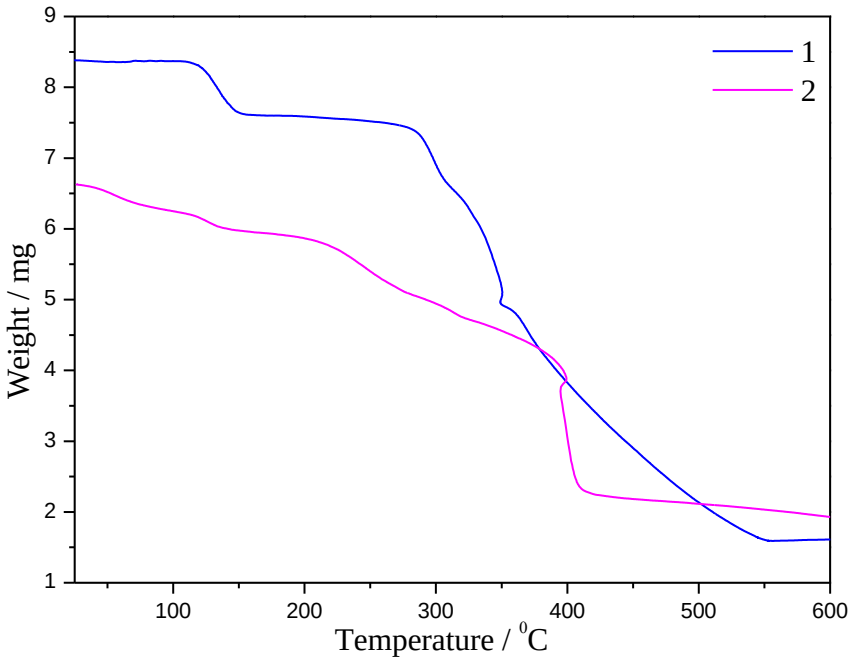

Fig. 22. Thermogravimetric analysis (TGA) for **1** and **2**.

Hirshfeld surface analysis

The Hirshfeld surfaces [27] of **1** and **2** are illustrated in Figs. **23**(a) and (b) revealing surfaces mapped over a d_{norm} range of −0.5 to 1.5 Å. The surfaces are transparently shown to visualize the moieties around which it was calculated. The deep red depressions [28] visible on the d_{norm} surfaces are indicative of hydrogen bonding contacts. The dominant interactions viz. C–H···π, C–H···H, C–O···C, N–O···N and N–O···Cu for **1** and C–H···π, C–H···H, C–O···H for **2** are shown in the Hirshfeld surface plots as the red-shaded area in **Figs. 24**(a) and (b).

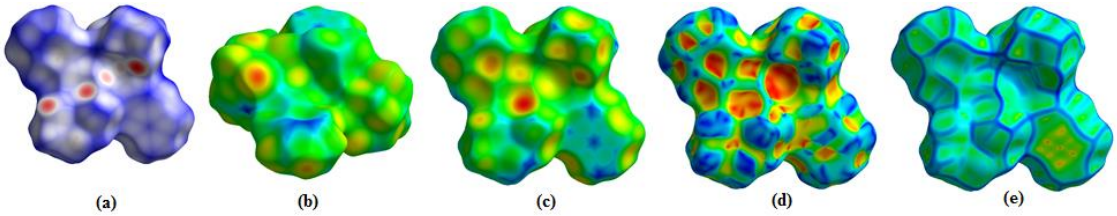

Fig. 23(a). Hirshfeld surface of **1** mapped with d_{norm} (a) d_i (b) d_e (c) shape index (d) and curvedness (e).

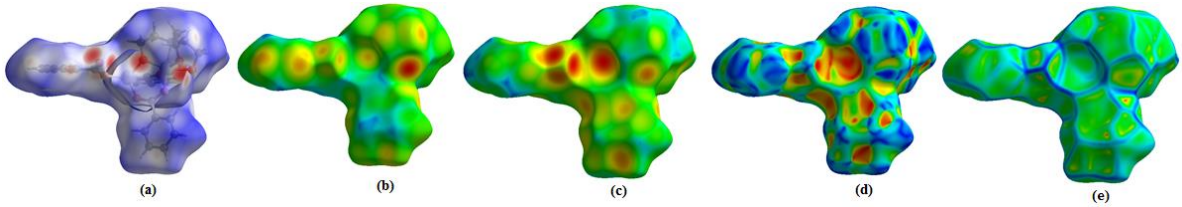

Fig. 23(b). Hirshfeld surface of **2** mapped with d_{norm} (a) d_i (b) d_e (c) shape index (d) and curvedness (e).

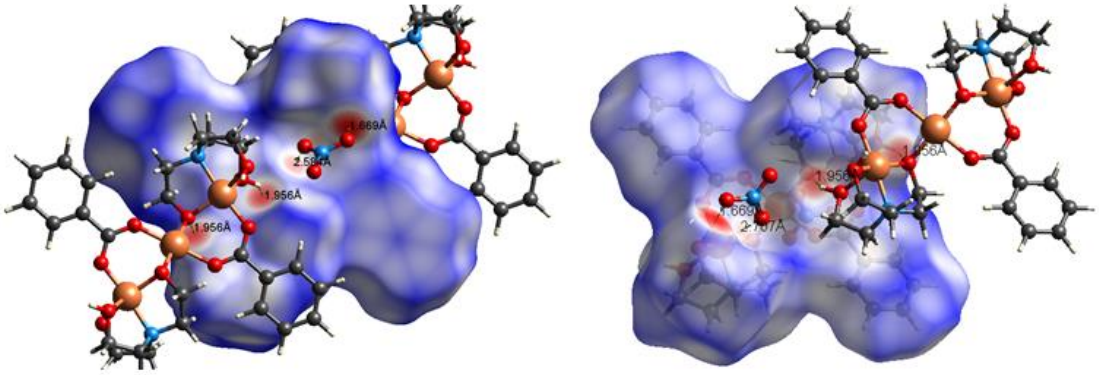

Fig. 24(a). Intermolecular N–O···H and N–O···Cu Interactions in **1** through red spots shown at different orientations by Hirshfeld surface.

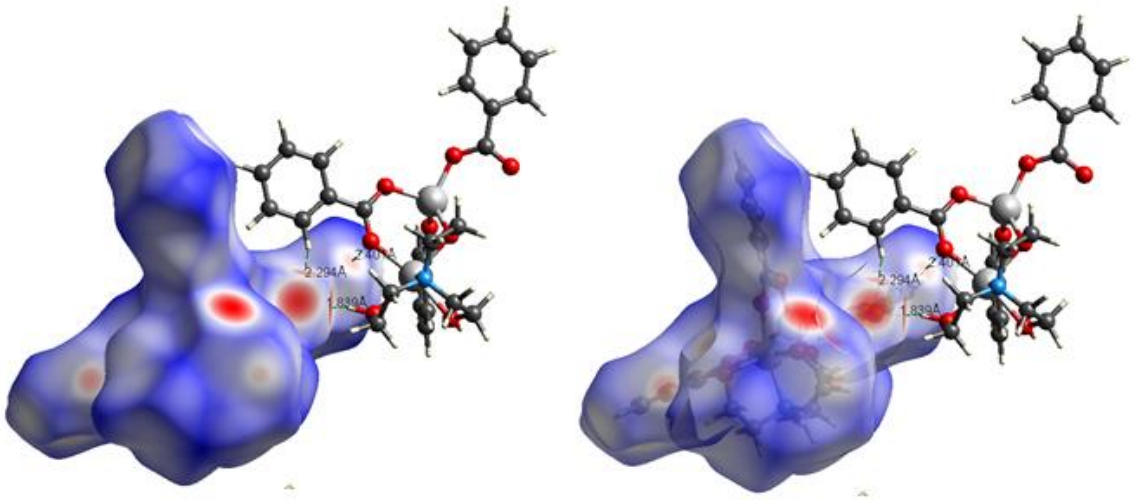

Fig. 24(b). Intermolecular C–O···H interactions in **2** through red spots shown at different orientations by Hirshfeld surface.

The 2D-fingerprint plots provide quantitative information about the decomposition of the Hirshfeld surfaces into contributions from the various intermolecular interactions present in the crystal structures [29]. The fingerprint plots are presented in **Figs. 25**(a) and (b).

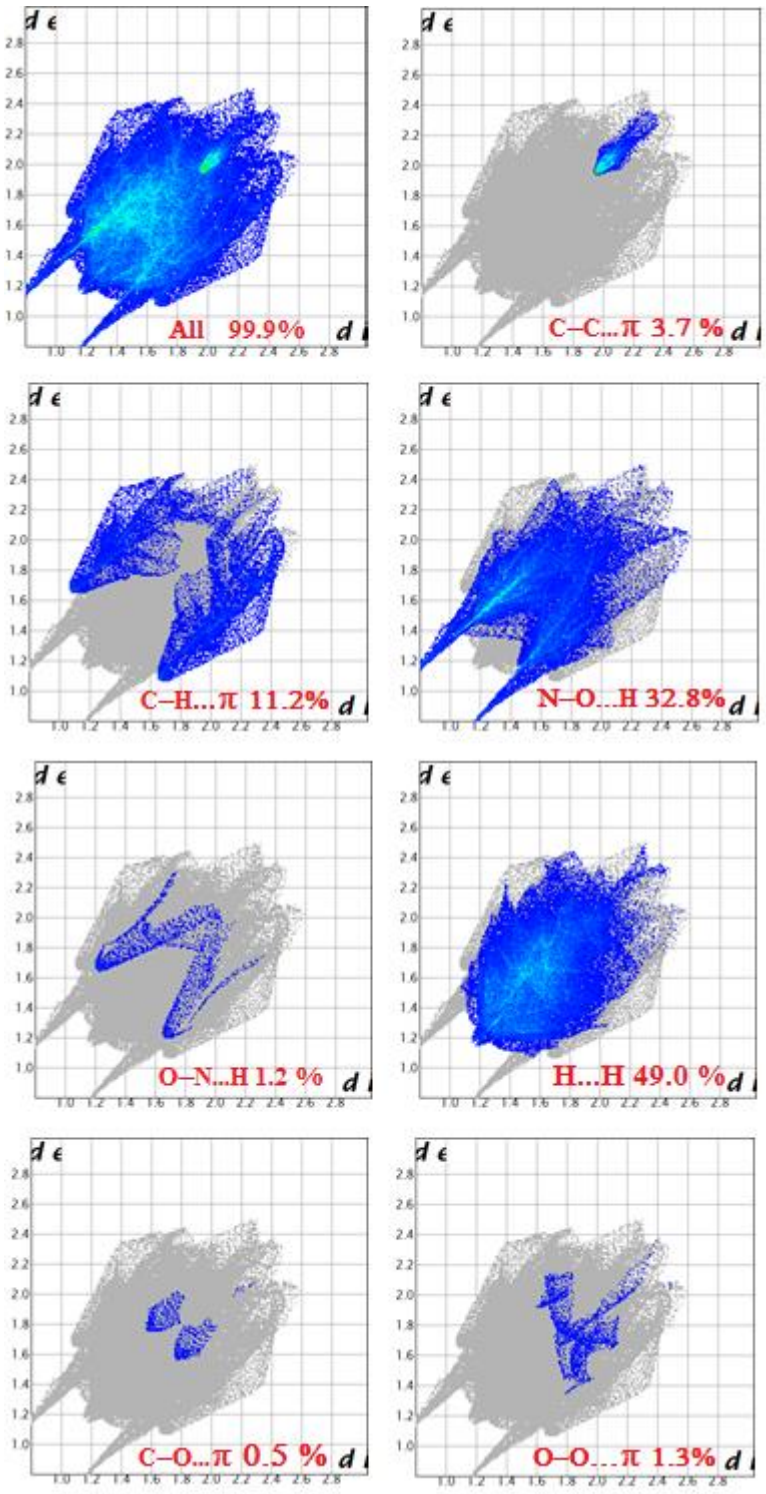

Fig. 25(a). 2D-fingerprint plots of **1** showing different interactions**.**

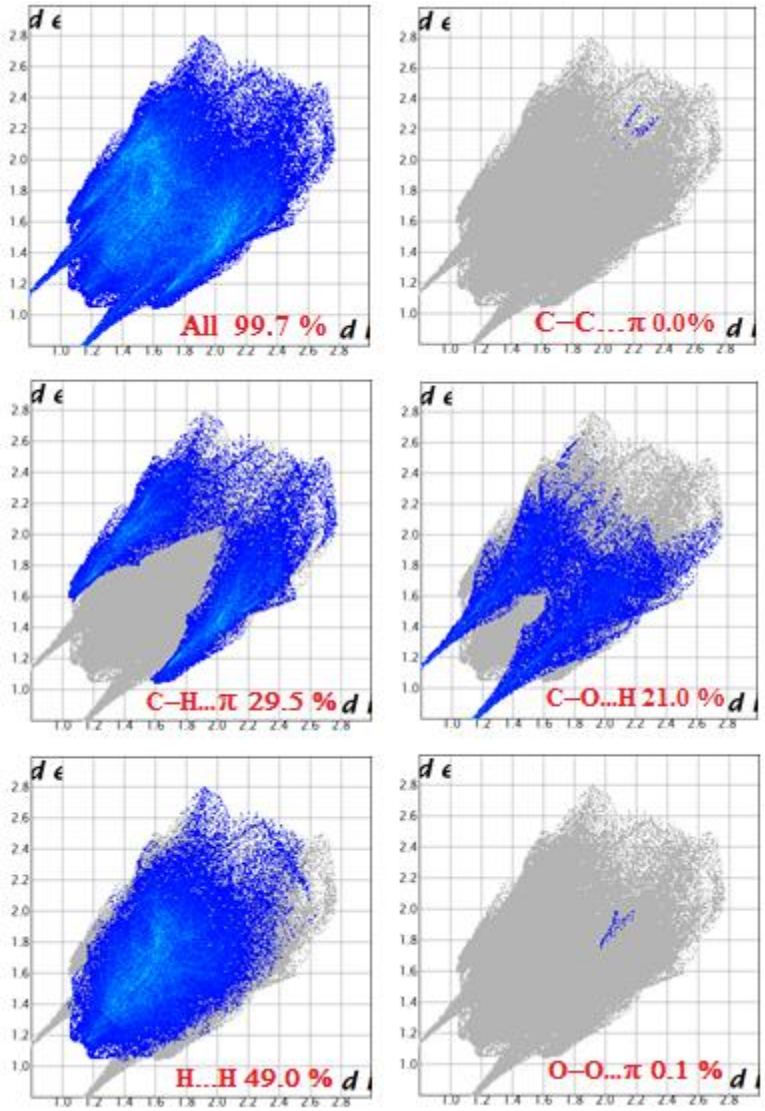

Fig. 25(b). 2D-fingerprint plots of **2** showing different interactions.

The intermolecular N–O···H interactions in **1** appear as two distinct spikes of almost equal length in the 2D fingerprint plots in the region 2.40 Å < (d_e + d_i) < 2.85 Å shown as a light sky-blue pattern whereas the same pattern appears for C–O···H in **2** in the region 2.36 Å < (d_e + d_i) < 3.40 Å. Complementary regions are visible in the fingerprint plots where one molecule acts as a donor (d_e > d_i) and the other as an acceptor (d_e < d_i). The fingerprint plots

can be used to highlight a particular atom-pair close contacts. This enables the separation of contributions from different interaction types, which overlap in the full fingerprint.

The electrostatic potential (ESP) for the complexes has also been mapped on the Hirshfeld surface displaying the presence of a positive ESP on the H atom (σ-hole) of H_2tea^- of magnitude +0.164 au and +0.185 au, respectively, for **1** and **2 (Figs. 26** and **27)**.

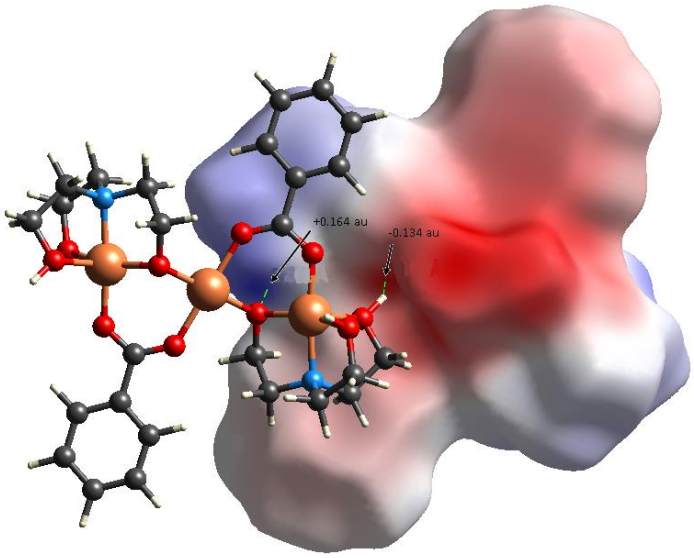

Fig. 26(a). Hirshfeld surface mapped with electrostatic potential (ESP) for **1**, showing the σ-hole on the non-protonated H atom of H_2tea^- with potential values at two different interacting sites for O···H contacts.

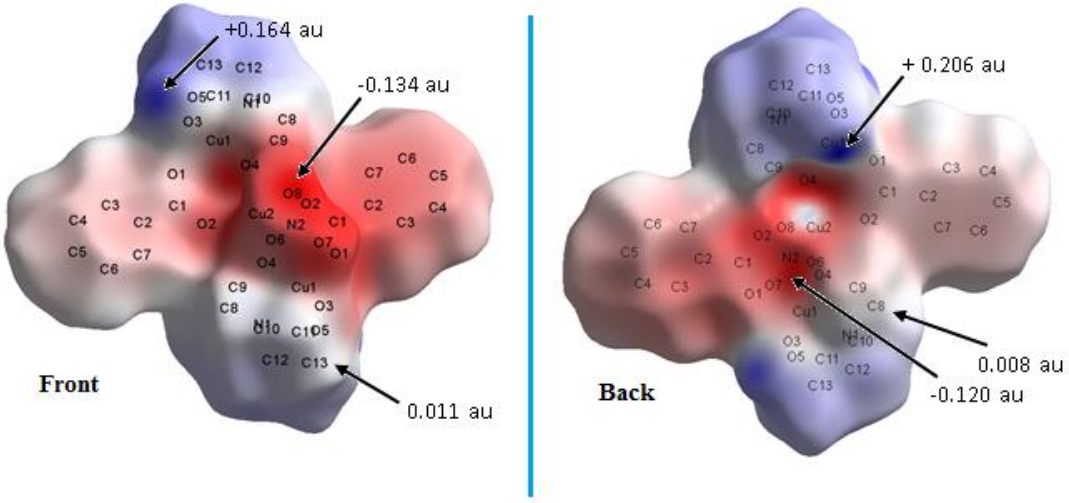

Fig. 26(b). Front and rear views of the electrostatic potential (ESP) mapped over the Hirshfeld surface for **1** over the range −0.139 au (red) through 0.000 (white) to 0.225 au (blue).

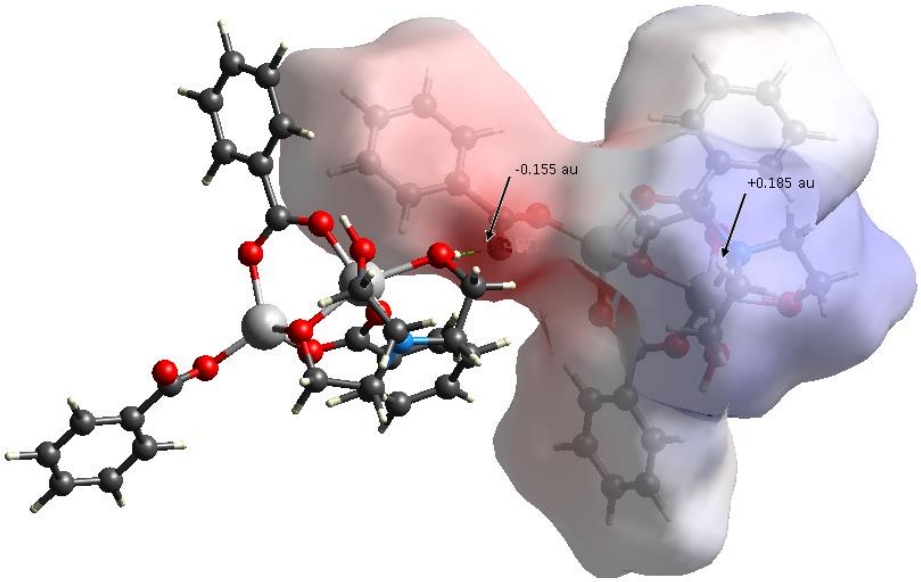

Fig. 27(a). Hirshfeld surface mapped with electrostatic potential (ESP) for **2**, showing the σ-hole on the non-protonated H atom of H_2tea^- with potential values at two different interacting sites for O···H contacts.

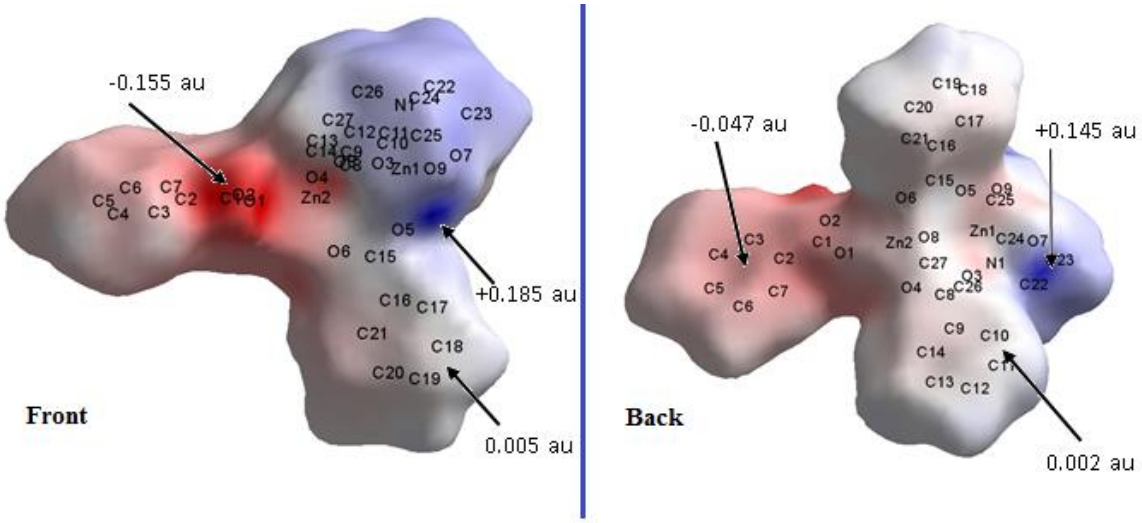

Fig. 27(b). Front and rear views of the electrostatic potential (ESP) mapped over the Hirshfeld surface for **1** over the range −0.161 au (red) through 0.000 (white) to 0.208 au (blue).

This electropositive region on the H atom interacts with an electronegative region over the O atom (−0.134 au for **1** and −0.120 au for **2**), resulting in the formation of the short dimeric O···H contact in the crystal packing. Its contribution to the Hirshfeld surface are 32.8 % **1** and

21.0 % **2** (**Fig. 25**). A pair of spikes for the O···H contacts were observed on the decomposed 2D fingerprint plots.

The deformation density calculations for **1** and **2** are also performed (**Fig. 28**) revealing, for **1**, the presence of a charge depletion (CD) region at the non-protonated H atom of H_2tea^-, which is directed towards the charge concentration (CC) region over bridged O atom of H_2tea^-, facilitating formation of the O···H contacts in the crystal. For **2**, the presence of a charge depletion (CD) region at the non-protonated H atom of H_2tea^- is also directed towards the charge concentration (CC) region over non-bridged O atom of benzoic acid, facilitating the formation of the O···H contacts in **2**.

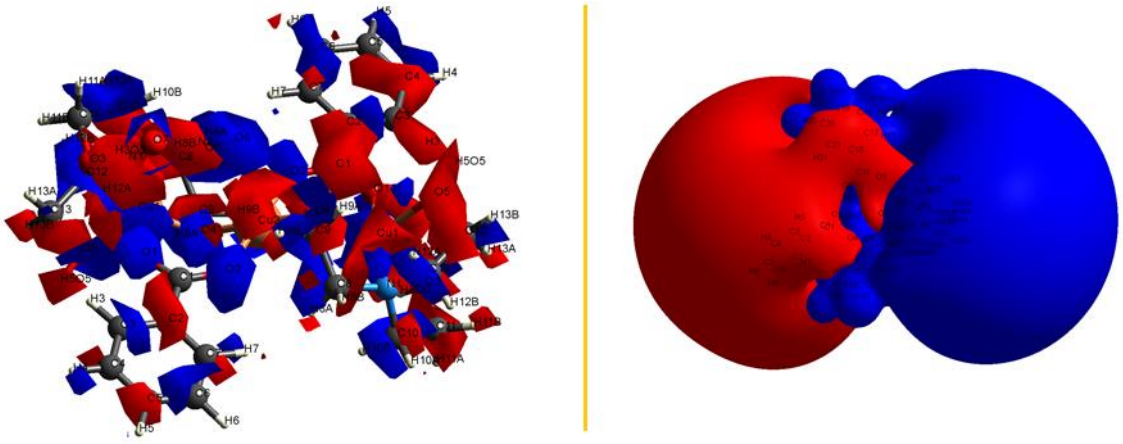

Fig. 28. 3D-deformation density map for **1** (left) and **2** (right) showing the presence of CD regions (in red) and CC regions (in blue), mapped using Crystal Explorer 3.0. The iso surfaces are drawn at 0.008 eau^{-3}.

Magnetic studies

There are a few examples of copper carboxylate bridged complexes where antiferromagnetic interaction leads to almost diamagnetic behaviour up to room temperature. The carboxylate linkers have been widely used to build magnetic units with transition-metal ions. The carboxylate group of benzoic acid can adopt syn−syn, syn−anti, and anti−anti coordination modes, and corresponding compounds often show ferro - or antiferromagnetic behaviors [**30**]. The magnetic susceptibility of compound **1** and **2** have been measured at the room temperature (300 K). Magnetic susceptibility is measured using very sensitive instrument

known as a magnetic susceptibility balance. The balance contains a pair of magnets mounted at opposite ends of a beam, initially in equilibrium, when sample is introduced into the balance, a disruption of the magnetic field results. A current through a coil located between the poles of a second pair of magnets returns the beam to equilibrium. The current through the coil is measured and transformed into a numerical reading. Diamagnetic materials are weakly repelled by an external magnetic field, resulting in a negative reading. Paramagnetic materials are attracted to an external magnetic field and give a positive reading. The magnetic moment of the complexes was calculated using by the formula as follows:

$$\chi_{g=} \, LC_{bal}(R-Ro)/10^{9}(m)$$

L = height of sample in tube in units of centimeters

C_{bal} = balance calibration constant = 1.0

R = reading for tube plus sample

R_o = reading for the empty tube

m = mass of the sample in units of grams

The molar magnetic susceptibility is then calculated from the gram magnetic susceptibility using the following equation:

$$\chi_m = \chi_g \times (\text{molar mass})$$

$\chi_A = \chi_m$ – diamagnetic correction

The magnetic susceptibility for a particular substance is not particularly useful in itself. However, the effective magnetic moment for a particular substance can be calculated from the gram magnetic susceptibility using the following equation.

$$\mu_{eff} = 2.283\sqrt{\chi_A . T}\; B.M.$$

{χ_g magnetic susceptibility erg.G^{-2}.gm^{-1}, χ_m molar susceptibility erg.G^{-2}.mol^{-1}, and μ_{eff} effective magnetic moment B. M.}.

Magnetic data indicates that μ_{eff} for complexes (3.9 (**1**) and 0.0 B.M. (**2**)) are suggestive of highly paramagnetic behavior of **1** and diamagnetic nature of **2** [31].

Catalytic properties

Alkane functionalization reactions have been tested using **1** and **2** as catalysts for the mild hydrocarboxylations of alkanes (C_n) into carboxylic acids (C_{n+1}) [**18**] the promoting behaviours of the **1** and **2** using various C_2–C_7 linear and C_5–C_7 cyclic alkanes as substrates are examined by reaction with carbon monoxide (CO), water (H_2O) and potassium peroxodisulfate ($K_2S_2O_8$) in a neutral H_2O–MeCN medium at low temperature (60 °C) (**Scheme 5**).

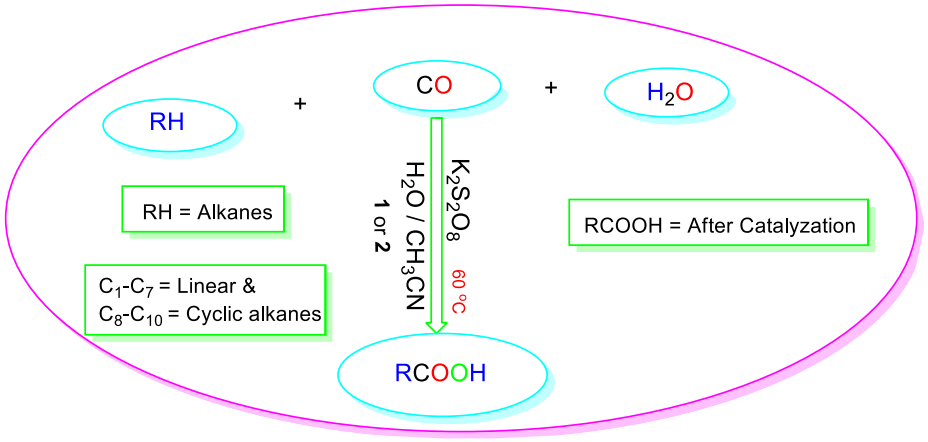

Scheme 5. Hydrocarboxylation of alkanes to carboxylic acids catalyzed by **1** and **2**.

Both the **1** and **2** exhibited similar catalytic behaviours except the yield of the product. The complex **1** is proven tobe more efficient than **2** as can be seen from data given in **Table 4**. For alkanes bearing a single type of carbon atom (ethane and all cycloalkanes), the formation of only one carboxylic acid product is detected as shown in **Table 4 (**entries **1-8)**, whereas linear C_3–C_8 alkanes containing secondary and primary carbon atoms generate two to four isomeric acid products (entries 2–6). Among them, the branched acids derived from the carboxylations at different secondary C atoms always constitute the major products**.** For the linear C_5–C_7 alkanes, a mixture of three or four isomeric products is formed.

Although the hydrocarboxylations can proceed to some extent in the absence of **1** and **2** boosters [18], the yields of the reactions promoted by **1** and **2** are typically three to four times higher than those of the metal-free systems under similar reaction conditions. Hence, in the

systems promoted by **1** and **2** (**Table 4**), maximum yields (based on alkane) of carboxylic acids in the 47–24% range are achieved in the hydrocarboxylations of C_3H_8 (46.2%), C_5H_{10} (42.4%), C_6H_{12} (40%), n-C_6H_{14} (35%), n-C_4H_{10} (28.6%), n-C_2H_6 (31.4%), n-C_5H_{12} (25.8%), C_7H_{14} (38.2%) and n-C_7H_{16} (24.2%). The formation of the oxidation products (cyclic ketones and alcohols) in up to~10% yields also takes place when using cycloalkanes as substrates (entries 8–10). In contrast, the yields of ketones and alcohols are negligible (typically below 1%) in the transformations of linear C_2–C_7 alkanes.

From the catalytic data, it is concluded that **1** and **2** are potent catalyst for consume of alkane/cycloalkane to carboxylic acids under ecofriendly conditions (**1** being more efficient than **2**).

Table 4. Catalytic activity data of **1** and **2**.

Entry[a]	Alkane C_n	C_{n+1} carboxylic acid (yield, %[b]) with **1**	C_{n+1} carboxylic acid (yield, %[b]) with **2**	Regioselectivity[c] C(1) : C(2) : C(3) :C(n)
1	C_2H_6	n-C_2H_5COOH (31.4)	n-C_2H_5COOH (28.5)	
2	C_3H_8	$CH_3CH(COOH)CH_3$ (40.5), n-C_3H_7COOH (6.2)	$CH_3CH(COOH)CH_3$ (38.6), n-C_3H_7COOH (6.8)	[1º:2º = 1:24] (**1**) [1º:2º = 1:23] (**2**)
3	n-C_4H_{10}	$C_2H_5CH(COOH)CH_3$ (25.4), n-C_4H_9COOH (3.2)	$C_2H_5CH(COOH)CH_3$ (24.6), n-C_4H_9COOH (2.8)	[1º:2º = 1:13] (**1**) [1º:2º = 1:12] (**2**)
4	n-C_5H_{12}	$C_2H_5CH(COOH)C_2H_5$ (7.4), $C_3H_7CH(COOH)CH_3$ (17.2) n-$C_5H_{11}COOH$ (1.2)	$C_2H_5CH(COOH)C_2H_5$ (8.2), $C_3H_7CH(COOH)CH_3$ (16.4) n-$C_5H_{11}COOH$ (1.0)	1:20:20 (**1**) 1:22:21 (**2**)
5	n-C_6H_{14}	$C_3H_7CH(COOH)C_2H_5$ (15.6) $C_4H_9CH(COOH)CH_3$ (18.6) n-$C_6H_{13}COOH$ (0.8)	$C_3H_7CH(COOH)C_2H_5$ (13.4) $C_4H_9CH(COOH)CH_3$ (17.5) n-$C_6H_{13}COOH$ (0.6)	1:20:19 (**1**) 1:22:21 (**2**)
6	n-C_7H_{16}	$C_3H_7CH(COOH)C_3H_7$ (4.2) $C_4H_9CH(COOH)C_2H_5$ (9.2) $C_5H_{11}CH(COOH)CH_3$ (9.8) n-$C_7H_{15}COOH$ (1.0)	$C_3H_7CH(COOH)C_3H_7$ (4.3) $C_4H_9CH(COOH)C_2H_5$ (8.8) $C_5H_{11}CH(COOH)CH_3$ (9.0) n-$C_7H_{15}COOH$ (1.0)	1:18:16:14 (**1**) 1:19:17:13 (**2**)
7	C_5H_{10}	C_5H_9COOH (40.0) C_5H_8O/C_5H_9OH[d] (2.2/0.2)	C_5H_9COOH (36.0) C_5H_8O/C_5H_9OH[d] (2.0/0.1)	
8	C_6H_{12}	C6H11COOH (28.6) $C_6H_{10}O/C_6H_{11}OH$[d] (8.4/3.0)	C6H11COOH (24.5) $C_6H_{10}O/C_6H_{11}OH$[d] (8.3/2.8)	
9	C_7H_{14}	$C_7H_{13}COOH$ (28.8) $C_7H_{12}O/C_7H_{13}OH$[d] (9.4/1.6)	$C_7H_{13}COOH$ (26.4) $C_7H_{12}O/C_7H_{13}OH$[d] (8.2/1.3)	

[a]Reaction conditions: *p*(gaseous alkane) = 1.0 (C_2H_6, C_3H_8) or 0.75 (*n*-C_4H_{10}) atm + *p*(CO) = 10 and 2 atm (1 atm = 0.266 mol); liquid alkane (1.0 mmol) + *p*(CO) = 20 atm; compound **1** or **2** (4.0 mmol); $K_2S_2O_8$ = 1.0 (entries 1–3) or 1.5 (entries 4–11) mmol; H_2O (2.0 mL)–MeCN (4.0 mL); 60 °C, 6 h, 13.0 mL autoclave. [b]Moles of product/100 moles of alkane. [c]one/ol = cyclic ketones and alcohols (products of oxidation).

Conclusions

We report here in this work, two novel complexes with stoichiometry $[Cu_3(H_2tea)_2(ba)_2(NO_3)_2]$ (**1**) and $[Zn_2(H_2tea)(ba)_3]\cdot H_2O$ (**2**), where triethanolamine in mono deprotonated form act as primary ligand and benzoate ion is introduced as supporting auxiliary to result in trinuclear **1** and dinuclear **2** complexes. The two complexes have been characterized using various spectral and single crystal X-ray studies. Bonding modes of primary and auxiliary ligands are ascertained from FTIR data. single crystal X-ray studies reveal that all the Cu(II) in trinuclear complex are distorted octahedral while in dinuclear complex the two zinc metal ions are present in tetrahedral and distorted octahedral environment. This is a rare case of the unique geometry of the **2**. The complexes show various non-covalent interactions like C–H···O, C–H···O, O–H···O, C–H···π and C–H···C which have been supported by crystallographic studied and Hirshfeld surface analysis. The complexes are examined for catalytic property in conversion of alkane to carboxylic acids and it is concluded that Cu_3 complex is more active for such catalytic transformations while Zn_2 complex is slightly less potent. Luminescent spectral studies of the complexes confirmed that **2** is more promising luminescent material than **1**. Furthermore, red shift of the emission peaks in solid state spectra is attributed the presence of non-covalent interactions in solid state which are absent in solution state.

References

[1] (a) W. Hasse, S.J. Gehring, Chem. Soc., Dalton Trans. (1985) 2609 (b) The Cambridge Structural Database (CSD), version 5.28 (Jan. 2007). (c) F.H. Allen, Acta Crystallogr. (2002) B58 380. (d) U. Riaz, O.J. Curnow, M.D. Curtis, J. Am. Chem. Soc., 116 (1994) 4357. (e) R.D. Adams, B. Captain, Angew. Chem., Int. Ed., 47 (2008) 252. (f) R.E.P. Winpenny, J.A. McCleverty, T.J. Meyer, 2004: Comprehensive Coordination Chemistry; Pergamon Press: Oxford, Vol. 7, Chapter 7.3, 125. (g) R.E.P. Winpenny, Adv. Inorg. Chem., 52 (2001) 1. (h) Y. Hayashi, T. Ohshima, Y. Fujii, Y. Matsushima, K. Mashima, Catal. Sci. Technol., 1 (2011) 230. (i) H. Li, M. Eddaoudi, T.L.; Groy, O.M. Yaghi, J. Am. Chem. Soc., 120 (1998) 8571. (j) H. Li, M. Eddaoudi, M. O'Keeffe, O.M. Yaghi, Nature, 402 (1999) 276.

[2] (a) Q, Jr, L.W.B. Tolman, Nature, 455 (2008) 333. (b) C. Cambillau, M. Tegoni, M. Prudencio, A.S. Pereira, S. Besson, J.J. Moura, I. Moura, K. Brown, Nat. Struct. Biol., 7 (2000) 191. (c) T.D. Westmoreland, D.E. Wilcox, M.J. Baldwin, W.B. Mims, E.I.J. Solomon, Am. Chem. Soc., 111 (1989) 6106. (d) A. Granata, E. Monzani, L. Casella, J. Biol. Inorg. Chem., 9 (2004) 903. (e) M. Costas, K. Chen, L.J. Que, Coord. Chem. Rev., 200–202 (2000) 517. (f) G.T. Babcock, M. Wikström, Nature, 356 (1992) 301. (g) N. Mano, V. Soukharev, A.J. Heller, Phys. Chem., 110 (2006) 11180. (h) M.A. Thorseth, C.E. Tornow, E.C.M. Tse, A.A. Gewirth, Coord. Chem. Rev., 257 (2013) 130. (i) C.C.L. McCrory, A. Devadoss, X. Ottenwaelder, R.D. Lowe, T. Daniel, P. Stack, C.E.D. Chidsey, J. Am. Chem. Soc., 133 (2011) 3696.

[3] (a) F.A. Cotton, Wilkinson, G. (1988) Advanced Inorganic Chemistry: A Comprehensive Text 5th ed., vol. 1. John Wiley & Sons New York. (b) Y. Hayashi, T. Ohshima, Y. Fujii, Y. Matsushima, K. Mashima, Catal. Sci. Technol., 1 (2011) 230. (c) T. Iwasaki, K. Agura, Y. Maegawa, Y. Hayashi, T. Ohshima, K. Mashima, Chem. Eur. J., 16 (2010) 11567. (d) Y. Maegawa, T. Ohshima, Y. Hayashi, K. Agura, T. Iwasaki, K. Mashima, ACS Catal., 1 (2011) 1178.

[4] (a) P.G. Cozzi, Chem. Soc. Rev., 33 (2004) 410. (b) C. Di Nicola, Y. Yu. Karabach, A. M. Kirillov, M. Monari, L. Pandolfo, C. Pettinari, A.J.L. Pombeiro, Inorg. Chem., 46 (2007)

221. (c) S.J. Elliot, M. Zhu, L. Tso, H.-H.T. Nguyen, Yip, S.I.J. Chan, Am. Chem. Soc., 119 (1997) 9949. (d) B. Ding, L. Yi, P. Cheng, D.-Z. Liao, S.-P. Yan, Inorg. Chem., 45 (2006) 5799.

[5] (a) W. Joseph D.C. Sharples, Coord. Chem. Rev. 260 (2014) 1. (b) R.E.P. Winpenny, Adv. Inorg. Chem., 52 (2001) 1. (ed. A. G. Sykes). (c) M. Murrie, Chem. Soc. Rev., 39 (2010) 1986. (d) M. Nakano, H. Oshio, Chem. Soc. Rev., 40 (2011) 3239. (e) G. Rajaraman, M. Murugesu, E.C. Sañudo, M. Soler, W. Wernsdorfer, M. Helliwell, C. Muryn, J. Raftery, S.J. Teat, G. Christou, E.K. Brechin, J. Am. Chem. Soc., 126 (2004) 15445. (f) S. Goswami, A.K. Mondal, S. Konar, Inorg. Chem. Front., 2 (2015) 687.

[6] (a) G. Abbas, Y. Lan, V. Mereacre, W. Wernsdorfer, R. Clérac, G. Buth, M.T. Sougrati, F. Grandjean, G.J. Long, C.E. Anson, A.K. Powell, Inorg. Chem., 48 (2009) 9345. (b) A.M. Ako, V. Mereacre, R. Clérac, I.J. Hewitt, Y. Lan, C.E. Anson, A.K. Powell, Dalton Trans. (2007) 5245. (c) A. Singh, R.C. Mehrotra, Coord. Chem. Rev., 248 (2004) 101. (d) J.G. Verkade, Coord. Chem. Rev., 137 (1994) 233. (e) A.M. Kirillov, Y.Y. Karabach, M. Haukka, M. C. Fatima, G. da Silva, J. Sanchiz, M.N. Kopylovich, A.J.L. Pombeiro, Inorg. Chem., 47 (2008) 162.

[7] (a) B.L. Chen, B.L.F. Mok, K.S.C. Ng, Y.L. Feng, S.X. Liu, Polyhedron, 17 (1998) 4237. (b) Y. Li, R. Cao, S.J. Lippard, Org. Lett., 13 (2011) 5052. (c) R.M. Escovar, J.H. Thurston, T. Ould-Ely, A. Kumar, K.H.Z. Whitmire, Anorg. Allg. Chem., 631 (2005) 2867. (d) O.V. Nesterova, M.V. Kirillova, M. Fatima, C. G. da Silva, R. Boca, A.J.L. Pombeiro, CrystEngComm, 16 (2014) 775. (e) S.K. Langley, K.J. Berry, B. Moubaraki, K.S. Murray, Dalton Trans. (2009) 973. (f) E.K. Brechin, M. Soler, J. Davidson, D. N. Hendrickson, S. Parsonsc, G. Christou, Chem. Comm. (2002) 2252. (g) M. Casarin, C. Corvaja, C. di Nicola, D, Falcomer, L, Franco, M, Monari, L, Pandolfo, C, Pettinari, F, Piccinelli, P. Tagliatesta, Inorg. Chem., 43 (2004) 5865. (h) M, Casarin, C, Corvaja, C, Di Nicola, D, Falcomer, L, Franco, M. Monari, L. Pandolfo, C. Pettinari, F. Piccinelli, Inorg. Chem., 44 (2005) 6265. (i) E.K. Brechin, Chem. Commun. (2005) 5141. (j) S.J. Shah, C.M. Ramsey, K.J. Heroux, J.R. O'Brien, A.G. Di-Pasquale, A.L. Rheingold, E. Del Barco, D.N. Hendrickson, Inorg. Chem., 47 (2008) 6245. (k) S.K. Langley, B.

Moubaraki, C.M. Forsyth, I.A. Gass, K.S. Murray, Dalton Trans., 39 (2010) 1705. (l) C.D. Samara, C.A. Muryn, F. Tuna, R.E.P. Winpenny, Eur. J. Inorg. Chem., (2010) 3097.

[8] J.A. Ibers, W.C. Hamilton, International Tables for X-ray Crystallography, Kynoch Press, Birmingham, England, 1974, vol. IV.

[9] SMART & SAINT Software Reference manuals, Version 6.45, Bruker Analytical X-ray Systems, Inc., Madison, WI, 2003.

[10] G. M. Sheldrick, SADABS, software for empirical absorption correction, Ver. 2.05, University of Göttingen, Göttingen, Germany, 2002.

[11] XPREP, version 5.1, Siemens Industrial Automation Inc., Madison, WI, 1995.

[12] G. M. Sheldrick, SHELXL97, Program for Crystal Structure Refinement, University of Göttingen, Göttingen, Germany 2008.

[13] A. Altomare, M.C. Burla, M. Camalli, G.L. Cascarano, C. Giacovazzo, A. Guagliardi, A.G. G. Moliterni, G. Polidori, R.J. Spagna, J. Appl. Crystallogr., 32 (1999) 115.

[14] S. K. Wolff, D. J. Grimwood, J.J. McKinnon, M.J. Turner, D. Jayatilaka, M.A. Spackman, Crystal Explorer, Version 3.0; University of Western Australia: 2012.

[15] M.A. Spackman, D. Jayatilaka, CrystEngComm, 11 (2009) 19.

[16] T. Dey, P. Chatterjee, A. Bhattacharya, S. Pal, A.K. Mukherjee, Cryst. Growth Des., 16 (2016) 1442.

[17] M.A. Spackman, J.J. McKinnon, D. Jayatilaka, CrystEngComm. 10 (2008) 377-388.

[18] (a) M.V. Kirillova, A.M. Kirillov, M.L. Kuznetsov, J.A.L. da Silva, J.J.R. Frausto da Silva, A.J.L. Pombeiro, Chem. Commun. (2009) 2353. (b) M.V. Kirillova, A.M. Kirillov, A.J.L. Pombeiro, Adv. Synth. Catal, 351 (2009) 2936. (c) M.V. Kirillova, A.M. Kirillov, A.J.L. Pombeiro, Chem. Eur. J., 16 (2010) 9485. (d) M.V. Kirillova, A.M. Kirillov, A.J.L. Pombeiro, Appl. Catal., A, 401 (2011) 106.

[19] (a) Z.-G. Li, J.-W. Xu, H.-Q. Jia, N.-H. Hu, Hu, Inorg. Chem. Commun., 9 (2006) 969. (b) Z. Boulsourani, V. Tangoulis, C.P. Raptopoulou, V. Psycharis, C. Dendrinou-Samara, Dalton Trans., 40 (2011) 7946. (c) E.G. Bakalbassis, G.A. Katsoulos, C.A. Tsipis, Inorg. Chem., 26 (1987) 3151.

[20] (a) M. Gatehouse, S.E. Livingstone, R.S.J. Nyholm, Inorg. Nucl. Chem., 8 (1958) 75. (b) N.T. Madhu, P.K. Radhakrishnan, Transition Met. Chem., 25 (2000) 287. (c) K. Nakamoto, Infrared and Raman Spectra of Inorganic and Coordination Compounds, Wiley, New York (1986). (d) K.-E. Lee, S.W.J. Lee, Mol. Struct., 975 (2010) 247.

[21] (a) R.S. Amim, M.R.L. Oliveira, G.J. Perpetuo, J. Janczak, L.D.L. Miranda, M.M.M. Rubinger, Polyhedron, 27 (2008) 1891. (b) A.B.P. Lever, Inorganic Electronic Spectroscopy (Elsevier, Amsterdam (1984). (c) E.G. Bakalbassis, G.A. Katsoulos, C.A. Tsipis, Inorg. Chem., 26 (1987) 3151.

[22] (a) K. Gudasi, R. Vadavi, R. Shenoy, M. Patil, S.A. Patil, M. Nethaji, Inorg. Chim. Acta., 358 (2005) 3799. (b) A. Abragam, B. Bleaney, in Electron Paramagnetic Resonance of Transition Ions, Clarendon Press, Oxford, U. K. (1970).

[23] (a) U.T. Mueller-Westerhoff, A. Nazzal, W. Prossdorf, J. Am. Chem. Soc., 103 (1981) 7678. (b) S. Gronert, J.R.J. Keeffe, Am. Chem. Soc., 127 (2005) 2324. (c) S. Das, P.K. Bharadwaj, Inorg. Chem., 45 (2006) 5257.

[24] (b) S. Zhang, F. Jiang, Y. Bu, M. Wu, J. Ma, X. Shan, K. Xiong, M. Hong, CrystEngComm, 14 (2012) 6394. (b) Q. Guo, C. Xu, B. Zhao, Y. Jia, H. Hou, Y. Fan, Cryst. Growth Des., 12 (2012) 5439. (c) X. Guo, G. Zhu, Q. Fang, M. Xue, G. Tian, J. Sun, X. Li, S. Qiu, Inorg. Chem., 44 (2005) 3850. (d) W.Q. Kan, J. Yang, Y.Y. Liu, J.F. Ma, CrystEngComm, 14 (2012) 6934. (e) F.P. Doty, C.A. Bauer, A.J. Skulan, P.G. Grant, M.D. Allendorf, Adv. Mater, 21 (2009) 95. (f) B. Gole, A.K. Bar, P.S. Mukherjee, Chem. Commun., 47 (2011) 12137. (g) L.P. Zhang, J.F. Ma, J. Yang, Y.Y. Pang, J.C. Ma, Inorg. Chem. 49 (2010) 1535. (h) A.J. Lan, K.H. Li, H.H. Wu, L.Z. Kong, N. Nijem, D.H. Olson, T.J. Emge, Y.J. Chabal, D.C. Langreth, M.C. Hong, J. Li, Inorg. Chem., 48 (2009) 7165. (i) H.-F. Zhu, J. Fan, T. Okamura, W.-Y. Sunand, N. Ueyama, Cryst. Growth Des., 5 (2005) 289.

[25] (a) C.D. Samara, P.D. Janakoudakis, D.P. Kessissaglou, G.E. Manoyussakis, D. Mentzapfos, A. Terzis, J. Chem. Soc., Dalton Trans. (1992) 3259. (b) Z.A. Siddiqi, V.J. Mathew, Polyhedron, 13 (1994) 799. (c) K. Dimitrou, A.D. Brown, T.E. Concolino, A.L. Rheingold, G. Christou, Chem. Commun. (2001) 1284. (d) R.A. Sheldon, J.A. Kochi,

Metal Catalysed Oxidations of Organic Compounds; Academic Press: New York. (1981).

[26] O. Yesilel, H.J. Ölmez, Therm. Anal. Calorim. 89 (2007) 261.

[27] (a) S.K. Seth, D. Sarkar, A.D. Jana, T. Kar, Cryst. Growth Des., 11 (2011) 4837. (b) M. Mitra, S.K. Seth, S.R. Choudhury, P. Manna, A. Das, M. Helliwell, A. Bauzá, A. Frontera, S. Mukhopadhyay, Eur. J. Inorg. Chem. (2013) 4679. (c) S.K. Seth, Inorg. Chem. Commun., 43 (2014) 60.

[28] R. Yadav, M. Trivedi, G. Kociok-Köhn, R. Prasad, A. Kumar, CrystEngComm, 17 (2015) 9175.

[29] I. Khan, P. Panini, S.U.D. Khan, U.A. Rana, H. Andleeb, D. Chopra, S. Hameed, J. Simpson, Cryst. Growth Des., 16 (2016) 1371.

[30] (a) X.-H. Bu, M.-L. Tong, Y.-B. Xie, J.-R. Li, H.-C. Chang, S. Kitagawa, J. Ribas, Inorg. Chem., 44 (2005) 9837. (b) D.L. Reger, A. Debreczeni, B. Reinecke, V. Rassolov, M.D. Smith, R.F. Semeniuc, Inorg. Chem., 48 (2009) 8911.

[31] (a) B.N. Figgis, J. Lewis, in Modern Coordination Chemistry, ed. Lewis and R. G. Wilkins, Interscience Publishers Inc,New York, (1960) 400. (b) R.J. Angelici, W.B. Saunders, Synthesis and technique in inorganic chemistry, (1977) 198. (c) C.E. Housecroft, A.G. Sharpe, Inorg. Chem., Pearson Education Limited (2008) vol. 3.

Chapter 3

New proton transfer complexes containing 4–picolinium as cation and pyridine–2,6–dicarboxylate complex as anion: synthesis, crystal structures, spectral investigations, antioxidant activities and molecular docking studies

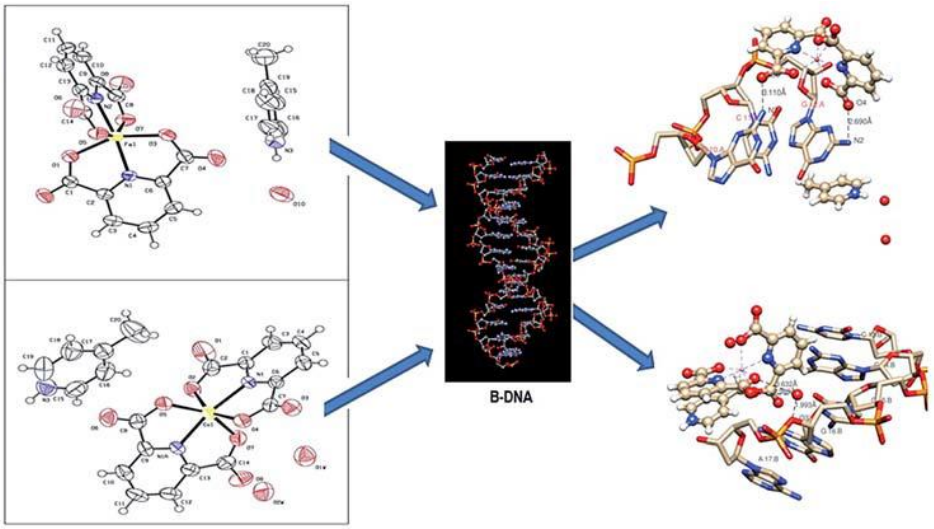

Introduction

The coordinating nature and type of ligands with specific symmetry are key factors to the structures and properties of the final products. Functionalized polycarboxylic acids are among the multidentate ligands, which can yield a number of mono and poly metallic coordination complexes. Pyridine–2,6–dicarboxylic acid (H_2pda) has played a key role to participate in interesting coordination chemistry [1,2]. The reasons for this interest is the ability of H_2pda to give stable chelates with different versatile flexible [N,O,O] coordination modes with metal ions, the great affinity to form strong hydrogen bonds and its biological activities [3,4]. H_2pda is a planer ligand with rigid 120° angle between the central pyridine ring and the two carboxylate groups, and therefore could potentially provide various coordination modes to form both discrete and consecutive metal complexes under appropriate synthesis conditions. The most important reactions of H_2pda are proton transfer in acid/base systems with specific interaction such as hydrogen bonding. There acid-base/proton transfer reactions are important in inorganic chemistry [5-8]. Polycarboxylic acids are most probably used in building blocks for construction of metal coordination complexes by the proton transfer processes. The binding of two or more carboxylic groups in different angles allow the creation of 1D (long chain), 2D (sheet) or 3D (cage) structure [9-12]. Non covalent interaction is backbone of supra molecular and molecular recognition chemistry. Non covalent interactions help to build molecular clusters while a covalent interaction is to form classical molecules [13]. Non covalent molecular clusters affect the properties of the subsystem, and these changes are important for the detection of cluster formation. The stronger non-covalent interaction causes larger changes in the properties of the subsystem [14,15]. Many proton transfer complexes have been prepared using H_2pda and other ligand like propanol amine [16]. However the chemistry of proton transfer complexes of H_2pda with a heterocyclic moiety has not been reported to the best of our knowledge. We have used H_2pda and 4–picoline (4–pic) in our system. H_2pda behaves as a proton donor and 4–picoline acts as a proton acceptor, which is interacting by Vander Waals force as H–bonding. Since such proton transfer complexes also exhibited

biological (like SOD) activities, the antioxidant (free radical scavenging) properties are also explored. Moreover, molecular docking studies are performed to investigate the effect of the complexes on DNA receptor.

Experimental

Materials and methods

All reagents of analytical grade were obtained from commercial sources and used without further purification. The infrared (IR) spectrum of the compound was recorded within the range 400–4000 cm–1 using KBr pellets on Perkin Elmer Model spectrum GX spectrophotometer. Melting points was determined by open capillary method and are uncorrected. An electronic spectrum and molar conductivity of 10^{-3} M solution in MeOH was recorded on Perkin Elmer λ-25 UV-visible spectrophotometer, cu-vettes of 1 cm path length and Systronics-305 digital conductivity bridge, respectively at room temperature. The elemental C, H and N analyses were obtained from Micro-Analytical Laboratory of Central Drug Research Institute (CDRI), Lucknow, India. ESI mass spectra were recorded on a WATERS Q-TOF Premier mass spectrometer. Fluorescence measurements were determined on Hitachi F-2700 spectrophotometer. ^{1}H and ^{13}C NMR spectra were recorded on a Bruker Avance II 400 NMR spectrometer from Punjab, university Chandigarh, India. The EPR spectrum of the complexes was acquired on a Perkin-Elmer spectrometer using X-band frequency (9.1 GHz) at room temperature in solid. Thermal gravimetric analysis (TGA) data were recorded from room temperature up to 800 °C at a heating rate of 20 °C/min. The data were obtained using a Shimadzu TGA-50H instrument. Magnetic susceptibility was measured by magnetic susceptibility balance, Sherwood scientific Cambridge U. K. at room temperature. Cyclic voltammetry (CV) was performed on EG&G PAR 273 Potentiostat/Galvanostat an IBM PS2 computer with EG&G M270 software for data acquisition. The three-electrode cell configuration comprised of, a platinum sphere, a platinum plate and Ag(s)/$AgNO_3$ were used as working, auxiliary and reference electrodes, respectively. The supporting electrolyte used was [$^{n}Bu_4N$]ClO_4. Platinum sphere electrode was sonicated for 2 min in dilute nitric acid, dilute hydrazine hydrate and then in double distilled water to remove the impurities. The solutions were deoxygenated by bubbling research grade

nitrogen gas and an atmosphere of nitrogen was maintained over the solution during measurements.

Antioxidant (scavenging) activity

DPPH free radical scavenging activity

The antioxidant activity of the complex (3) was determined by DPPH free radical assay [17,18]. The mixture solution (10^{-3} M ethanol) contains 1 mL of sample, 1 mL of DPPH radical solution and 5 mL of absolute ethanol (1:1:5). On the basis of reaction of antioxidant compounds with 2,2-Diphenyl-1-picrylhydrazyl (DPPH), compound donates proton and which is reduced. All the sample solution were incubated 60 °C on water bath for 100 minutes and the color of the sample solution changes from violet to yellow and absorption band is recorded at 515 nm by using a UV-Vis. spectrophotometer (Perkin Elmer, λ- 40). The mixture of 6 mL ethanol and 1 mL sample solution was used as blank while the control was prepared by mixing ethanol (6 mL) and DPPH radical solution (1 mL). The scavenging activity percentage (AA%) was determined by the following relation:

$$\%\ \text{Inhibition} = \frac{A_{\text{control}} - A_{\text{sample}}}{A_{\text{control}}} \times 100$$

Where $A_{control}$ = absorbance of DPPH in ethanol without an antioxidant and A_{sample} = absorbance of DPPH in the presence of an antioxidant.

Hydrogen peroxide scavenging activity

The hydrogen peroxide scavenging ability of the complex (3) was determined by standard method [19]. Hydrogen peroxide solution (2 mM) was prepared in phosphate buffer (50 mM, pH 7.4). The reaction mixture contains 3 ml of sample and 1.8 ml of H_2O_2 solution and phosphate buffer solution without H_2O_2 as a blank. Hydrogen peroxide concentration was determined by UV-Vis. spectrophotometer (Perkin Elmer,

λ-40) at 240 nm as a control. Absorbance of each sample was recorded after 10 minutes against the blank solution. The scavenging ability of hydrogen peroxide was calculated by the following equation:

$$\% \text{ Inhibition } = \frac{A_{control} - A_{sample}}{A_{control}} \times 100$$

Where $A_{control}$ = absorbance of H_2O_2 in ethanol without an antioxidant and A_{sample} = absorbance of H_2O_2 in the presence of an antioxidant.

Molecular docking

The rigid molecular docking studies were performed using HEX 8.0.0 software [20], which is an interactive molecular graphics program for calculating and displaying feasible docking modes of pairs of protein, enzymes and DNA molecule. The structure of the complexes (**2** and **3**) were sketched by CHEMSKETCH (http://www.acdlabs.com) and converted to pdb format from mol format by OPENBABEL (http://www.vcclab.org/lab/babel/). The crystal structure of the B-DNA dodecamer $d(CGCGAATTCGCG)_2$ (PDB ID: 1BNA) was downloaded from the protein data bank (http://www.rcsb.org./pdb). Visualization of the docked pose has been done by using CHIMERA (www.cgl.ucsf.edu/chimera) and PyMol (http://pymol. sourceforget.net/) molecular graphics program.

Synthesis

Synthesis of [4–pic–H][Cr(pda)$_2$]·2H$_2$O (1)

An ethanolic solution of pyridine–2,6–dicorbaxylic acid (5.0 mmol, 0.84 g) was refluxed with 4–picoline (5.0 mmol, 0.50 ml) for 6 h then cooled at room temperature. An ethanolic solution of $CrCl_2 \cdot 6H_2O$ (5.0 mmol, 1.18 g) was added dropwise to the above mixture, which produced green color solid. Stirring was continued for 4 h at room temperature. The solid obtained was filtered off, washed with ethanol and dried in

vacuum. After repeated recrystallization in various solvents, the solid could not provide single crystals suitable for X-ray studies.

[Green, Yield 65%, m.p. >300°C] Anal. Calcd. (%) for $C_{20}H_{14}CrN_3O_{10}$: C 46.38; H 2.70; N 8.25. Found (%): C 46.87; H 2.65; N 8.32. Molar conductance, Λ_m (10^{-3} M, methanol): 85 $\Omega^{-1}cm^2mol^{-1}$. FT–IR (as KBr disks, cm^{-1}): 1392s $\nu_{sym}(COO^-)$, 1619s $\nu_{asym}(COO^-)$, 3250w (N–H), 1583s (C=N), 1436w, 730m, 773s (C=C) pyridine ring stretching vibrations.

Synthesis of [4–pic–H][Fe(pda)$_2$]·2H$_2$O (2)

Synthetic procedure for **2** was similar to that for **1** except addition of $FeCl_3$ (5.0 mmol, 0.81 g) instead of $CrCl_2 \cdot 6H_2O$. The dark brown solid was obtained which was recrystallized in double distilled water yielding single crystals suitable for X–ray studies.

[Dark brown, Yield 60%, m.p. >300°C]Anal. Calcd. (%) for $C_{20}H_{14}FeN_3O_{10}$: C 46.62; H 2.70; N 8.22. Found (%): C 46.96; H 2.70; N 8.35. Molar conductance, Λ_m (10^{-3} M, methanol): 92 $\Omega^{-1}cm^2mol^{-1}$. FT–IR (as KBr disks, cm^{-1}): 1329s $\nu_{sym}(COO^-)$, 1654s $\nu_{asym}(COO^-)$, 3305w (N–H), 1591s (C=N), 1428w, 740m, 775s (C=C) pyridine ring stretching vibrations.

Synthesis of [4–pic–H][Co(pda)$_2$]·2H$_2$O (3)

Synthetic procedure for **3** was similar to that for **1** except addition of $CoCl_2 \cdot 6H_2O$ (5.0 mmol, 1.18 g) instead of $CrCl_2 \cdot 6H_2O$. The pink colour solid was obtained which was recrystallized in double distilled water yielding single crystals suitable for X–ray studies.

[Pink, Yield 60%, m.p. >300°C] Anal. Calcd. (%) for $C_{20}H_{14}CoN_3O_{10}$: C 46.58; H 2.72; N 8.15. Found (%): C 46.92; H 2.68; N 8.27. Molar conductance, Λ_m (10^{-3} M,

methanol): 90 $\Omega^{-1}cm^2mol^{-1}$. FT–IR (as KBr disks, cm^{-1}): 1386s $\nu_{sym}(COO^-)$, 1618s ν_{asym} (COO^-), 3300w (N–H), 1587s (C=N), 1430w, 730m, 762s (C=C) pyridine ring stretching vibrations.

Crystallographic data collection and refinements

Single crystal X-ray diffraction of compounds (**2** and **3**) was performed at 100 K on a Bruker SMART APEX CCD diffractometer, X–ray data was collected using graphite monochromated Mo-Kα radiation (λ = 0.71073 Å). The linear absorption coefficients, scattering factors for the atoms, and the anomalous dispersion corrections were taken from the International Tables for X–ray Crystallography [21]. The data integration and reduction were processed with SAINT Software [22]. An empirical absorption correction was applied to the collected reflections with SADABS [23] and the space group was determined using XPREP [24]. Several DIFX command has been given to fix the bond length parameters. The structures were solved by direct methods using SHELXL-97 [25] and refined on F2 by full matrix least squares using the SHELXL-97 program package [26]. All non-hydrogen atoms were refined with anisotropic displacement parameters. A summary of the crystallographic data and the structure refinement for the complexes is given in **Table 1**. CCDC reference numbers for **2** and **3** are 1440315 and 1405365, respectively.

Table 1. Crystallographic parameters for complexes (**2** and **3**)

Parameters	Complex **2**	Complex **3**
Empirical formula	$C_{20}H_{14}FeN_3O_{10}$	$C_{20}H_{14}CoN_3O_{10}$
Formula weight	512.19	515.27
Temp (K)	296(2)	273(2)
Crystal system	Monoclinic	Monoclinic
Space group	P 21/n	P 21/n
Unit cell dimensions		
a (Å)	15.0469(3)	15.020(7)
b (Å)	9.2868(2)	9.275(4)
c (Å)	15.5703(4)	15.524(7)
α (°)	90.00	90.00
β **(°)**	94.0110(10)	93.849(7)
γ (°)	90.00	90.00
V ($Å^3$)	2170.43	2157.8(18)
Z	4	4
ρ (calc) (g cm^{-3})	1.567	1.586
F (000)	1044	1048
Crystal size (mm3)	0.31×0.29×0.24	0.29 × 0.21 × 0.16
Index ranges	$-18 \le h \le 18$	$-17 \le h \le 17$
	$-11 \le k \le 11$	$-11 \le k \le 11$
	$-18 \le l \le 18$	$-18 \le l \le 18$
No of independent reflection	4031	2783
No. of reflections collected	26129	3794
GOF	1.014	1.087
Final R indices [$I > 2\sigma(I)$]	$R_1 = 0.0489$	$R_1 = 0.0822$
	$wR_2 = 0.1395$	$wR_2 = 0.1903$
R indices all data	$R_2 = 0.0399$	$R_2 = 0.0604$
	$wR_2 = 0.1299$	$wR_2 = 0.1692$
μ (mm^{-1})	0.758	0.859
Θ Range (°)	1.82-25.50	1.18-25.0

Results and discussion

The formation of the compounds can be regarded to involve two step mechanisms (**Scheme 1**). The first step is the proton transfer process from the dicarboxylic function of the pyridine–2,6–dicorboxylic acid (H_2pda) to 4–picoline (4–pic), which acts as proton acceptor to create the strong H–bonded species $[4–Pic–H]^+$ in the solution. The second step involves the in situ complexation reaction of this species with the M^{3+} ion to create the complex anion $[M(pda)_2]^-$, which is stabilized by the counter cation $[4–pic–H]^+$ to finally give the product $[4–pic–H][M(pda)_2]\cdot 2H_2O$ [M = Cr (**1**), Fe (**2**) and Co (**3**)]. The analytical and ESI Mass data are consistent with the proposed stoichiometry of the complexes (**1**–**3**). The molar conductance exhibits the 1:1 electrolytic nature of the complexes. The structure and bonding features were investigated by spectroscopic and X–ray data.

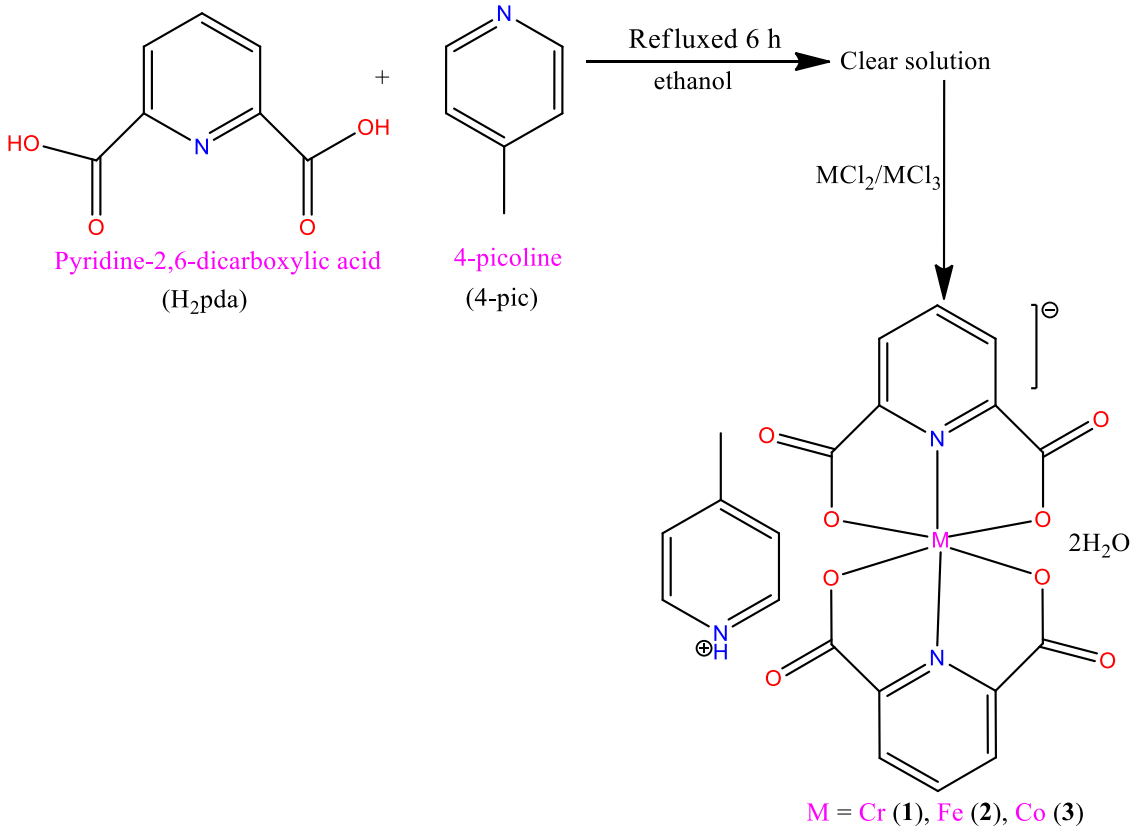

Scheme 1. Synthetic procedure of the complexes (**1**–**3**).

FT–IR, ^{1}H and ^{13}C NMR spectra

The bonding modes of the compounds (**1**–**3**) were observed by FT–IR spectral analysis. IR spectra were nearly the same and show vibrations due to the water and carboxylic acid fragments, ν(M–C), ν(M–O) and ν(M–O–O) frequencies. The FT–IR spectra of the complexes (**1**–**3**) contained strong intense bands at the ranges ~1620 and ~1340 cm^{-1}, which are characteristic peaks of the $\nu_{asym}(COO^{-})$ and $\nu_{sym}(COO^{-})$ fundamental stretching vibrations, respectively, of the pda^{2-} moiety coordinated to the metal ions. These symmetric and asymmetric vibrational bands are used to diagnose the coordination modes in the carboxylate ligands [27]. The separation (Δν) between $\nu_{asym}(COO^{-})$ and $\nu_{sym}(COO^{-})$ stretching vibration bands [i.e., $\Delta\nu = \nu_{asym}(COO^{-})–\nu_{sym}(COO^{-})$] provides ample information and ascertains the binding mode of coordination of the functionalized carboxylate moiety to the metal ions in the complexes (**1**–**3**). The carboxylate anion (COO^{-}) may bind the metal ion in four possible coordination modes as asymmetric monodentate (A), symmetric bidentate (B) and asymmetric bidentate (C and D) as presented in **Scheme 2**.

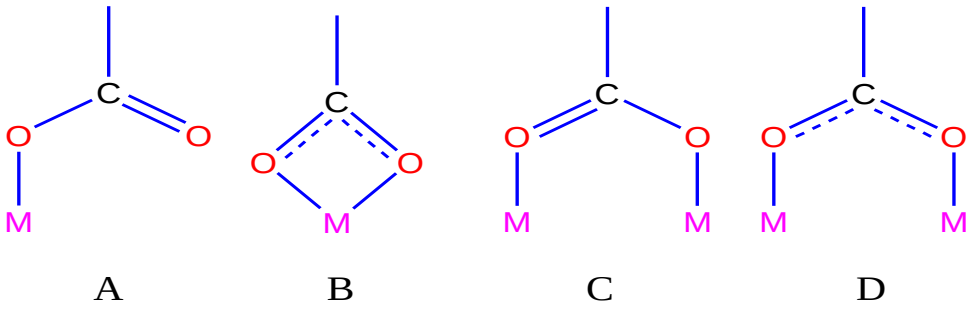

Scheme. 2. Important coordination modes of carboxylate (COO^{-}) group [i.e, asymmetric monodentate (A), symmetric bidentate (B) and asymmetric bidentate (C and D)].

If the magnitude of Δν lies in the range 250–300 cm^{-1}, the monodentate coordination mode (A) is present [28,29]. However, for the modes depicted in B, C and D the magnitude of Δν is much lower ($\Delta\nu \leq 200$ cm^{-1}). In the present complexes, the observed magnitude of Δν (~300 cm^{-1}) suggests that the carboxylate moieties of the pda^{2-} involve the asymmetric monodentate coordination (A). This fact has been further confirmed from the X–ray crystallography of the

complexes (**1** and **2**). The absence of the characteristic bands at around 1700 cm^{-1} attributed to the carboxyl groups indicates that complete deprotonating of all carboxylate groups in (**1**–**3**) has occurred upon reaction with metal ions. The ν(C=N) and ν(C=C) stretching vibration bands in the spectra were indicated in the region 1578–1583 and 1428–1436 cm^{-1}. The observed broad bands in 3492–3456 cm^{-1} region for the complexes were characteristic of the presence of lattice water molecules in the complex moiety. The appearance of an additional band in the high frequency region cantered at 3305–3311 cm^{-1} corresponds to the presence of H– bonded, N–H bond [30,31] in the cationic species of [4–Pic–H]. The medium intensity bands appearing at 432–436 and 542–595 cm^{-1} are characteristic of M–O and M–N bond(s) stretching vibrations, respectively [32].

^{1}H NMR spectra of the complexes showed a singlet in the high field side i.e., (at 2.3, 2.0 and 2.1 ppm for **1**, **2** and **3**, respectively) attributable to aliphatic protons of the $–CH_3$ group of 4–pic–H^+ moiety. A multiplet in the low field side (~6 ppm) corresponds to the pyridine ring protons in the complexes. An important peak characteristic of NH^+ proton is observed around ~9 ppm in all the complexes indicating the formation of proton transfer complexes (**1**–**3**) [9,33]. ^{13}C NMR spectra of the complexes contained three sets of resonance signals i.e., at 120–150 ppm due to aromatic carbons, at ~180 ppm due to carboxylate carbon and at ~25 ppm due to methyl carbon [33].

Electronic and EPR spectral studies

The electronic absorption spectra of the complexes (**1**–**3**) were recorded in methanol solution at room temperature (**Fig. 1**). The high-energy band at ~37,500, 30,000 and 26,000 cm^{-1} can be assigned to n→π*, π→π* and CT as shown in **Table 2** [34]. The charge transfers are LMCT due to M←pda^{2-} transition, involving oxygen atoms of the ligand. Low energy transitions are d–d bands assignable to high spin ground state of the metal ions i.e., Cr^{3+} ($t^3_{2g}e_g^0$) with $^4T_{1g}(F)←^4A_{2g}$ and $^4T_{2g}(F)←^4A_{2g}$ (**1**), Fe^{3+} ($t^3_{2g}e_g^2$) with $^4T_{2g}←^6A_{1g}$ and [$^4T_{2g}$, $^4T_{1g}$]←$^6A_{1g}$ (**2**) and Co^{3+} ($t^4_{2g}e_g^2$) with $^1E_{1g}←^1A_{1g}(F)$ and $^1A_{2g}←^1A_{1g}$ (**3**), assignments. The electronic spectral data are attributed to hexa-coordinate environment around the metal ions [35,36].

The solid state X–band EPR spectral data of the complexes (**1**–**3**) **Fig. 2** provide isotropic signal with g = 3.9-4.2 corroborating a distorted octahedral geometry of the complexes as revealed by electronic spectra.

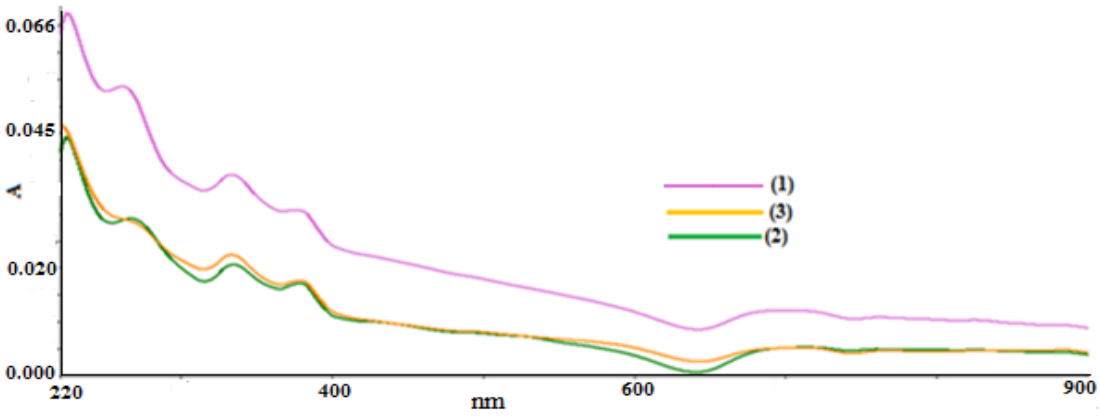

Fig. 1. Absorption spectra for the complexes (**1**–**3**).

Table 2. Electronic transitions with their assignments.

Complexes	Band positions (cm^{-1})	Assignments
[4-Pic-H][Cr(pda)$_2$]·2H$_2$O **1**	37453	n → π*
	32120	π → π*
	29247	CT
	23007	$^4T_1g(F) \leftarrow {}^4A_{2g}$
	22306	$^4T_2g(F) \leftarrow {}^4A_{2g}$
[4-Pic-H][Fe(pda)$_2$]·2H$_2$O **2**	37594	n → π*
	30030	π → π*
	26110	CT
	16920	$^4T_2g \leftarrow {}^6A_1g$
	14286	$[^4T_2g, {}^4T_1g] \leftarrow {}^6A_1g$
[4-Pic-H][Co(pda)$_2$]·2H$_2$O **3**	37594	n → π*
	30120	π → π*
	26178	CT
	16949	$^1E_1g \leftarrow {}^1A_1g(F)$
	14286	$^1A_2g \leftarrow {}^1A_1g$

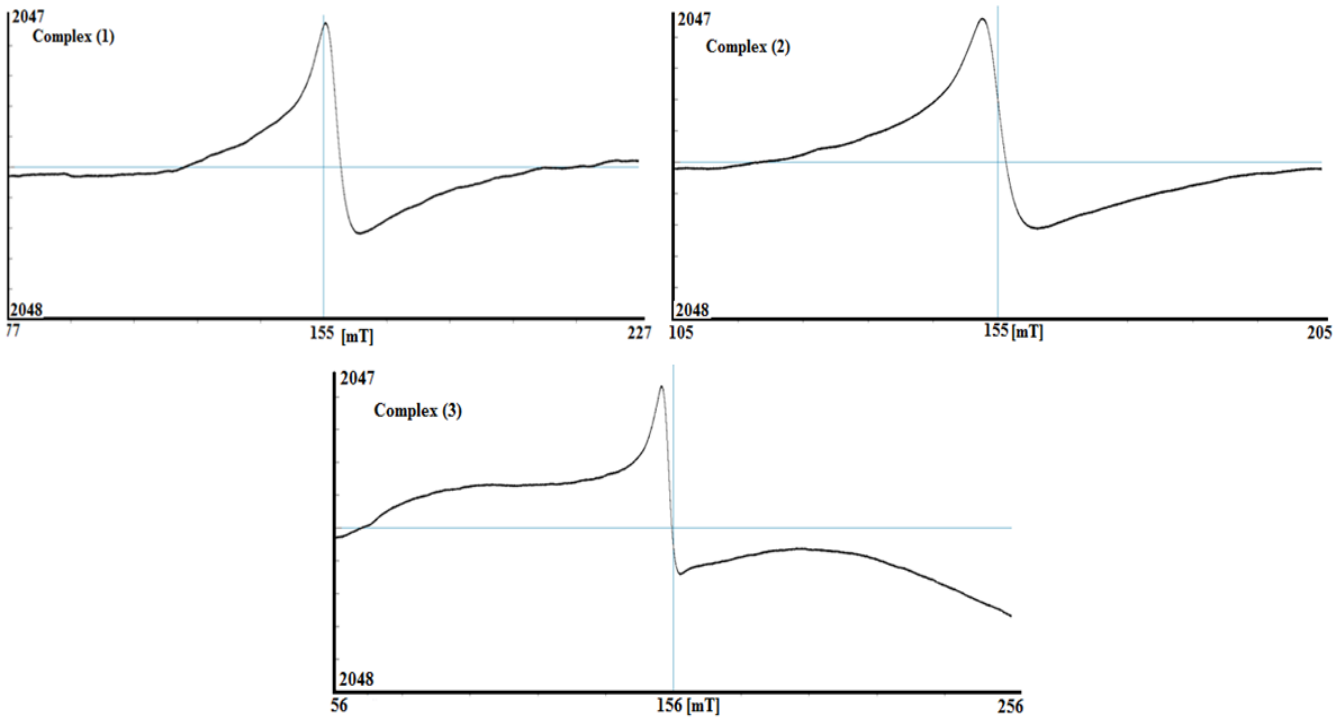

Fig. 2. EPR spectra of the complexes (**1**–**3**).

Luminescence spectra

Fluorescence spectra of the complexes (**1**–**3**) were also recorded in methanolic solution at room temperature as shown in **Fig. 3**. Upon excitation at ~265 and ~330 nm, an emission peak at~270 nd 390 nm, respectively were obtained with moderate intensity in all the complexes. The emission spectral data are indicative of the luminescence properties of the complexes.

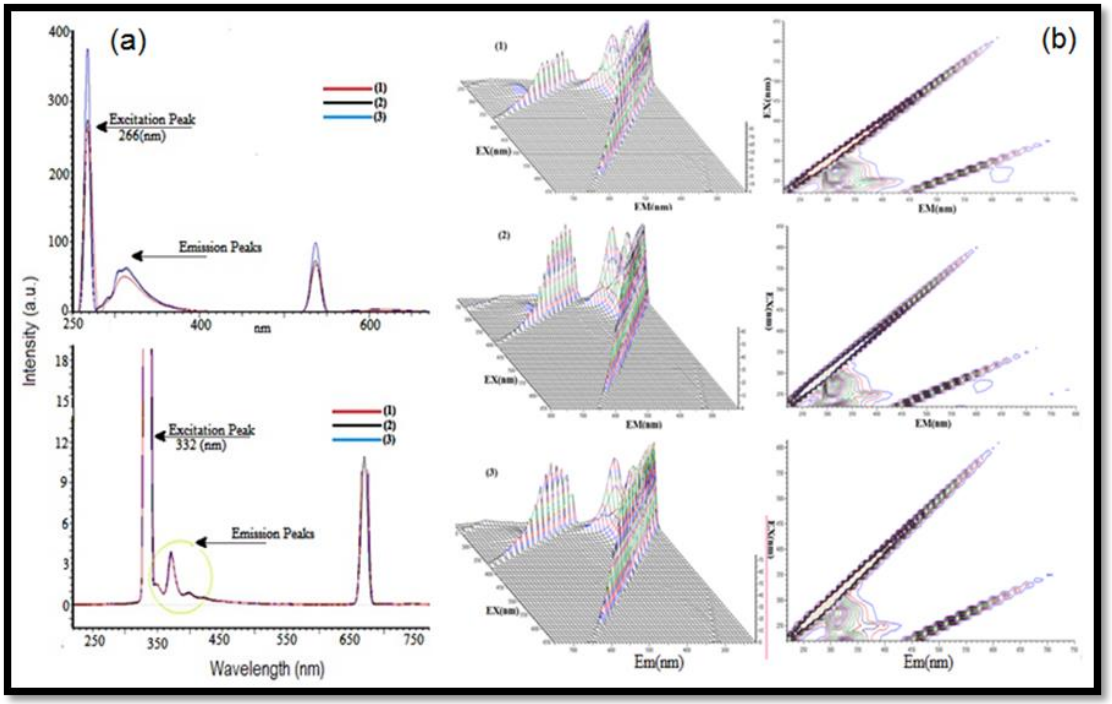

Fig. 3(a). Emission spectra of the complexes (**1**–**3**) and **(b)** 3D fluorescence spectra of the complexes (**1**–**3**).

Electrospray ionization mass (ESI–MS) spectra

Electrospray ionization mass (ESI–MS) spectrometry was performed to ascertain the proposed stoichiometry of the complexes (**1**–**3**). The complexes exhibited molecular ion peaks at m/z = 478 (**1**), 475 (**2**) and 479 (**3**) assignable to $[M(pda)_2][4\text{–pic–H}]^+$. All the complexes showed a peak at m/z = 94 (60%) assignable to $[4\text{–picH}]^+$ moiety. The complexes also exhibited peaks at m/z = 392 (**1**), 389 (**2**) and 393 (**3**) characteristic of the $[M(pda)_2]^+$ species. The ultimate species $[M(pda)]^+$ was formed as observed by peaks at m/z = 225 (**1**), 222 (**2**) and 226 (**3**).

Description of the crystal structures

X-ray crystal structure analysis for **2** and **3** reveals that both the complexes have identical molecular formula, i.e., $[4\text{–pic–H}][M(pda)_2]\cdot 2H_2O$, where **2** has iron and **3** cobalt ion. Both the compounds crystallize in the monoclinic space group $P2_1/n$. The complexes contain one $[4\text{–pic–H}]^+$ cation, one $[M(pda)_2]^-$ anion and two uncoordinated water molecules present in lattice (**Fig. 4**). The metal ion is present in +3 oxidation state and coordinated to two perpendicular tridentate pda^{2-} ligands. The geometry around the M^{3+} ion is distorted octahedral.

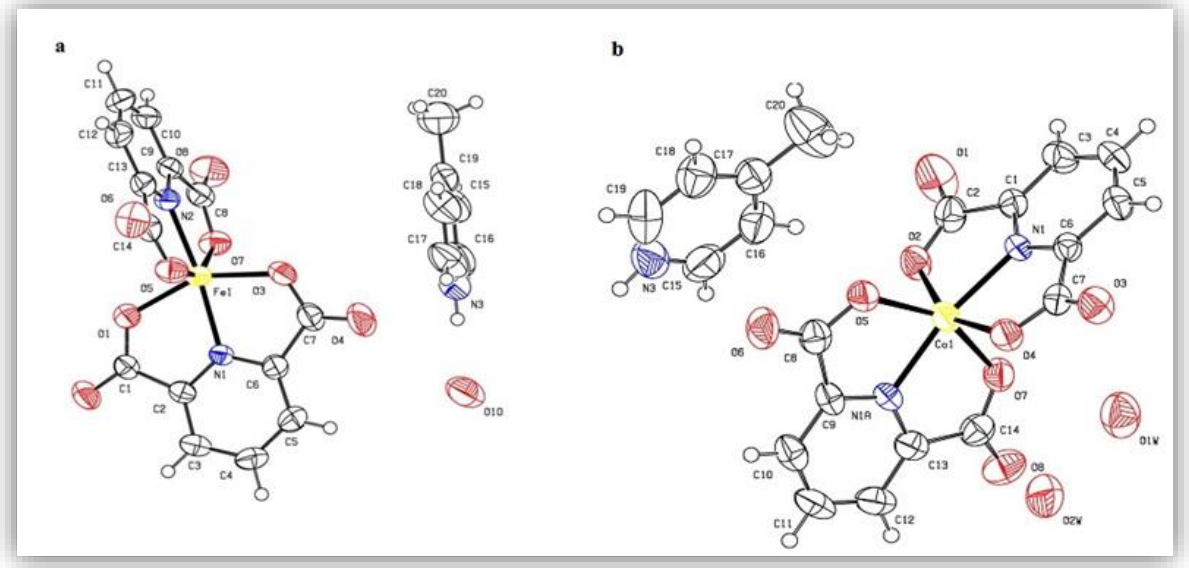

Fig. 4. ORTEP views of the complexes (a) **2** and (b) **3**.

The axial positions are occupied by pyridine nitrogen atoms N1 and N2, with bond lengths Fe1–N1 = 2.058, Fe1–N2 = 2.060 Å (**2**) and Co1–N1 = 2.056(3), Co1–N1A = 2.052(3) (**3**) while the equatorial plane is constructed by four carboxylic groups, with Fe–O bond distances ranging from 2.0030(17) to 2.0092(17) (**2**) and Co–O, from 1.998(3) to 2.034(3) (**3**) Å. The presence of picolinium cation $[4\text{–pic–H}]^+$ shows that the proton transfer process helps the formation of M(III) complex. The M–O and M–N bond distances also support the +3 oxidation state of metal ion. In the molecular structure of the complexes, H_2pda are joined to the metal ion centre in its dianionic form (pda^{2-}), resulting in monoanionic complexes. The

N1–Co1–N1A and N1–Fe1–N2 angle deviate from linear to 169.02 and 168.99(8)°, in **2** and **3**, respectively, confirming the coordination geometry around M(III) atom as distorted octahedral (**Fig. 5)**. The value of the O4–Co1–O2, O7–Co1–O5 angles are 151.96 and 151.51°, and the O3–Fe1–O1, O7–Fe1–O5 angles are 151.68(7) and 151.28(7)°, respectively, which are much deviated from the expected (180°) angle for the perfect planarity, indicating that the four oxygen atoms of the carboxylic groups of two pda^{2-} moieties are not planar. In complexes (**2** and **3**), $[4–pic–H]^+$ cation, $[M(pda)_2]^-$ anion and two uncoordinated H_2O molecules are joined through H-bonds (N–H···O and O–H···O bond lengths vary from 1.811 to 2.989 Å), which are shown in **Fig 6**.

The N–H···O hydrogen bonds exist between pyridine nitrogen atom (N3) of $[4–pic–H]^+$ cation and uncoordinated water molecules. The O–H···O hydrogen bonds are located between uncoordinated water molecules as donor atoms and oxygen acceptor atoms from carboxylate groups of $[M(pda)_2]^-$ anions or neighbouring water molecules **(Fig. 5)**. Selected bond lengths and angles for **2** and **3** are given in **Table 2**.

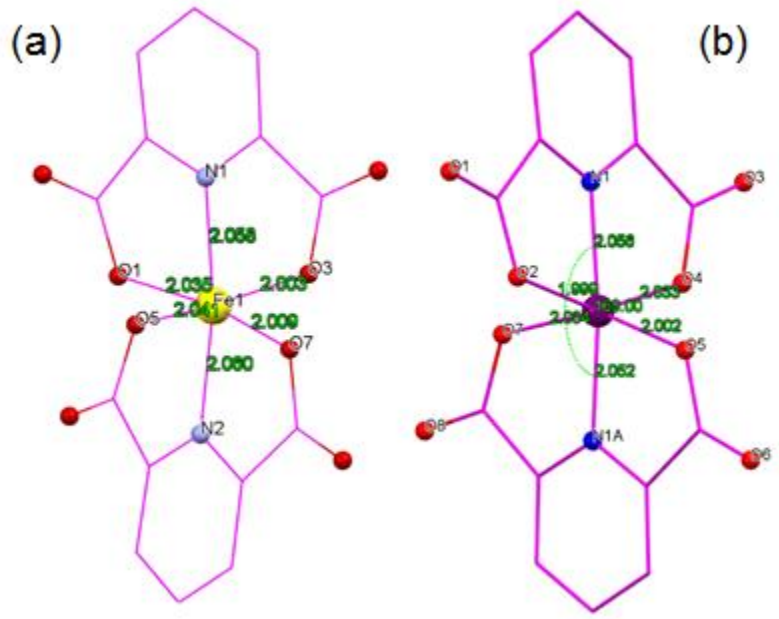

Fig. 5. Selected bond lengths and angle of the complexes (a) **2** and (b) **3**.

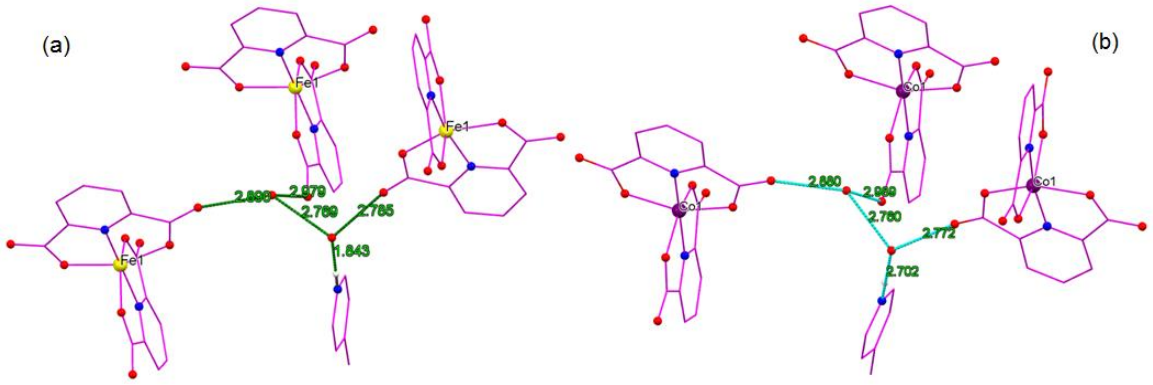

Fig. 6(a). The extensive H-bonding (shown by dotted lines C─H…O) in (**a**) **2** and (**b**) **3**.

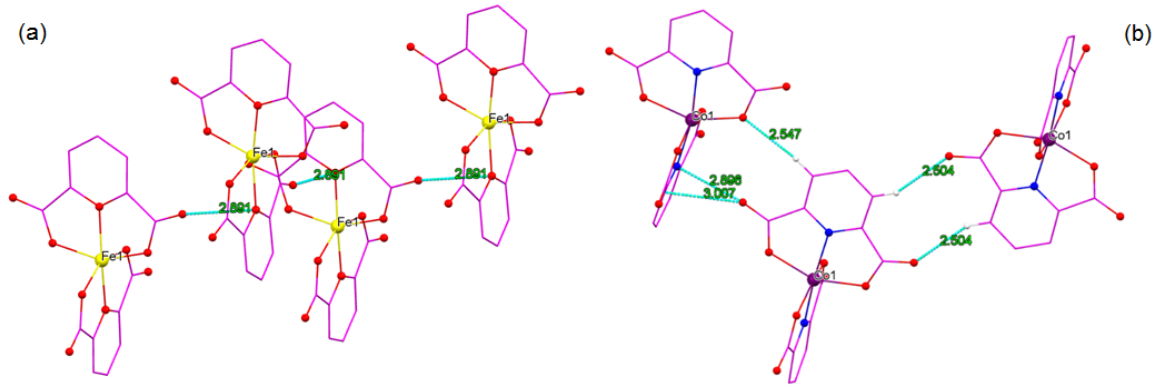

Fig. 6(b). The extensive H-bonding (shown by dotted lines O–H···O) in (a) **2** and (b) **3**.

Table 2. Selected bond lengths (Å) and bond angles (°) of the complexes (**2** and **3**).

Complex **2**		Complex **3**	
Bond lengths (Å)			
O1–Fe1	2.0347(17)	O2–Co1	1.998(3)
O7–Fe1	2.0092(17)	O4–Co1	2.033(3)
O3–Fe1	2.0030(17)	O5–Co1	2.003(3)
O5– Fe1	2.0403(18)	O7–Co1	2.034(3)
N1–Fe1	2.058(2)	N1–Co1	2.056(3)
N2–Fe1	2.061(2)	N1A–Co1	2.052(3)
Bond angles (°)			
O3–Fe1–O7	92.83(8)	C6 –N1–Co1	119.6(3)
O3–Fe1–O1	151.68(7)	C1–N1–Co1	118.0(3)
O7–Fe1–O1	95.24(8)	C9–N1A–Co1	118.4(3)
O3–Fe1–O5	92.29(8)	C13–N1A–Co1	118.9(3)
O7–Fe1–O5	151.28(7)	C2–O2–Co1	120.3(3)
O1–Fe1–O5	93.52(8)	O2–Co1–O5	92.82(13)
O3–Fe1–N1	76.46(7)	O2–Co1–O4	151.97(12)
O7–Fe1–N1	114.36(7)	O5–Co1–O4	95.17(13)
O1–Fe1–N1	75.48(7)	O2–Co1–N1A	106.61(12)
O5–Fe1–N2	75.28(7)	O5–Co1–N1A	76.14(13)
N1–Fe1–N2	168.99(8)	O7–Co1–N1A	75.55(13)

Thermogravimetric analysis (TGA)

TGA was carried out for polycrystalline samples of complexes (**1**–**3**) as shown in **Fig. 7** in 25–800 °C temperature range. Thermal stability of the complex has provided enough information regarding stoichiometry. The thermal fragmentation was examined in a nitrogen atmosphere with the heating rate of 20 °C/minute. The thermograms of the complexes (**1**–**3**) shows the release of two water molecules and one 4-pic moiety between the temperature range 25 to 130 °C (found 25%, calculated 26%) [37]. Further, as the temperature increases above 400 °C, elimination of one H_2pda moiety from the complexes takes place. The final residual product appears to be [M(pda)] [37,38].

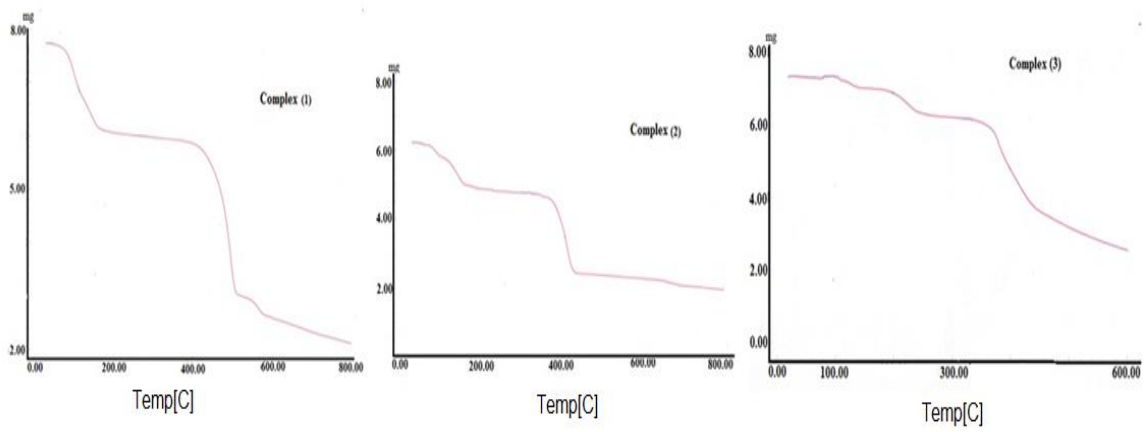

Fig. 7. Thermogravimetric analysis (TGA) of the complexes (**1-3**).

Cyclic voltammetric studies

The cyclic voltammograms of the complexes (**1**–**3**) for the electrochemical redox properties in the potential range +1.0 to –1.0 V with reference to Ag/AgCl electrode at 27 °C in the presence of $[^{n}Bu_4N]\cdot ClO_4$ were recorded at 200 Vs^{-1} scan rate to investigate the changes in oxidation state of metal ions in solution. Complexes (**1**–**3**) show nearly similar electrochemical behaviour and show two cathodic and one anodic peak [**Fig. 8**]

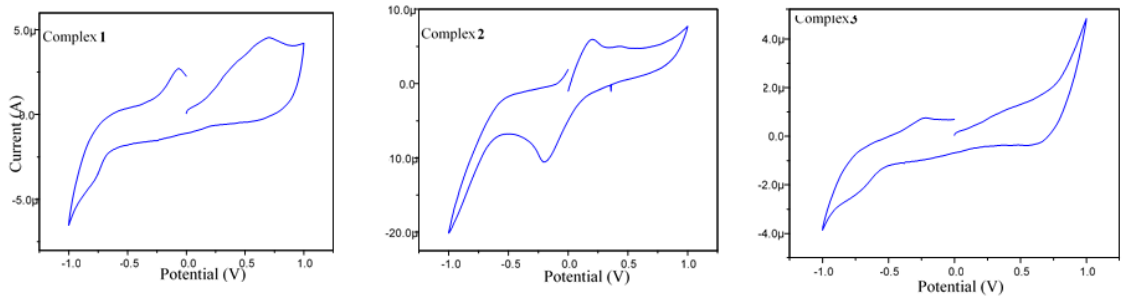

Fig. 8. Cyclic voltammogram for complex (**1**–**3**).

One of the cathodic peaks couples with the anodic peak to form a quasi reversible redox couple at $E^{0}_{1/2}$ = 0.34 V (**1**), 0.37 V (**2**) and 0.33 V (**3**) [39]. An additional cathodic peak in all the complexes are consistence with irreversible reaction in solution [40,41].

Magnetic studies

Magnetic study was performed to investigate the paramagnetic behaviour of the complex. Magnetic susceptibility is measured using a very sensitive instrument known as a magnetic susceptibility balance. The balance contains a pair of magnets mounted at opposite ends of the beam, initially in equilibrium. When a sample is introduce into the balance, a disruption of the magnetic field results. A current through a coil located between the poles of the second pair of magnets returns the beam to equilibrium. The current through the coil is measured and transferred into ta numerical reading. Diamagnetic materials are weakly repelled by an external magnetic field, resulting in a negative reading. Paramagnetic materials are attracted to an external magnetic field and give a positive reading.

The magnetic moment of the complexes was calculated using by the formula as follows:

$$\chi_{g=}\, LC_{bal}(R-Ro)/10^{9}(m)$$

L = height of sample in tube in units of centimetres

m = mass of the sample in units of grams

R = reading for tube plus sample

R_o = reading for the empty tube

C_{bal} = balance calibration constant = 1.0

The molar magnetic susceptibility is then calculated from the gram magnetic susceptibility using the following equation

$\chi_m = \chi_g$.(molar mass),

$\chi_A = \chi_m$ – diamagnetic correction, and

The magnetic susceptibility for a particular substance is not particularly useful in itself. However, the effective magnetic moment for a particular substance can be calculated from the gram magnetic susceptibility using the following equation.

$$\mu_{eff} = 2.283\sqrt{\chi_A.T}$$

{χ_g magnetic susceptibility erg.G^{-2}.gm^{-1}, χ_m molar susceptibility erg.G^{-2}.mol^{-1}, and μ_{eff} effective magnetic moment B. M.}.

Magnetic data indicate that μ_{eff} for the complexes 4.1 (**1**), 6.2 (**2**) and 5.1 (**3**) BM is suggestive of highly paramagnetic behaviour of the complexes. It is clear from magnetic data that Cr^{+3} ($t^3_{2g}e_g^0$) (**1**), Fe^{+3} ($t^3_{2g}e_g^2$) (**2**) and Co^{+3} ($t^4_{2g}e_g^2$) (**3**) are high spin configurations having +3 oxidation state [42-44].

Biological activities

Antioxidant (free radical scavenging) properties

DPPH free radical scavenging activity is very suitable and significant method for the evaluation of antioxidant activity because DPPH is a stable free radical that accepts a hydrogen free radical and becomes a stable diamagnetic molecule [18]. The reducing properties are associated with the antioxidant activity. After 100 minutes reaction, colour changes from violet to yellow which gives λ_{max} at 515 nm (absorbance of the sample and control = 1.63 and 2.39, respectively) (**Fig. 9)**, revealing that some antioxidants are present in the solution. **3** exhibited 32% anti-oxidant activity. This activity can be attributed to the fact that chelating agents are effective as secondary antioxidants because they can reduce the redox potential thereby stabilizing the oxidized form of the metal ion [45].

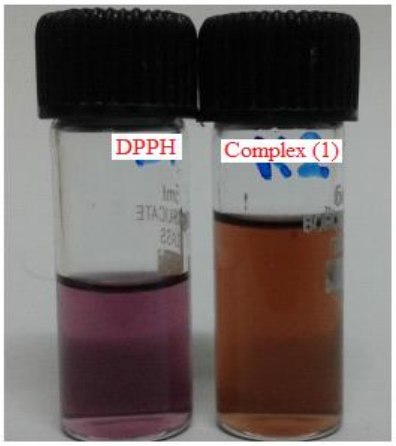

Fig. 9. DPPH assay of the complex (**3**)

Additionally, hydrogen peroxide assay was also used to investigate the antioxidant property of **3**. The hydrogen peroxide radicals are the most reactive among all oxygen containing reactive species used for the estimation of antioxidant properties of the compound during aerobic metabolism [46]. The hydrogen peroxide scavenging activity result was in good agreement with DPPH free radical scavenging assay.

Molecular docking studies

The designing of molecules can lead to the recognition of specific sequences and structures of nucleic acids and plays an important role in the development of new chemotherapeutic drugs. Molecular docking studies have played a very significant role in understanding the drug–DNA interaction in the rational drug design, as well as in the mechanistic study by placing a small molecule into the binding site of the DNA target specific region mainly in a non-covalent fashion, which predicts interactions between the drug molecules and the nucleic acids of DNA. Conformation of docked complexes was analyzed in terms of energy, hydrogen bonding, and hydrophobic interaction between complexes and DNA. Targeting the DNA minor groove for a small molecule has long been regarded as an important pattern in molecular recognition of a specific DNA sequence [47]. The energetically favourable docked poses obtained from the rigid molecular docking of the complexes (**2** and **3**) with a DNA duplex of sequence d(CGCGAATTCGCG)$_2$ dodecamer (PDB ID: 1BNA) are shown in **figures 10 (a** and **b)**. Obviously, complexes (**2** and **3**) fit snugly into the curved contour of the DNA target in the minor groove and are situated within the G–C rich region. It is well known that the interactions of chemical species with the minor groove of B-DNA differ from those occurring in the major groove, both in terms of electrostatic potential and steric effects, because of the narrow shape of the former. Small molecules interact with the minor groove, while large molecules tend to recognize the major groove binding site [48]. The results of molecular docking show that complexes (**2** and **3**) bind efficiently with the DNA receptor (in minor groove) and exhibit free energy of binding (FEB) values of –314 (**2**) and –276.8 kcal mol^{-1} **(3)**. The more negative relative binding energy of complex **2** indicated its strong binding ability to the DNA compared to complex **3** [49].

The mechanism of binding can also be better understood by the docking results. As illustrated in the **figure 10 (a** and **b)**, the carbonyl oxygen and lattice water molecule of the complexes displayed a strong hydrogen-bonding interaction with DNA bases [49]. The compounds exhibited stabilization through hydrophobic and Vander Waals interactions with nearby nucleotides. The results of the docking studies reveal that compounds fit in the minor groove region of B-DNA. The compound **2** forms two hydrogen bonds with B-DNA at G10/G12 (**2**) [N2 (G10)···O8 = 3.110 A, N2(G12)···O4 = 2.690 Å], while compound **3** forms only one hydrogen bond at A17/G16 [O3′(G16/A17)...OW = 1.993 Å]. This also indicates that **2** has stronger interactions with the B-DNA as compared to **3**.

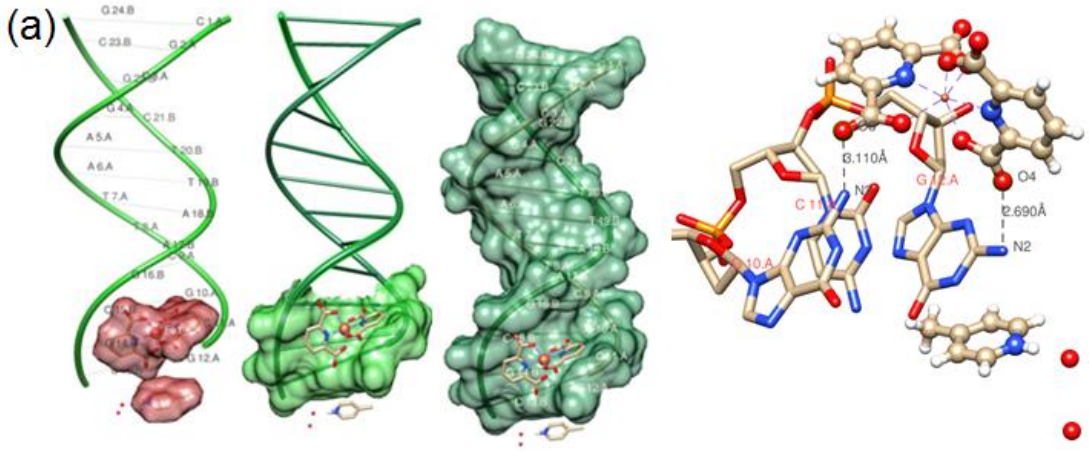

Fig. 10(a). Molecular docked model of the complex (**2**) and showing H-bonding interaction of **2** with B-DNA.

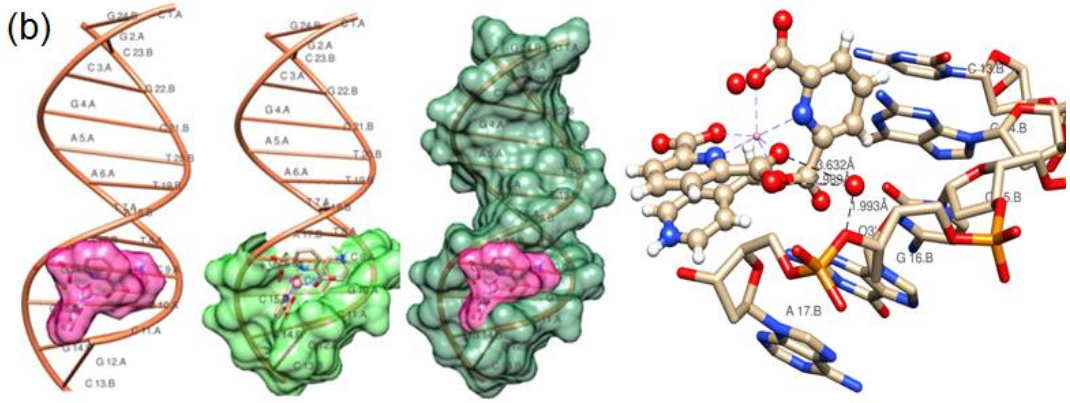

Fig. 10(b). Molecular docked model of the complex (**2**) and showing H-bonding interaction of **2** with B-DNA.

Conclusions

A series of novel proton transfer complexes bearing composition [4–pic–H][M(pda)$_2$]·2H$_2$O [M = Cr^{3+} **(1)**, Fe^{3+} **(2)** and Co^{3+} **(3)**] using pyridine–2,6–dicarboxylic acid (H_2pda) as a proton donor and 4–picoline (4–pic) as a proton acceptor has been synthesized and characterized using FT–IR, ^{1}H and ^{13}C NMR, ESI Mass, EPR, UV–Visible and fluorescence spectral studies. Single crystal X–ray crystallographic data of **2** and **3** ascertained the structure and binding modes of the ligand. The pda^{2-} ligand binds the metal ion in dianionic tridentate [N,O,O] form resulting in distorted octahedral geometry around the M^{3+} ion. ESI and thermal studies confirmed the presence of cation [4–pic–H], anion $[M(pda)_2]^-$ and two lattice water molecules. Cyclic voltammetric studies indicate the presence of quasi-reversible redox couple in solution. DPPH and hydrogen peroxide scavenging study confirmed the antioxidant property of the complexes. The results of molecular docking show that complexes **2** and **3** bind efficiently with the DNA receptor and exhibit free energy of binding (FEB) values of –314 (**2**) and –276.8 kcal mol^{-1} (**3**), respectively. The docking data exhibits that **2** has stronger binding ability to the DNA (1BNA) compared to that of **3**.

References

[1] S.R. Baten, B.F. Hoskins, R. Robson, J. Am. Chem. Soc., 117 (1995) 5385.

[2] B. F. Hoskins, R. Robson, J. Am. Chem. Soc., 112 (1990) 1546.

[3] D. Min, S.S. Yoon, D.Y. Jung, C.Y. Lee, Y. Kim, W.S. Han, S.W. Lee, Inorg. Chim. Acta., 324 (2001) 293.

[4] L.M. Sayre, G. Perry, M.A. Smith, Chem. Res. Toxicol., 21 (2008) 172.

[5] G. Gregoire, C. Jouvet, C. Dedonderand, A.L. Sobolewski, J. Chem. Phys., 324 (2006) 398.

[6] U. Casellato, R. Graziani, P.R. Bonomo, A.J. D. Bilio, Chem. Soc. Dalton Trans. (1991) 23.

[7] W. Furst, P. Gouzerh, J.Y. Jeannin, Coord. Chem., 8 (1979) 237.

[8] Y.E. Alexeev, B.I. Kharisov, T.C. Hermandez, A.D. Garnovski, Coord. Chem. Rev., 254 (2010) 794.

[9] Z.A. Siddiqi, P.K. Sharma, M. Shahid, M. Khalid, S. Kumar, J. of Mol. Structure., 994 (2011) 295.

[10] H.E. Hosseini, M. Mirzaei, Mendeleev Commun., 22 (2012) 323.

[11] J.D. Ranford, P.J. Sadler, D.A. Toucher, J. Chem. Soc. Dalton Trans., 64 (1993) 3393.

[12] (a) D.R. Weyna, T. Shattock, P. Vishweshwar, M.J. Zaworotko, Cryst. Growth Des. 9 (2009) 1106. (b) S. Jin, L. Liu, D. Wang, J. Guo, J. Mol. Struct., 1005 (2011) 59.

[13] Z.A. Siddiqi, A. Siddique, M. Shahid, M. Khalid, P.K. Sharma, Anjuli, M. Ahmad, S. Kumar, Y. Lan, A.K. Powell, Dalton Trans., 42 (2013) 9513; I.A. Ansari, F. Sama, M. Shahid, M. Khalid, P.K. Sharma, M. Ahmad, Z.A. Siddiqi, J Inorg Organomet Polym 26 (2016) 178; M. Shahid, A. Siddique, I.A. Ansari, F. Sama, S. Chibber, M. Khalid, Z.A. Siddiqi, M.S.H. Faizi, J. Coord. Chem., 68 (2015) 848.

[14] M. Mirzaei, H. Aghabozorg, H.E. Hosseini, J. Iran. Chem. Soc., 8 (2011) 580.

[15] K.M. Dethlefs, P. Hobza, Chem. Rev., 100 (2000) 143.

[16] Z.A. Siddiqi, M. Khalid, M. Shahid, S. Kumar, P.K. Sharma, A. Siddique, Anjuli, J. of Mol. Structure., 1033 (2013) 98.

[17] Zhou, K., Yu, L. Effects of extraction solvent on wheat bran antioxidant activity estimation. LWT–Food Sci. Tech. Leb., 37 (2004) 717.

[18] Loo, A.Y., Jain, K., Darah, I. Antioxidant and radical scavenging activities of the pyroligneous acid from a mangrove plant, Rhizophor piculata. Food Chem., 104 (2007) 300.

[19] Ruch, R.J., Cheng, S.J., Klaininig, J.E. Prevention of cytotoxicity and inhibition of intracellular communication by antioxidant catechins isolated from Chinese green tea. Carcinogen, 10 (1980) 1003.

[20] D.W. Ritche, V. Venkataraman, Bioinformatics, 26 (2010) 2398.

[21] International Tables for X-ray Crystallography, Kynoch Press, Birmingham, England IV, 1974.

[22] SMART & SAINT Software Reference manuals, Version 6.45, Bruker Analytical X-ray Systems, Inc., Madison, WI (2003).

[23] G. M. Sheldrick, SADABS, software for empirical absorption correction, Ver. 2.05, University of Göttingen, Göttingen, Germany (2002).

[24] XPREP, version 5.1; Siemens Industrial Automation Inc.: Madison, WI, (1995).

[25] G. M. Sheldrick, SHELXL97, Program for Crystal Structure Refinement, University of Göttingen, Göttingen, Germany (2008).

[26] A. Altomare, M.C. Burla, M. Camalli, G.L. Cascarano, C. Giacovazzo, A. Guagliardi, A.G.G. Moliterni, G. Polidori, R.J. Spagna, J. Appl. Crystallogr., 32 (1999) 115.

[27] P. Laine, A. Gourdon, J.P. Launay, Inorg. Chem., 34 (1995) 5129.

[28] G.B. Deacon, R. J. Philips, Coord. Chem. Rev., 33 (1980) 227.

[29] Z.A. Siddiqi, M. Shahid, S. Kumar, M. Khalid, S. Noor, J. Organomet. Chem., 694 (2009) 3768.

[30] J. Stare, J. Mavri, J. Grdadolnik, J. Zidar, Z.B. Maksic, R. Vianello, J. Phys. Chem. B, 115 (2011) 5999.

[31] L.J. Bellamy, the Infrared Spectra of Complex Molecule, John Wiley & Sons, New York, (1971).

[32] K. Nakamoto Infrared and Raman Spectra of Inorganic and Coordination Compounds, Wiley-Interscience, New York Publication, 191 (1886).

[33] Z.A. Siddiqi, S. Kumar, M. Khalid, M. Shahid, Spectrochim. Acta Part A, 72 (2009) 616.

[34] A.C.G. Baro, R.P. Diez, E.O.E. Piro, B.S.P. Costa, Polyhedron, 27 (2008) 502.

[35] Z.A. Siddiqi, M.M. Khan, M. Khalid, S. Kumar, Trans. Met., Chem., 32 (2007) 927.

[36] A.B.P. Lever, Inorganic Electronic Spectroscopy, Elsevier, Amsterdam, (1984).

[37] A.A.A. Emara, F.S.M. Abd EI-Hameed, S.M.E. Khalil, Phosphorus Sulphur Silicon, 114 (1996).

[38] Z.A. Siddiqi, P.K. Sharma, M. Shahid, S. Kumar, Anjuli, A. Siddique, Spectrochim. Acta Part A., 93 (2012) 280.

[39] J.P. Battioni, D. Lexa, D. Mansuy, J.M. Seveant, J. Am. Chem. Soc., 105 (1983) 207.

[40] Z.A. Siddiqi, M. Shahid, M. Khalid, S. Noor, S. Kumar, Spectrochim. Acta Part A., 74 (2009) 391.

[41] C.D. Samara, P.D. Janakoudakis, D.P. Kessissaglou, G.E. Manoyussakis, D. Mentzapfos, A. Terzis, J. Chem. Soc., Dalton Trans. (1992) 3259.

[42] B.N. Figgis, J. Lewis, In Lewis, R.G. Wilkins, Eds. Modern Coordination Chemistry. Interscience Publishers Inc. New York, 400 (1960).

[43] R.J. Angelici, W.B. Saunders, synthesis and technique in inorganic chemistry, 198 (1977).

[44] C.E. Housecroft, A.G. Sharpe, Pearson Education Limited, Inorg. Chem., 3 (2008).

[45] Yin, J., Heo, S., Wang, M. Antioxidant and antidiabetic activities of extracts from Cirsium japonicum roots. Nutrition Res. Prac., 2 (2008) 247.

[46] Waling, C. Fenton's reagent revisited. Acc. Chem. Res., 8 (1975) 125.

[47] Rohs, I. Bloch, H. Sklenar, Z. Shakked, Nucleic Acids Res., 33 (2005) 7048.

[48] R. Corradini, S. Sforza, T. Tedeshi, R. Marchelli, Chirality, 19 (2007) 269.

[49] P. Yang and M. Guo, Met.-Based Drugs, 5 (1998) 41.

Chapter 4

Synthesis, spectroscopic analysis and X-ray crystal structures of cis-μ-1,2-peroxo dicobalt(III) complexes

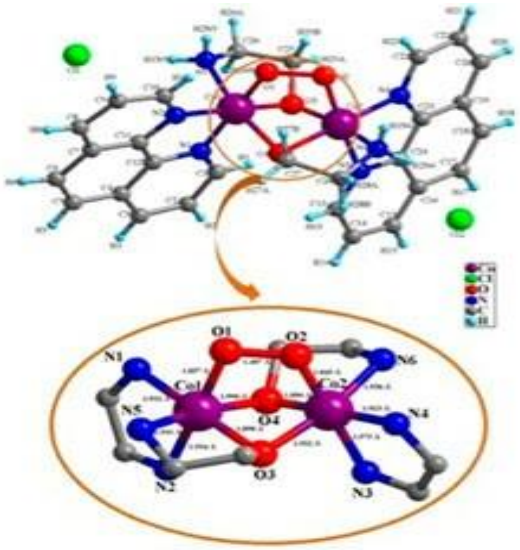

Introduction

Dioxygen-bridged polynuclear metal complexes have attracted attention [1,2] of coordination and bio-inorganic chemists, owing to their potential applications in biological copper metalloproteins such as in dioxygen carrying hemocyanins in arthropods and mollusks [3–5]. Dioxygen-iron(III) complex was implicated as intermediate in the mechanisms of oxygen activating biomolecules such as cytochrome P450 and heme oxygenase [6,7]. Peroxo-iron(III) and copper(II) species were proposed in mimicking the dioxygen activation by simple iron(III) [8–11] and copper(II) compounds [12–18]. A number of dioxygen-bridged coordination compounds have been reported in which the bridging dioxygen is generally a peroxide ion [19], but there are also some reports providing the binding of superoxide as bridging ligand [20–22]. Dicobalt(III) complexes involving peroxide (O_2^{2-}) [19,23,24] or superoxide as the only bridging unit were crystallographically characterized [25–29]. But other dioxygen-bridged dicobalt complexes also had an additional μ-amido or μ- hydroxo bridge [30–32]. In these doubly bridged dicobalt complexes, the resulting five-membered rings were almost flat.

The nature of the O–O bond in dinuclear cobalt complexes was the subject of much controversy. X-ray diffraction, vibrational, and EPR spectroscopic studies eventually allowed the distinction to be made between superoxo and peroxo ligands. There are four dioxygen (peroxo or superoxo) metal-binding coordination modes found in the bridged dinuclear compounds, trans- and cis-μ-η^1: η^1 – (end-on), μ-η^2: η^2 – (side-on), and μ-η^1 : η^2 – (end-on/side-on) bridging (**scheme 1**) [5, 24].

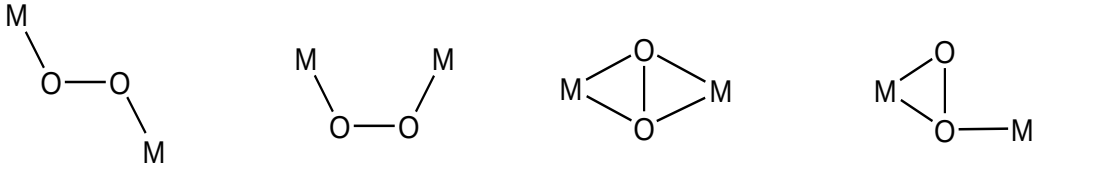

Scheme 1. Coordination modes found in the bridged dinuclear compounds.

While the trans-end-on bridging mode was found in a number of Cu(II), Fe(III), and Co(III) complexes [5,15,23], the corresponding cis-end-on bridging mode was found only in complexes where the two metal centers are simultaneously doubly bridged by a peroxide and another bridging ligand such as OH^{-}, O_2^{-}, NH_2^{-}, $S_2O_3^{2-}$, CH_3COO^{-}, $phCOO^{-}$, $phCH_2^{-}COO^{-}$, and α-D-glucopyranosyl-(14)-D-glucose [5,8–10, 23, 24]. μ_4-bridging peroxo was found in high-nuclearity cluster compounds [33–36]. Flexible amino alcohols are versatile ligands to generate di- and tetra-nuclear-bridged cobalt complexes [37]. Mixed ligand complexes of cobalt with amino alcohols (such as diethanol amine and propanol amine) and α-diimine chelator involving alkoxo or hydroxo bridging have recently been reported by our group [37]. However, dicobalt complexes of ethanolamine (Hea) with cis-μ-1,2 binding of bridged peroxide ion consisting of a chelator (Phen or Bipy) are not known to the best of our knowledge. Moreover, since for medicinal uses, any compound is tested first for its toxicity or side effects, genotoxic studies have also been examined for the compounds.

Experimental

Materials

All the reagents used were of analytical grade. Ethanolamine (E. Merck), 1,10-phenanthroline (Aldrich) and 2,2′-bipyridine (Aldrich) were used as received while metal salts were recrystallized and solvents were purified by standard procedures before use [38].

Physico-chemical methods and instrumentation

IR spectra were recorded on a Perkin-Elmer spectrum GX automatic recording spectrophotometer as KBr disc. ^{1}H and ^{13}C NMR spectra of compounds dissolved in CD_3OD were recorded on a Brucker DRC-300 spectrometer using $SiMe_4$ (TMS) as internal standard. Microanalysis for C, H and N were obtained from Microanalytical Laboratories, CDRI, Lucknow. Thermal gravimetric analysis (TGA) data was measured from room temperature upto 600 °C at a heating rate of 20 °C/min. The data were obtained using a Shimadzu TGA-50H instrument.

Crystallographic data collection and structure analysis

Single crystal X-ray data of **1** and **2** were collected at 100 K on a Bruker SMART APEX CCD diffractometer using graphite monochromated MoK_α radiation (λ = 0.71073 Å). The linear absorption coefficients, scattering factors for the atoms, and the anomalous dispersion corrections were taken from the International Tables for X-ray Crystallography [39]. The data integration and reduction were carried out with SAINT [40] software. Empirical absorption correction was applied to the collected reflections with SADABS [41] and the space group was determined using XPREP [42]. Several DFIX command has been given to fix the bond length parameters. The structure was solved by the direct methods using SHELXTL-97 [43] and refined on F^2 by full-matrix least-squares using the SHELXL-97 [44] program package. All non-hydrogen atoms were refined anisotropically. For **1**, squeeze refinement has been performed using PLATON that shows five and half water molecules per formula weight. The contribution of both the hydrogen atoms and the oxygen atoms have been incorporated in

both the empirical formula and formula weight in **Table 1**. Pertinent crystallographic data for the compounds are summarized in **Tables 1** and **2**.

Table 1. Crystal data with refinement parameters for the complexes **1** and **2**.

	Complex **1**	Complex **2**
Empirical formula	$C_{28}H_{39}Cl_2Co_2N_6O_{9.5}$	$C_{24}H_{32}Co_2N_8O_{12}$
Formula wt.	800.40	742.44
Crystal system	Triclinic	Monoclinic
Space group	P-1	P 2_1/c
a, Å	11.5852(18)	12.1158(8)
b, Å	12.621(2)	18.6341(12)
c, Å	13.011(2)	14.3254(10)
α (°)	64.663(3)	90
β (°)	74.819(3)	110.778(2)
γ (°)	80.711(2)	90
U, Å^3	1656.8(4)	3023.9(3)
Z	2	4
ρ_{calc} g/m^3	1.406	1.631
μ, mm^{-1}	1.203	1.631
F(000)	716	1528
Refl. collected	8488	5307
Independent refl.	5725	3703
GOF	1.093	1.032
Final R indices	R_1 = 0.0692	R_1 = 0.0745
[$I>2\sigma(I)$]	wR_2 = 0.2252	wR_2 = 0.1019
R indices	R_1 = 0.0929	R_1 = 0.0420
(all data)	wR_2 = 0.2457	wR_2 = 0.0894

Table 2. Selected bond distances (Å) and angles (°) of **1** and **2**.

	Complex **1**				Complex **2**		
Bond lengths				Bond lengths			
Co1-O1	1.857(4)	Co2-O2	1.845(4)	Co1-O1	1.841(2)	Co2-O2	1.853(2)
Co1-O3	1.898(5)	Co2-O3	1.922(5)	Co1-O3	1.895(2)	Co2-O3	1.918(2)
Co1-O4	1.906(4)	Co2-O4	1.890(5)	Co1-O4	1.914(2)	Co2-O4	1.893(2)
Co1-N1	1.932(6)	Co2-N3	1.975(5)	Co1-N1	1.912(3)	Co2-N3	1.916(3)
Co1-N2	1.934(6)	Co2-N4	1.923(6)	Co1-N2	1.950(3)	Co2-N4	1.948(3)
Co1-N5	1.941(7)	Co2-N6	1.936(5)	Co1-N5	1.926(3)	Co2-N6	1.930(3)
O1-O2	1.487(6)	Co1-Co2	2.731(12)	O-O2	1.462(3)	Co1-Co2	2.7426(6)
Bond Angles							
O1-Co1-O3	91.7(2)	O2-Co2-O4	92.89(18)	O1-Co1-O3	92.29(9)	O2-Co2-O4	92.39(9)
O1-Co1-O4	87.69(19)	O4-Co2-O3	80.6(2)	O1-Co1-O4	88.43(9)	O4-Co2-O3	79.25(9)
O3-Co1-O4	80.77(19)	O4-Co2-N4	91.58(19)	O3-Co1-O4	79.29(9)	O4-Co2-N4	93.94(10)
O1-Co1-N2	174.2(3)	O2-Co2-N3	91.5(2)	O1-Co1-N2	173.42(11)	O2-Co2-N3	91.14(11)
O3-Co1-N2	92.5(3)	O3-Co2-N3	100.7(3)	O3-Co1-N2	94.27(11)	O3-Co2-N3	87.81(9)
O4-Co1-N2	89.1(2)	O2-Co2-N6	89.4(2)	O4-Co1-N2	92.24(10)	O2-Co2-N6	89.71(11)
O1-Co1- N5	91.0(3)	O3-Co2-N6	167.0(2)	O1-Co1-N5	88.69(11)	O3-Co2-N6	166.13(10)
O3-Co1-N5	87.2(3)	N3-Co2-N6	91.9(3)	O3-Co1-N5	87.30(10)	N3-Co2-N6	93.46(11)
O4-Co1-N5	167.08(3)	O4-Co2-Co1	44.21(13)	O4-Co1-N5	166.16(10)	O4-Co2-Co1	44.22(6)
N2-Co1-N5	93.1(3)	N4-Co2-Co1	110.96(15)	N2-Co1-N5	92.17(11)	N4-Co2-Co1	114.81(8)
O3-Co1-N1	175.0(2)	O2-Co2-O4	92.89(18)	O3-Co1-N1	176.02(11)	O2-Co2-O4	92.39(9)
O4-Co1-N1	95.0(2)	O4-Co2-O3	80.6(2)	O4-Co1-N1	98.46(10)	O4-Co2-O3	79.25(9)
N2-Co1-N1	84.8(3)	O4-Co2-N4	91.58 (19)	N2-Co1-N1	82.50(12)	O4-Co2-N4	93.94(10)
O2-Co2-O3	87.13(19)	O2 -Co2-Co1	70.32(13)	O2-Co2-O3	87.81(9)	O2-Co2-Co1	69.33(7)
O2-Co2-N4	174.4(2)	O3-Co2-Co1	44.09(15)	O2-Co2-N4	173.57(11)	O3-Co2-Co1	43.68(6)
O3-Co2-N4	90.2(2)	N3-Co2-Co1	138.92(19)	O3-Co2-N4	92.23(10)	N3-Co2-Co1	137.06(8)
O4-Co2-N3	175.3(2)	O2-Co2-O3	87.13(19)	O4-Co2-N3	176.41(11)	O2-Co2-O3	87.81(9)
N4-Co2-N3	84.1(2)	O2-Co2-N4	174.4(2)	N4-Co2-N3	82.52(11)	O2-Co2-N4	173.57(11)
O4-Co2-N6	87.1(2)	O3-Co2-N4	90.3(2)	O4-Co2-N6	87.23(10)	O3-Co2-N4	92.23(10)
N4 -Co2-N6	94.2(2)	O2-Co2-Co1	70.32(13)	N4-Co2-N6	91.75(11)	O2-Co2-Co1	69.33(7)
O2- Co2-O3	87.13(19)	O3-Co2-Co1	44.02(15)	O2-Co2-O3	87.81(9)	O3-Co2-Co1	43.68(6)

Cyclic voltammetric studies

Cyclic voltammetry (CV) was performed on EG&G PAR 273 Potentiostat/Galvanostat and an IBM PS2 computer along with EG&G M270 software to carry out the experiments and to acquire the data. The three-electrode cell configuration comprised of, a platinum sphere, a platinum plate and Ag(s)/$AgNO_3$ were used as working, auxiliary and reference electrodes, respectively. The supporting electrolyte used was $[^nBu_4N]ClO_4$. Platinum sphere electrode was sonicated for 2 min in dilute nitric acid, dilute hydrazine hydrate and then in double-distilled water to remove the impurities. The solution was deoxygenated by bubbling research grade nitrogen gas and an atmosphere of nitrogen was maintained over the solution during measurements.

Biology

Treatment of plasmid pUC19 DNA with compound

Reaction mixture (50 µl) contained 10 mM Tris-HCl (pH 7.5), 0.5 µg plasmid pUC19 DNA and varied concentration of **1**. Oxidative stress generated by compound with increase in concentration was determined. Incubation was performed at 4 ºC for 2 hour. After incubation, 30 µl of a solution containing 40 mM EDTA, 0.05 % bromophenol blue tracking dye and 50 % (v/v) glycerol was added and the solution was subjected to electrophoresis at 50 V in submarine 1 % agarose gel. Ethidium bromide stained gel was then viewed and photographed on a UV-trans illuminator.

Isolation of lymphocytes

Heparinized blood samples (3 ml) from a single healthy donor was obtained by venepuncture and diluted suitably in Ca^{2+} and Mg^{2+} free PBS of pH 7.5. Lymphocytes were isolated from blood using Histopaque 1077 and the cells were finally suspended in RPMI 1640 medium.

Treatment of Lymphocytes

Lymphocytes in a total reaction volume of 2ml were treated with varying concentration of **1**. Incubation was performed at 4 ºC for 2 hour, after the incubation the reaction was processed for comet assay [45].

Comet assay (single cell gel electrophoresis)

Comet assay was performed under alkaline conditions essentially according to the reported procedure [46] with slight modifications. Fully frosted microscopic slides pre-coated with 1.0 % normal melting agarose were used (dissolved in Ca^{+2} and Mg^{+2} free PBS of pH 7.5). Around 10 000 cells were mixed with 100 µl of 1.0 % low melting agarose to form a cell suspension and pipetted over the first layer and covered immediately by a cover slip. The slides were placed on a flat tray and kept on ice for 10 min to solidify the agarose. The cover slips were removed and a third layer of 0.5 % low melting agarose (100 µl) was pipetted. Cover slips were placed over it and it was allowed to solidify on ice for 5 min. The cover slips were removed and the slides were immersed in cold lysis solution containing 2.5 M NaCl, 100 mM EDTA and 10 mMTris, pH 10, 1 % Triton X-100 was added before use for a minimum of 1 h and 30 minutes at 4 ºC. After lysis, DNA was allowed to unwind for 20 min in alkaline electrophoretic solution consisting of 300 mMNaOH and 1mM EDTA, pH >13. Electrophoresis was performed at 4 ºC in field strength of 0.7 V/cm and 300 mA current. The slides were then neutralized with cold 0.4 M Tris, pH 7.5, stained with 75 µl ethidiumbromide (20 mg/ml) and covered with a cover slip. They were then placed in a humidified chamber to prevent drying of the gel and analyzed the same day. Slides were scored using an image analysis system (Komet 5.5; Kinetic Imaging, Liverpool, UK) attached to an Olympus (CX41) fluorescent microscope (Olympus Optical Co., Tokyo, Japan) and a COHU 4910-integrated CC camera (equipped with 510–560 nm excitation and 590 nm barrier filters) (COHU, San Diego, USA). Images from 50 cells (25 from each replicate slide) were analyzed. The parameter taken to assess lymphocytes DNA damage was tail length (migration of DNA from the nucleus in µ meter).

Synthesis

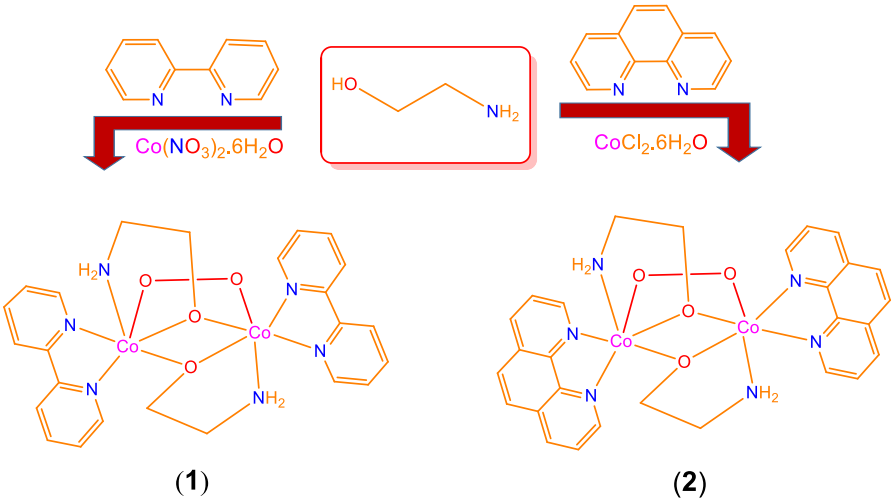

Scheme 1. Synthetic procedure of **1** and **2**.

Synthesis of {[Co_2(ea)$_2$(Phen)$_2$(O_2)]·5.5H_2O·2Cl} (1) and {[Co_2(ea)$_2$(Bipy)$_2$(O_2)]·2H_2O·2NO_3} (2)

All the reaction steps were carried out in aerobic conditions. Both **1** and **2** were prepared adopting similar procedure. An aqueous solution (10 mL) of $CoCl_2$·6H_2O or $Co(NO_3)_2$·6H_2O (5 mmol) was dropped to a stirred 1:1 mixture (clear solution) of the ligands Hea (5 mmol) and Phen or Bipy (5 mmol) taken in 20 mL methanol. The stirring was continued for 5 h at room temperature giving orange coloured solution. The resulting solution was kept in fridge giving beautiful orange colored cubic crystals of **1** and **2** after 2 days. These single crystals were suitable for X-ray crystallographic studies.

Complex (**1**): Yield = 59 %, Analytical data for $C_{28}H_{43}N_6O_{11.5}Co_2Cl$, Calculated (%): C = 41.94, H = 5.36, N = 10.48, Cl = 4.43; Observed (%): C = 41.87, H = 5.31, N = 10.41, Cl = 4.42.

Complex (**2**): Yield = 54 %, Analytical data for $C_{24}H_{32}N_8O_{12}Co_2$, Calculated (%): C = 38.83, H = 4.34, N = 15.09; Observed (%): C = 38.33, H = 4.31, N = 15.22.

Results and Discussion

FTIR, ^{1}H and ^{13}C NMR Spectra

The infrared spectra of **1** and **2** show a strong broad band at ~3350 cm^{-1} characteristic of the presence of lattice H_2O molecule(s) in the molecular unit [47]. The ligand (Hea) and its metal complexes are reported to exhibit broad bands in the range 3300-3350 cm^{-1} due to hydrogen bonded O–H bond stretching vibrations of unionized ethanolamine. This band is, however, absent in the present IR spectra of the present complexes indicating that the ligand binds the metal ions as an anionic moiety (ea^{-}). The band appearing at ~1000 cm^{-1} is characteristic of bridged υ(Co–O–Co) stretching vibrations in **1** and **2**. A considerable negative shift in υ(N–H) frequency in the complexes relative to that of the free ligand moiety indicates the additional coordination from the amino nitrogen. The ligand ea^{-}, therefore, acts as bridging ligand behaving as a bidentate [N,O] moiety. The peroxo O–O stretching frequency, ν(O–O) was observed as a medium intense band at 764 cm^{-1} (**1**) and 770 cm^{-1} (**2**), which is in the same range as that reported in structurally characterized dinuclear end-on bridged cobalt complexes [48]. The bands observed in the low frequency 450–550 cm^{-1} region are characteristic of M–N and M–O bond stretching vibrations [49]. The presence of the α-diimine i.e., Phen or Bipy in the complex moiety was ascertained from the appearance of characteristic υ(C=C) and υ(C=N) stretching vibrations.

^{1}H NMR spectrum of the complexes contained a resonance signal on the high field side (δ 3.0–3.5 ppm) arising from the skeleton CH_2 proton of the ligand (ea^{-}). However, the low field side (δ ~9.0 ppm) contained broad signal due to N–H proton resonance. The sharp well splitted resonance signals in 7.0–8.5 ppm region are characteristic of the aromatic protons of the α-diimine moiety. There is a considerable shift in the positions of the various signals compared to that of the uncomplexed ligands, which is not an uncommon behaviour because of the metal ion coordination [50]. The ^{13}C NMR spectra contained resonance signals in 35–43 and 125–155 ppm region due to the methylene (–CH_2–) and α-diimine (Phen or Bipy) carbons, respectively [51,52].

Crystal structures of {[$Co_2(ea)_2(Phen)_2(O_2)$]·$5.5H_2O$·2Cl} (1) and {[$Co_2(ea)_2(Bipy)_2(O_2)$]·$2H_2O$·$2NO_3$} (2)

Elemental analysis results were correlated well with the calculated values and confirmed the proposed stoichiometries of **1** and **2**. The complexes are stable in air and soluble in common organic solvents. Single-crystal X-ray diffraction study reveals that the **1**v crystallizes in the triclinic system with *P*-1 space group and **2** crystallizes in monoclinic system with $P2_1/c$ space group. The asymmetric unit of the complexes contains two crystallographically identical Co(III) metal ions, two Phen/Bipy ligands, one coordinated peroxide anion (bridged in cis manner), two coordinated ea^- and also two anions (chloride or nitrate) along with water molecules in the lattice [**Fig**. **1**(**a**) and (**b**)]. Crystal data with refinement parameters are given in **Table 1**. The selected bond lengths and bond angles for the molecule are provided in **Table 2**.

Each of the Co(III) atoms shows a distorted octahedral CoN_3O_3 coordination from two different oxygens of each of ligand, ea^- [Co–O = 1.890(4)–1.922(5) Å for **1** and 1.841(2) 1.918(2) Å for **2**], two nitrogen atoms from Phen/Bipy ligand[Co–N = 1.923(6)–1.975(5)Å for **1** and 1.912(3)–1.950(3) for **2**], and one nitrogen from ea^- [Co-N = 1.936(5), 1.941(7) Å for **1** and 1.926(3), 1.930(3) Å for **2**] . The remaining sixth site is occupied by bridged oxygen of O_2^{2-} [O–O = 1.487(6) (**1**), 1.462(3) (**2**)].

The bridging peroxide anion is coordinated to both the cobalt ions in a cis-1,2 fashion in both the complexes. All the Co–O and Co–N bond distances are within the range reported for octahedral Co(III) complexes (**Table 2**). The crystal structure shows that the molecule is stabilized by π–π aromatic stacking interactions between two neighboring Phen/Bipy ligands. The π–π aromatic stacking distances of the phen ligands are in range of 3.28–3.53 Å.These are further reinforced by intricate non-covalent H-bonding interactions involving lattice chloride/nitrate anions and aromatic H-atom to form an overall 3D supramolecular structure (**Fig. 2**).

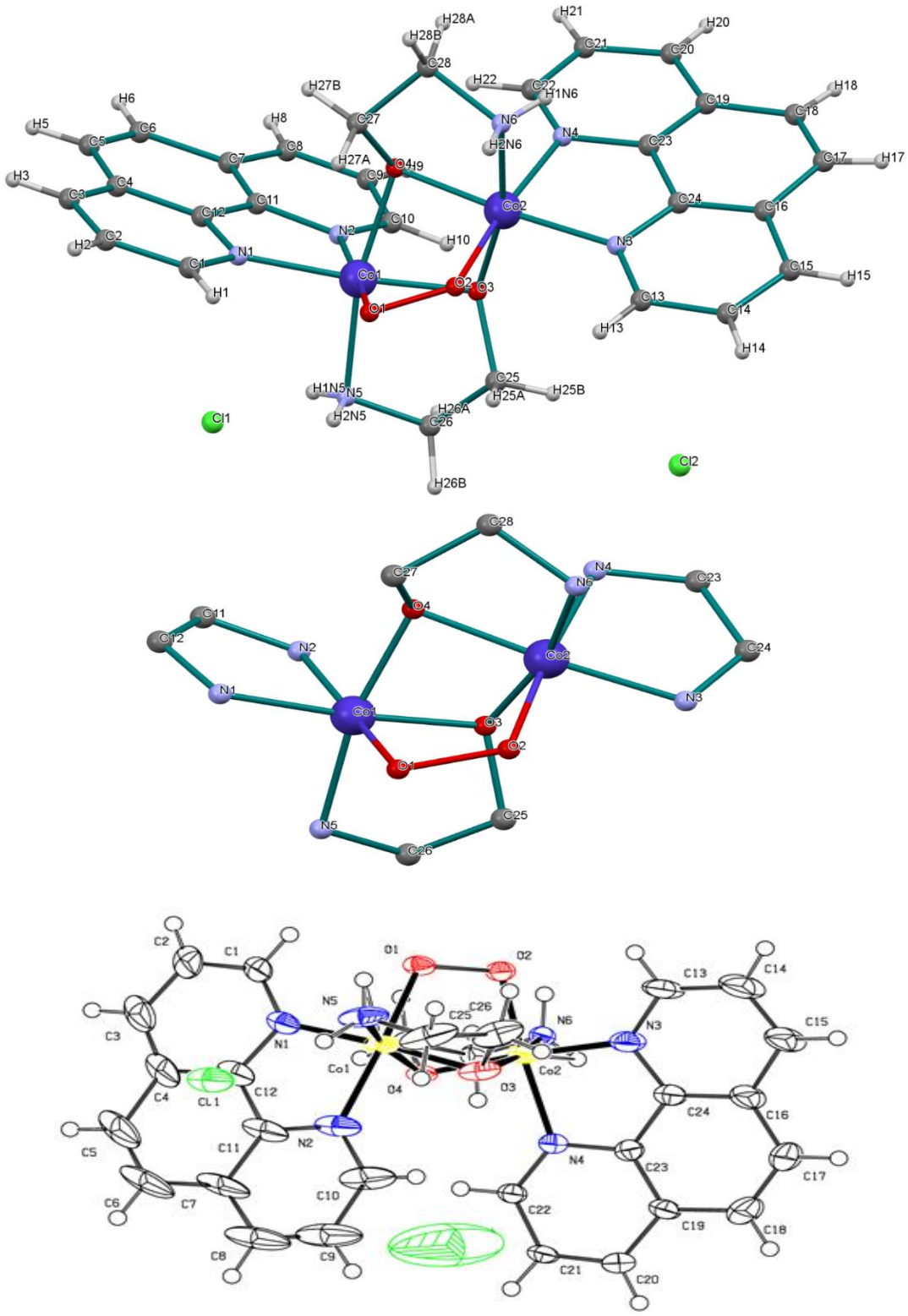

Fig. 1(a). Molecular structure, core and ORTEP views of **1**.

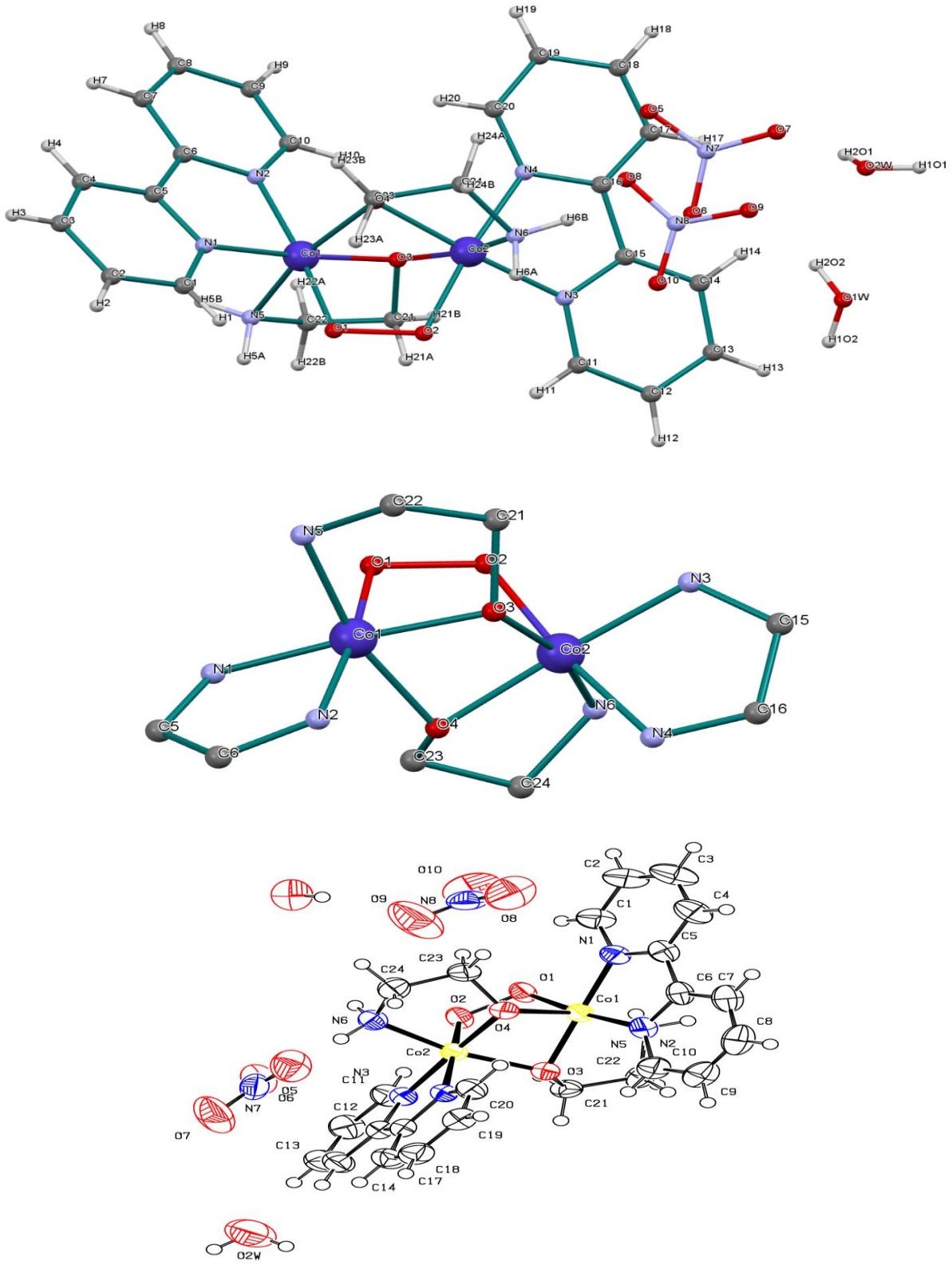

Fig. 1(b). Molecular structure, core and ORTEP views of **2**.

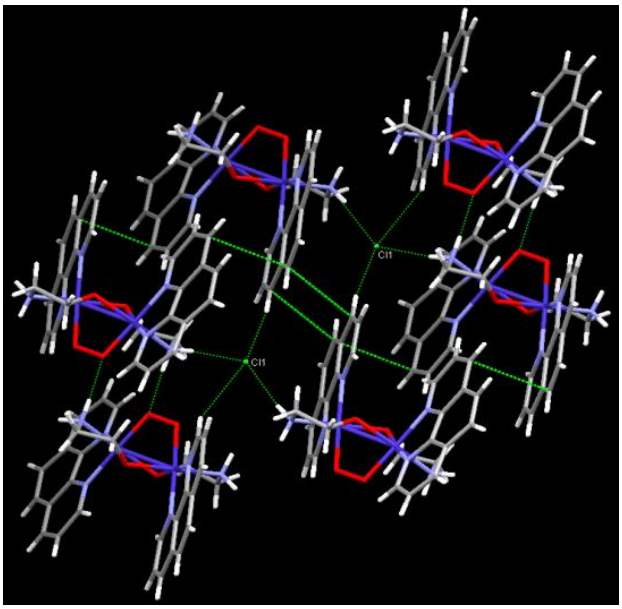

Fig. 2(a). 3D view of **1**.

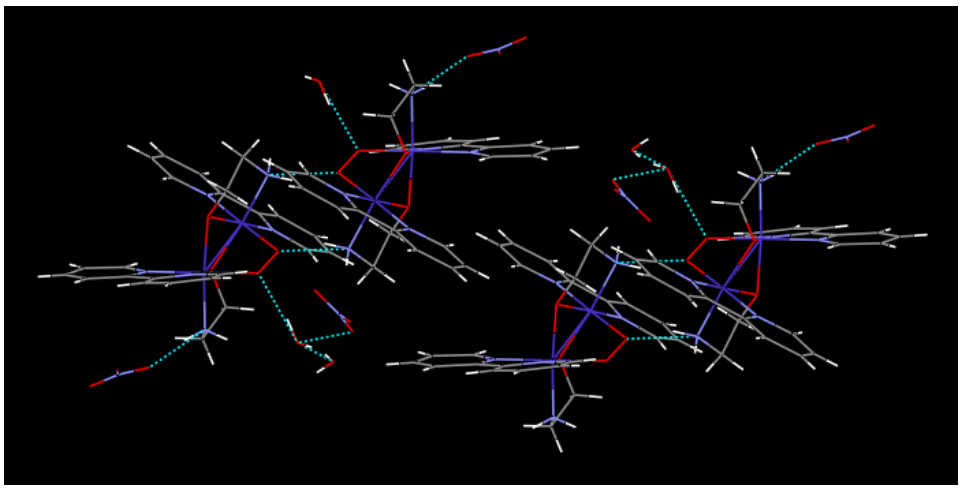

Fig. 2(b). 3D view of **2**.

PXRD and Thermal (TGA) studies

The simulated and as-synthesized powder X-ray diffraction (PXRD) patterns of **1** are in excellent agreement. All peaks pattern of as-synthesized and simulated PXRD of the

compound showed no extra peaks, confirming the phase purity. The differences in intensity may possibly be due to preferred orientations of the powdered samples as shown in **figure 3**.

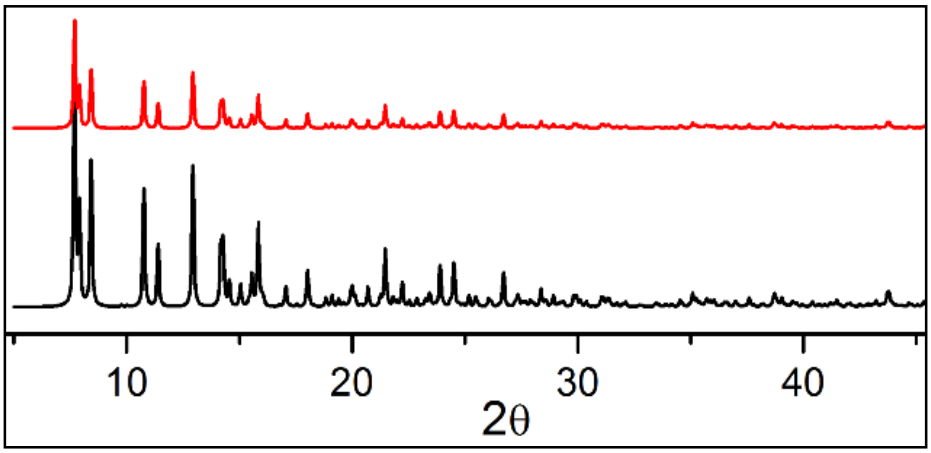

Fig. 3. PXRD pattern (top-Experimental, bottom-Simulated) of **1**.

In order to examine the thermal stability of complexes, thermal analysis of **1** was carried out in an N_2 atmosphere at the rate of 20 °C per minute. The TGA of compound shows a weight loss of ~12.89% (expected = 12.38%) within the temperature range 80-210 °C that corresponds to the release of all lattice water molecules [53]. Beyond this temperature (>400 °C) the compound starts to decompose (**Fig. 4**). Beyond 400 °C compound decomposes as oxide and peroxide moiety helps converting the molecule into the oxide.

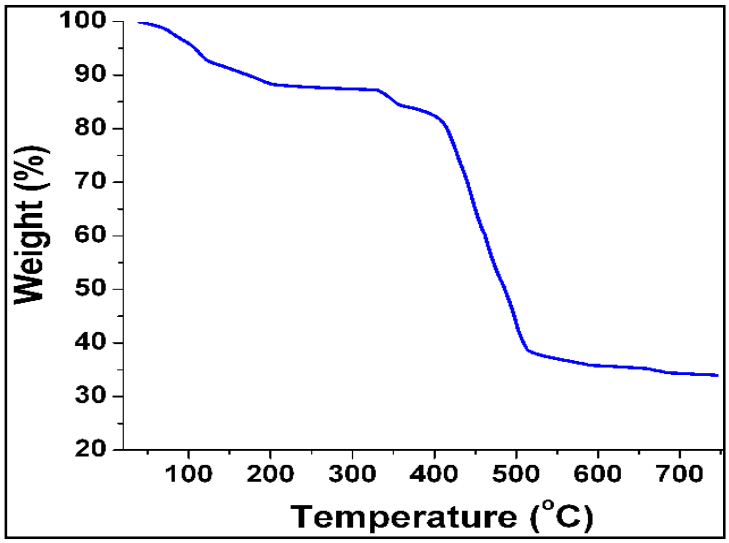

Fig. 4. Thermogram (TGA) of **1**.

Cyclic Voltammetric (CV) studies

The cyclic voltammogram for the complex (**1**) was recorded at various scan rates (0.1, 0.2 and 0.3 Vs^{-1}) and the voltammograms was similar at all the scan rates probability due to stability of the complex in solution. The voltammogram recorded at 0.2 Vs^{-1} is given in **figure 5**. The voltammogram for the complex exhibited cathodic peak in the forward scan which may be coupled with the anodic peak in the reverse cycle forming a quasi-reversible redox couple with $E^0_{1/2} = -0.17$ V. The probable electrochemical reaction involving a $2e^-$ redox mechanism may be given as follows:

$$[Co^{III}—L—Co^{III}] \underset{}{\overset{2e-}{\rightleftharpoons}} [Co^{II}—L—Co^{II}]$$

The voltammogram in the present case did not indicate the existence of possible electrochemical deposition process [54] unlike to that reported for the homo-dinuclear complexes of Cu(II) involving macrocyclic ligands [55,56].

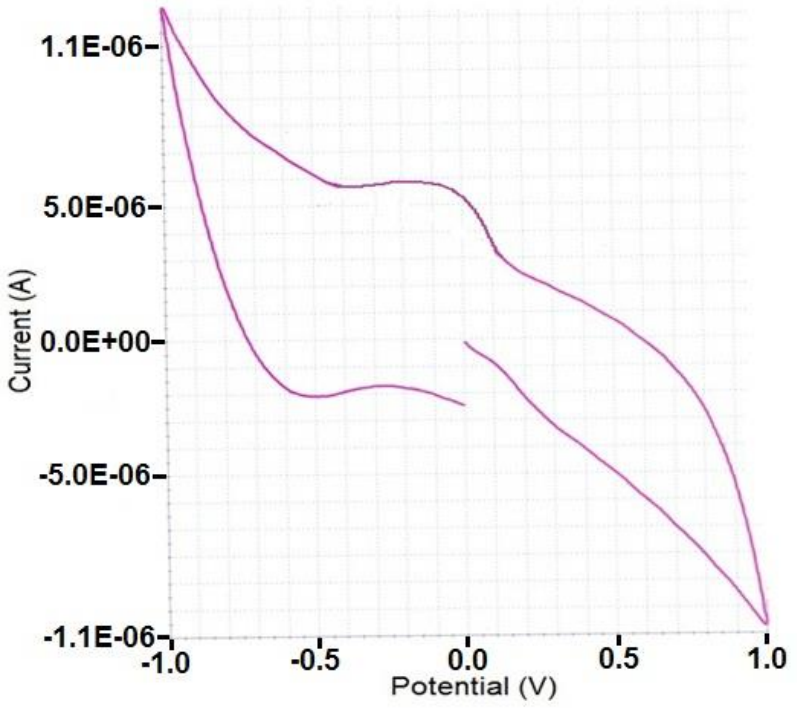

Fig. 5. Scanned cyclic voltammogram of **1**.

Biology

In order to evaluate the possible applications of the complexes in medicines and to ascertain the side effects or effect of the complexes on DNA, the genotoxic studies were performed on **1** using DNA nicking and comet assays.

Effect of compound on pUC19 DNA (DNA nicking assay)

Nicking of plasmid DNA and its conversion of open circular form is an indication of the genotoxic nature of the compound under test. Toxic action of the **1** was examined on plasmidpUC19 DNA at 50, 100, 200 and 300 µM concentrations with observation of the four farms of supercoiled DNA (**Fig. 6**). It is clear, in case of the present complex, that at lower concentration (50 µM) the supercoiled was neither converted to open circular nor was any linear formation observed (**Fig. 6**). But at higher concentrations of the complex (100, 200 or 300 µM) the plasmid DNA is nicked and converts to open circular form with increase in the intensity of band. This indicates that with increase in concentration of the compound, more of reactive oxygen species (ROS) are generated which enhance the nicking effect.

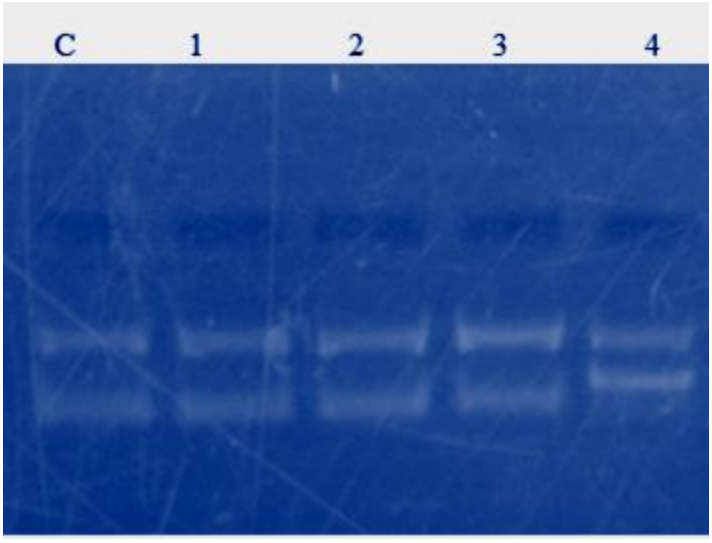

Fig. 6. Effect of compound on pUC19 DNA (Plasmid nicking assay).

Plasmid nicking assay attributed that only negligible amount of cytotoxic damage takes place with the complex at lower concentration. Thus we can extract that synthesized complex is non-toxic and can be exploited for medicinal applications at 50 µM concentration.

Effect of compound on nuclear DNA breakage (Comet assay)

In comet assay, the complex is treated with nuclear DNA and the tail formation and the apparent tail length relative to the control is the index of DNA damage or in other words a measure of the toxic effect by the compound [46]. It may be noted that when the compound **1** was added to reaction, the nuclear DNA breakage (tail length) was progressively increasing with increasing concentrations of compound. **Figure 7** shows that, for the complex, at a concentration of 50, the tail length is least but at higher concentrations, tail length increases remarkably. In **Figure 8**, the data is plotted as % DNA in tail of comet and the comparative genotoxic nature of the control and the compound (at various concentrations) can be observed. The nuclear DNA breakage (at higher concentrations of the compound) observed in our case exhibited radial movement probably due to larger fragment generation. This is presumably the result of direct interaction of compound with chromatin [57-60].

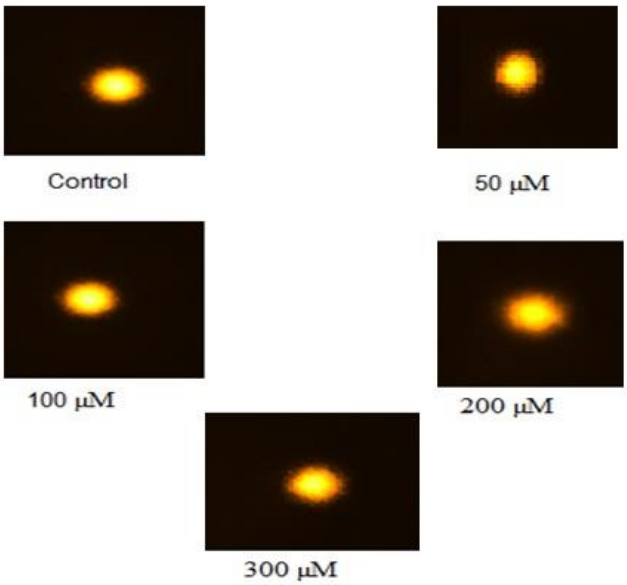

Fig. 7. Single cell gel electrophoresis (Comet assay) of human peripheral lymphocytes with **1**.

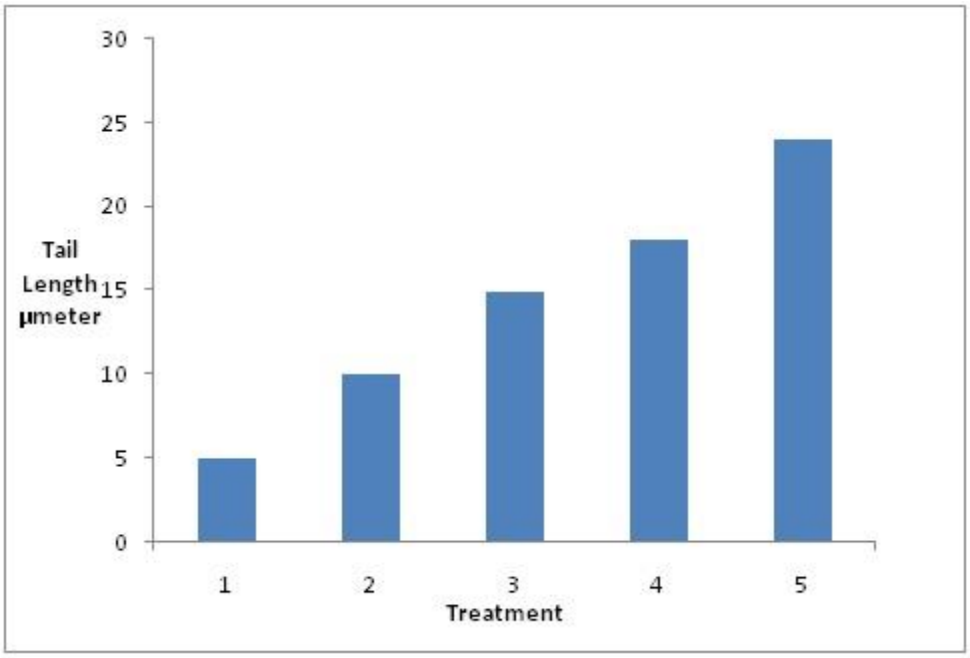

Fig. 8. Effect of complex (**1**) on lymphocyte DNA breakage (% Tail length).

Conclusions

A homodinuclear Co(III) complex with a cis-peroxide bridging is synthesized and characterized using spectral and X-ray crystallographic techniques. The peroxo bridging is in a cis-μ-1,2-fashion and the metal ions acquire a distorted octahedral environments. The genotoxic studies using DNA nicking and comet assays indicate the present complex does not cause harm to human DNA at lower concentration (50 μM) and can be exploited for industrial applications.

References

[1] M.C. Linder, C.A. Goode, Biochemistry of Copper, 1991, PlenumNew York. W. Kaim, B. Schwederski, Bioinorganic Chemistry: Inorganic Elements in the Chemistry of Life, 1994, Wiley, NewYork. K. DKarlin, Z. Tyeklar, Bioinorganic Chemistry of Copper, 1993, Ed. Chapman & Hall. New York.

[2] R.H. Holm, P. Kennepohl, E.I. Solomon.Chem. Rev., 96 (1996) 2239.

[3] K.D. Karlin, A.D. Zuberbühler, in: R.J. Reedijk, E. Bouwman (Eds.), Bioinorganic Catalysis (1999) 469. 2nd Ed. Revised and Expanded, M. Dekker, New York.

[4] H.-C. Liang, M. Dahan, K.D. Karlin. Curr.Opin.Chem. Biol., 3 (1999) 168.

[5] E.I. Solomon, U.M. Sundaram, T.E. Machonkin. Chem. Rev., 96 (1996) 2563.

[6] M. Sono, M.P. Roach, E.D. Coulter, J.H. Dawson. Chem. Rev., 96 (1996) 2841.

[7] D.E. Ortiz, P.R. Montllano. Acc. Chem. Res., 31 (1998) 543.

[8] A.L. Feig, M. Becker, S. Schindler, R. van Eldik, S.J. Lippard. Inorg.Chem. 35 (1996) 2590.

[9] A. Mukherjee, M.A. Cranswick, M. Chakrbarti, T.K. Paine, K. Fujisawa, E. Münck, L. Que, Jr. Inorg.Chem., 49 (2010) 3681.

[10] S.K. Kryatov, F.A. Chavez, A.M. Reynolds, E.V. Rybak-Akimova, L. Que Jr., W.B. Tollman. Inorg. Chem., 43 (2004) 2141.

[11] Y. Funahashi, T. Nishikawa, Y. Wasada-Tsutsui, Y. Kajita, S. Yamagucchi, H. Arii, T. Ozawa, K. Jitsukawa, T. Tosha, S. Hirota, T. Kitagawa, H. Masuda. J. Am. Chem. Soc., 130 (2008) 16444.

[12] H.-C. Liang, K.D. Karlin, R. Dyson, S. Kaderli, B. Jung, A.D. Zuberbühler. Inorg. Chem., 39 (2000) 5884.

[13] R.R. Jacobson, Z. Tyeklár, K. D. Karlin, S. Liu, J. Zubieta. J. Am. Chem. Soc., 110 (1988) 3690.

[14] Z. Tyeklár, R.R. Jacobson, N. Wei, N.N. Murthy, J. Zubieta, K.D. Karlin.J. Am. Chem. Soc., 115 (1993) 2677.

[15] Y. Lee, D.-H. Lee, G.Y. Park, H.R. Lucas, A.A.N. Sarjeant, M.-T.Kieber-Emmons, M.A. Vance, A.E. Milligan, E.I. Solomon, K.D. Karlin. Inorg. Chem., 49 (2010) 8873.

[16] K.D. Karlin, S. Kaderli, A.D. Zuberbühler, Acc. Chem. Res., 30 (1997) 139.

[17] J. Cohoy, P.L. Holland, W.B. Tolman. Inorg. Chem., 38 (1999) 2161.

[18] T.N. Sorrell, W.K. Allen, P.S. White. Inorg. Chem., 34 (1995) 952.

[19] K. Yamanari, M. Mori, S. Dogi, A. Fuyuhiro. Inorg. Chem., 33 (1994) 4807.

[20] B. Spingler, M. Scanavy-Grigorieff, A. Werner, H. Berke, S.J. Lippard, Inorg. Chem., 40 (2001) 1065.

[21] V.M. Miskowski, B.D. Santarsiero, W.P. Schaefer, G. Ansok., H.B. Gray. Inorg. Chem., 23 (1984) 172.

[22] R. Davies, A.G. Sykes. J. Chem. Soc. A (1968) 2237.

[23] W.R. Harris, G.L. McLendon, A.E. Martell, R.C. Bess, M. Mason. Inorg. Chem., 19 (1980) 21.

[24] T. Tanase, T. Onaka, M. Nakagoshi, I. Kinoshita, K. Shibata, M. Doe, J. Fujii, S. Yano. Inorg. Chem., 38 (1999) 3150.

[25] F.R. Fronczek, W.P. Schaefer, R.E. Marsh. Inorg. Chem., 14 (1975) 611.

[26] W.P. Schaefer, S.E. Ealick, R.E. Marsh. Acta Crystallogr., B37 (1981) 34.

[27] W.P. Schaefer, S.E. Ealick, D. Finley, R.E. Marsh. Acta Crystallogr., B38 (1982) 2232.

[28] P.V. Bernhardt, G.A. Lawrance, T.W. Hambley. J. Chem. Soc. Dalton Trans. (1990) 235.

[29] S. Schmidt, F.W. Heinemann, A. Grohmann. Eur. J. Inorg. Chem. (2000) 1657.

[30] G.G. Christoph, R.E. Marsh, W.P. Schaefer. Inorg.Chem. 8 (1969) 291.

[31] U. Thewalt, R.E. Marsh. Inorg. Chem., 11 (1972) 351.

[32] U. Thewalt, G.Z. Struckmeier. Anorg. Allg. Chem., 419 (1976) 163.

[33] I. Shweky, L.E. Pence, G.C. Papaefthymiou, R. Sessoli, J.W. Yun, A. Bino, S.J. Lippard.J. Am. Chem. Soc., 119 (1997) 1037.

[34] F. Meyer, H. Pritzkow. Angew. Chem. Int. Ed., 39 (2000) 2112.

[35] S. Konar, N. Bhuvanesh, A. Clearfield. J. Am. Chem. Soc., 128 (2006) 9604.

[36] S. Khanra, S. Konar, A. Clearfield, M. Helliwell, E.J.L. McInnes, E. Tolis, F. Tuna, R.E.P. Winpenny. Inorg. Chem., 48 (2009) 5338.

[37] Z.A. Siddiqi, A. Siddique, M. Shahid, M. Khalid, P.K. Sharma, Anjuli, M. Ahmad, S. Kumar, Y. Lan, A.K. Powell. Dalton Trans, 42 (2013) 9513.

[38] Z.A. Siddiqi, P.K. Sharma, M. Shahid, M. Khalid, Anjuli, A. Siddique, S. Kumar. Eur. J. Med. Chemistry, 57 (2012) 102.

[39] International Tables for X-Ray Crystallography, Kynoch Press, Vol. III, Birmingham, England, (1952).

[40] SAINT, version 6.02; Bruker AXS: Madison, WI, (1999).

[41] Sheldrick, G.M. SADABS: Empirical Absorption Correction Program; University of Göttingen: Göttingen, Germany, (1997).

[42] XPREP, version 5.1; Siemens Industrial Automation Inc.: Madison, WI, 1995.

[43] Sheldrick, G.M. SHELXTL Reference Manual, version 5.1; Bruker AXS: Madison, WI, (1997).

[44] Sheldrick, G.M. SHELXL-97: Program for Crystal Structure Refinement; University of Göttingen: Göttingen, Germany (1997).

[45] N.P. Singh, M.T. McCoy, R.R. Tice, E. L. Schneider. Exp. Cell. Res., 175 (1988) 184.

[46] U. Shamim, S. Hanif, M.F. Ullah, A.S. Azmi, S.H. Bhat, S.M. Hadi.Free Radic. Res., 42 (2008) 764.

[47] K. Nakamoto, Infrared and Raman Spectra of Inorganic and Coordination Compounds, Wiley-Interscience, New York (1986).

[48] T.N. Sorrell, W.K. Allen, P.S. White. Inorg. Chem., 34 (1995) 952.

[49] L. J. Bellamy, the Infra-Red Spectra of Complex Molecules, John Wiley & Sons, New York, (1958).

[50] D. Russels, Physical Methods In Inorganic Chemistry, Reinhold Pub. Corp., (1965).

[51] F. Lions, I.G. Dance, J. Lewis. J. Chem. Soc. A (1967) 565.

[52] B.F. Hoskins, R. Robson, G.A. Williams. Inorg. Chim. Acta, 16 (1976) 121.

[53] J.S. Kwag, M.H. Jeong, A.J. Lough, J.C. Kim. Bull. Korean Chem. Soc., 31 (2010) 2069.

[54] Z.A. Siddiqi, V.J. Mathew. Polyhedron, 13 (1994) 799.

[55] Z.A. Siddiqi, M.M. Khan, M. Khalid, S. Kumar. Trans. Met. Chem., 32 (2007) 927.

[56] C.D.-Samara, P.D. Janakoudakis, D.P. Kessissaglou, G.E. Manoyussakis, D. Mentzapfos, A. Terzis. J. Chem. Soc., Dalton Trans. (1992) 3259.

[57] S. Chibber, I. Hassan, M. Farhan, I. Naseem. Tumor Biology, 33 (2012) 701.

[58] J.H. Lee, S.Y. Kim, I.S. Kil. J Biol Chem., 282 (2007) 13385.

[59] M. Benhar, D. Engelberg, A. Levitzki. EMBO Rep., 3 (2002) 420.

[60] C.Y. Li, S. Shan, Q. Huang, R.D. Braun, J. Lanzen, K. Hu, P. Lin, M.W. Dewhirst. J Natl Cancer Inst., 92 (2000) 143.

Chapter 5

Synthesis, spectral and X-ray crystallographic characterization of tetranuclear cobalt clusters

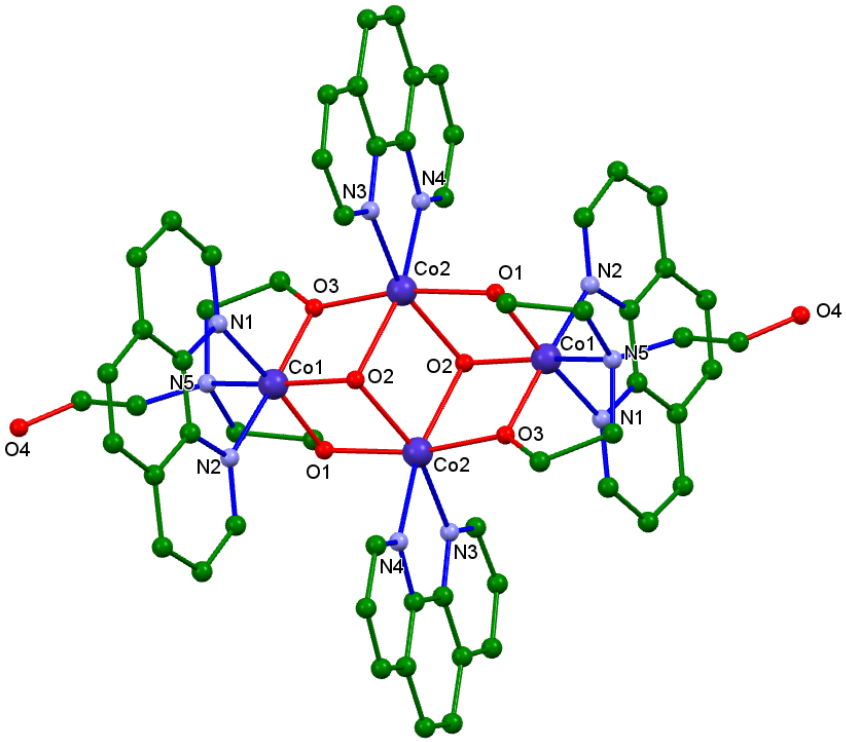

Introduction

One of the current challenges in inorganic chemistry is the synthesis and characterization of new molecular 3d metal polynuclear clusters at moderate oxidation states [1]. Reasons for this are the aesthetic beauty that develops as the high nuclearity of the clusters increases and the complexity of their molecular structures become apparent. From a more practical viewpoint, such large clusters can represent an alternative, 'bottom-up' route to nanoscale particles complementary to the traditional 'top-down' approach [2,3]. Tetranuclearity can be considered a common and representative class of high-nuclearity 3d-metal clusters showing interesting properties spanning from catalysis [4], and magnetism to modelling biochemical reactions [5]. A class of polynuclear metal-oxygen cluster complexes have unique chemical and physical properties with potential applications such as optics and meditational chemistry. Various coordination motifs have been described in the literature, in which the most important M_4 cores are butterfly, incomplete cubane, cubane, defect dicubane topologies (**Scheme 1**) [6].

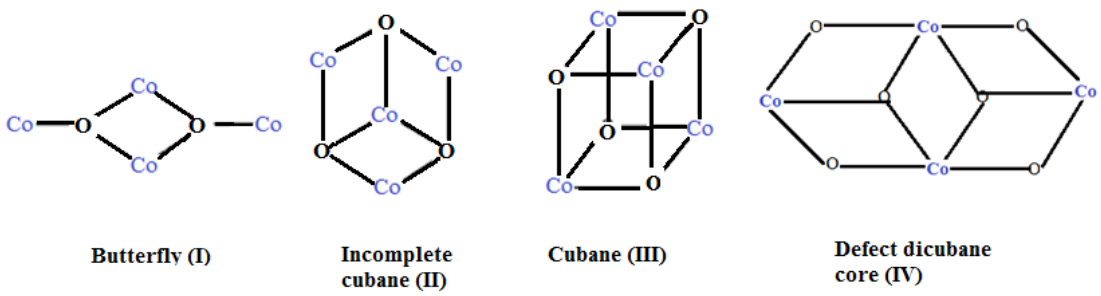

Scheme 1. Selected cores found in tetranuclear clusters.

Cubane-like clusters, found in a variety of transition metal complexes, exhibit interesting magnetic exchange properties and under certain circumstances act as SMMs. In biology, such systems are well known; [7] e.g. the Fe_4S_4 cubane units are present in the structure of a ferredoxin protein and act as electron transfer agents [8]. The heteronuclear

cubane Mn_3CaO_4 is present at the active site of the oxygen-evolving centre (OEC) of photosystem II, and the Fe_3MoS_4 has been identified at the active site of nitrogenase [9]. Cubane like structures are favored in iron, manganese and vanadium hydroxo- and/or alkoxo-bridged chemistry, while in cobalt systems relatively limited especially the mixed valence Co^{II}/Co^{III} compounds are reported [10]. Aliphatic amino alcohols belong to a group of ligands that are widely used for the construction of tetranuclear molecular complexes, including heterometallic ones, which are of continuous interest in modern chemistry [11]. The geometrical flexibility of aliphatic amino alcohols, their polydentate nature and ability to show a variety of coordination modes stipulate their broad coordination chemistry. Triethanolamine (H_3tea) is an ideal ligand act as deprotonated multidentate in the area of self-assembly chemistry with its [N,O,O,O] donor atoms to incorporate their oxygen atoms into a metal oxide framework with versatile bridging modes, as it can, in theory, bind to up to a number of metals at a time. The flexible nature of the H_3tea is what makes it so appealing and has thus far been known to display eight different modes of bonding (**Scheme 2**).

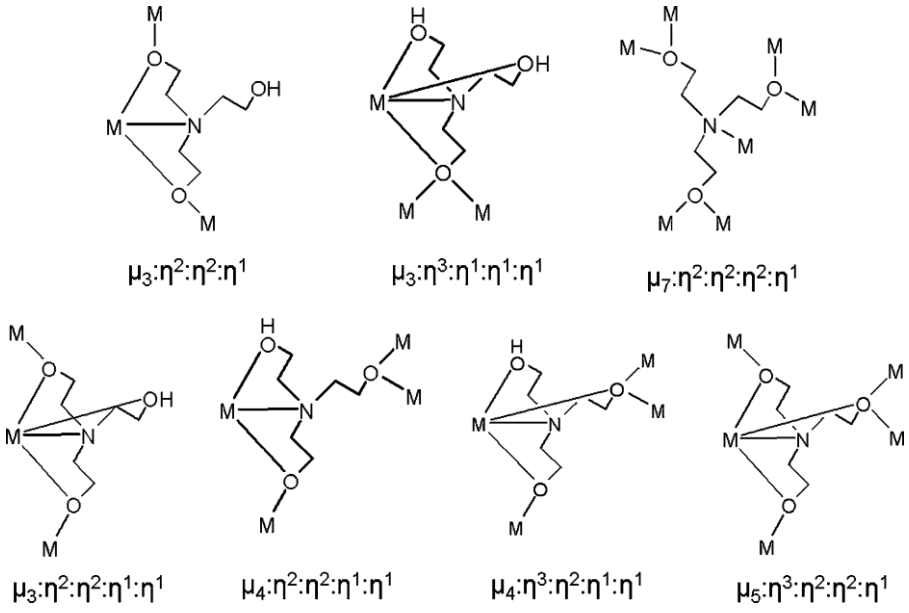

Scheme 2. Coordination modes of the ligand triethanolamine (H_3tea).

Examples of these include the μ_4:η^3: η^2: η^1: η^1 and μ_3: η^2: η^2: η^1:η^1 modes and allow us to stabilize a variety of novel metal topologies that possess novel magnetic properties [12,13]. The important structural properties of H_3tea led us to carry out synthesis of tetranuclear cobalt clusters containing α-diimine auxiliary ligand.

Experimental

Materials and methods

All experiments were carried out under aerobic conditions. Triethanolamine, 1,10-phenanthroline, 2,2'-bipyridine, triethylamine and $Co(NO_3)_2 \cdot 6H_2O$ (Merck) were used as received. The solvents used in the reactions were reagent grade and used without further purification.

Physical methods

FTIR spectra were recorded on a Perkin-Elmer spectrum GX automatic recording spectrophotometer with sample prepared as KBr discs. Melting points was determined by open capillary method and are uncorrected. The elemental C, H and N analyses were obtained from Micro-Analytical Laboratory of Central Drug Research Institute (CDRI), Lucknow, India. ^{1}HNMR and ^{13}CNMR spectra were recorded on a Bruker Avance II 400 NMR spectrometer from Punjab, university Chandigarh, India. Absorption spectroscopic measurements were carried out at room temperature; using a Perkin-Elmer Lambda-25 UV-visible spectrophotometer in 10^{-3} M solution in CH_3OH, cu-vettes of 1 cm path length. Molar conductivity of 10^{-3} M aqueous solution was recorded on Systronics-305 digital conductivity bridge, respectively at room temperature. The EPR spectrum of the complexes was acquired on a Perkin-Elmer spectrometer using X-band frequency (9.1 GHz) at room temperature in solid. Cyclic voltammetry (CV) was performed on EG&G PAR 273 Potentiostat/Galvanostat an IBM PS2 computer with EG&G M270 software for data acquisition. The three-electrode cell configuration comprised of, a platinum sphere, a platinum plate and Ag(s)/$AgNO_3$ were used as working, auxiliary and reference electrodes, respectively. The supporting electrolyte used was [^{n}Bu$_4$N]ClO_4. Platinum sphere electrode was sonicated for 2 min in dilute nitric acid,

dilute hydrazine hydrate and then in double distilled water to remove the impurities. The solutions were deoxygenated by bubbling research grade nitrogen gas and an atmosphere of nitrogen was maintained over the solution during measurements. Thermal gravimetric analysis (TGA) data were recorded from room temperature up to 600 $^{\circ}$C at a heating rate of 20 $^{\circ}$C/min. The data were obtained using a Shimadzu TGA-50H instrument. Magnetic susceptibility are measured by magnetic susceptibility balance, Sherwood scientific Cambridge U. K. at room temperature.

X–ray crystal structure determination and refinements

Single-crystal X-ray data of **1** and **2** were collected at 100 K on a Bruker SMART APEX CCD diffractometer using graphite monochromated Mo-Kα radiation (λ = 0.71073 Å). The linear absorption coefficients, scattering factors for the atoms and the anomalous dispersion corrections were taken from the International Tables for X–ray Crystallography [14]. The data integration and reduction were processed with SAINT Software [15]. An empirical absorption correction was applied to the collected reflections with SADABS [16] and the space group was determined using XPREP [17]. Several DIFX command has been given to fix the bond length parameters. The structures were solved by direct methods using SHELXL-97 [18] and refined on F^2 by full matrix least squares using the SHELXL-97 program package [19]. All non-hydrogen atoms were refined with anisotropic displacement parameters. CCDC reference numbers for **1** and **2** are 1026333 and 1026334, respectively.

Synthesis

General procedure

Synthetic procedure of **1** and **2** was same under aerobic condition (Scheme **3**). Metal salt, H_3tea and N-heterocyclic chelator were used in 1:1:1 molar ratio in methanol, triethylamine was added to the mixture and after 2 h stirring clear brown solution was obtained, which on standing over night produced beautiful crystals of **1** and **2**. Oxidation state of cobalt

changed from +2 to +3 in the product due to atmospheric oxygen molecules which is not unusual and has already been reported with manganese, iron metal ions.

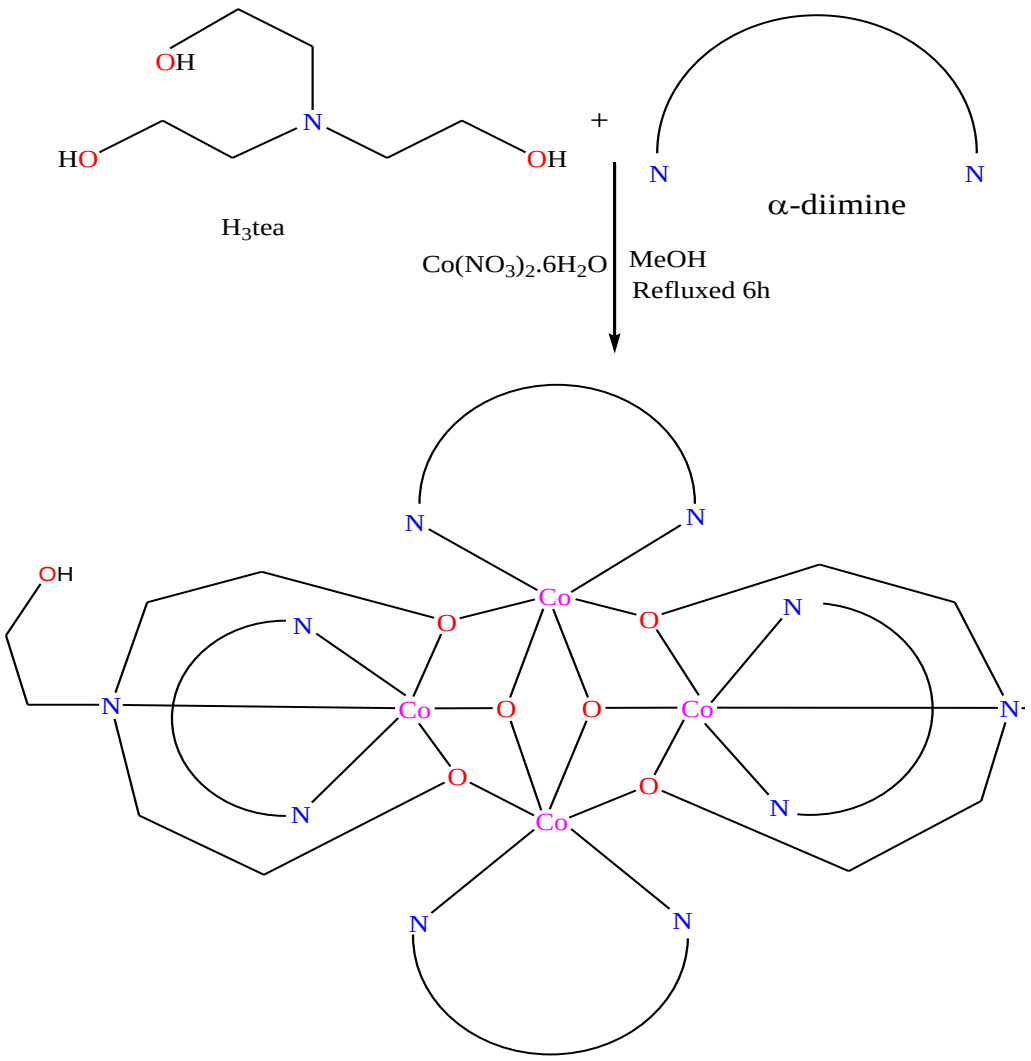

α -diimine = 1,10-phenanthroline (**1**) or 2, 2'-bipyridine (**2**)

Scheme 3. Synthetic procedure for **1** and **2**.

Synthesis of $[Co_4(\mu_3–O)_2(Htea)_2(Phen)_4]2NO_3·4H_2O$ (1)

$Co(NO_3)_2·6H_2O$ (0.50 mmol, 0.15g) was dissolved in 20 ml methanol. A mixture of equimolar quantity of H_3tea (0.50 mmol, 0.06 ml), 1,10-phenanthroline (0.50 mmol. 0.10 g) and 1.5 mmol of NEt_3 (0.20 ml) was dissolved in 10 ml methanol and metal solution was added dropwise. The reaction mixture was refluxed for 6 h. The obtained brown solution was filtered and 10 ml of acetonitrile was added to the filtrate. Brown crystals of **1** for X-ray structure determination were deposited by layering with diethyl ether.

[Yield: 70%, m.p. >300 °C] Anal. Calcd. (%) for $C_{60}H_{58}Co_4N_{14}O_{28}$: C 43.40; H 3.50; N 11.82. Found (%): C 43.92; H 3.38; N 11.67. Molar conductance, Λ_m (10^{-3} M, methanol): 240 Ω^{-1} $cm^2\,mol^{-1}$. IR spectra (KBr pellets, cm^{-1}): ν(O–H): 3373, ν(C–H): 2935, ν(C–O): 1090 ν(NO_3): 1384 ν(Co–O–Co): 946, νCo_3(μ_3–O): 650

Synthesis of $[Co_4(\mu_3–O)_2(Htea)_2(Bipy)_4]2NO_3$ (2)

Synthetic procedure for **2** was similar to that for **1** except addition of 2,2'-bipyridine (0.50 mmol, 0.08 g) instead of 1,10-phenanthroline.

[Yield: 67%, m.p. >300 °C] Anal. Calcd. (%) for $C_{52}H_{58}Co_4N_{14}O_{20}$: C 43.49; H 4.40; N 13.66. Found (%): C 43.85; H 4.22; N 13.72. Molar conductance, Λ_m (10^{-3} M, methanol): 245 Ω^{-1} $cm^2\,mol^{-1}$. IR spectra (KBr pellets, cm^{-1}): ν(O–H): 3270, ν(C–H): 2928, ν(C–O): 1090 ν(NO_3): 1385 ν(Co–O–Co): 942, νCo_3(μ_3–O): 645

Results and discussion

Triethanolamine (H_3tea) was reacted with $CoNO_3 \cdot 6H_2O$ in the presence of α-diimine (L–L) viz. 1,10-phenanthroline (Phen), or 2,2′-bipyridine (Bipy) affording stable crystalline products, which have been characterized as mixed valence tetranuclear species of **1** or **2**. The formation of **1** and **2** is represented in **Scheme 3**. The complexes were soluble in water and usual organic solvents whose analytical data are fully consistent with the coordination sphere $[Co_4(\mu_3\text{–}O)_2(Htea)_2(L\text{–}L)_4]^{2+}$ (Experimental section). The observed magnitude of molar conductivities ($\Lambda_m \sim 245\ \Omega^{-1}cm^2mol^{-1}$) indicates that in aqueous solution they tend to ionize as strong electrolytes suggesting that the counter anion (NO_3^-) is weakly bound to the bulky complex cation and preferably remains out of the coordination sphere. Suitable crystals of **1** and **2** were obtained on slow evaporation of the mother liquor and were characterized by various spectroscopic techniques and single crystal X-ray diffraction studies.

X-ray crystallographic studies

The crystal structures of **1** and **2** (**Fig. 1**) were determined by single crystal X-ray diffraction. The full crystallographic data and refinement parameters are given in **Table 1**. Selected bond distances and bond angles are shown in Table **2**. Both tetranuclear cationic units are nearly identical and discussed simultaneously. The complex **1** is triclinic with space group P-1 and complex **2** is monoclinic with space group P $2_1/c$. The complexes are coordinated by μ_3–oxo bridging ($Co_2\text{–}O_2\text{–}Co_2$). The μ_3–oxo bridge is rare in coordination compounds, and has rarely been observed in tetranuclear mixed valance cobalt clusters [20]. Each cluster is stabilized by two NO_3^- counter ions.

The molecular unit of the complexes contains four cobalt ions located in a manner to form a defect dicubane core (**Fig. 2**) [21]. The alkoxide oxygens (O1, O3 in **1** and O1, O2 in **2**) of $Htea^{2-}$ unit are bridging the internal Co2 ions with the external Co1 ions while one alkoxide arm of the $Htea^{2-}$ unit remains uncoordinated. Each cobalt ion has distorted octahedral geometry with six coordination number. Each cobalt is effectively surrounded by one α-diimine (Phen or Bipy) chelator and two $Htea^{2-}$ bridging moieties shared between the four

cobalt units of defect dicubane. The external Co1 has a {N3O3} chromophore composed of an oxo oxygen O2 (**1**), or O4 (**2**), two alkoxide oxygen [(O1, O3) (**1**) and (O1, O2) (**2**)], a nitrogen from the $Htea^{2-}$ and two nitrogen coming from the α-diimine. The central Co2 has N2O4 chromophore composed of two alkoxide oxygen from the $Htea^{2-}$ ligand [(O1, O3) (**1**) and (O1, O2) (**2**)], two oxo- bridged oxygen [O2 (**1**) and O4 (**2**)] atoms and two nitrogen of Phen {N3,N4} or Bipy {N1,N2} chelators, respectively.

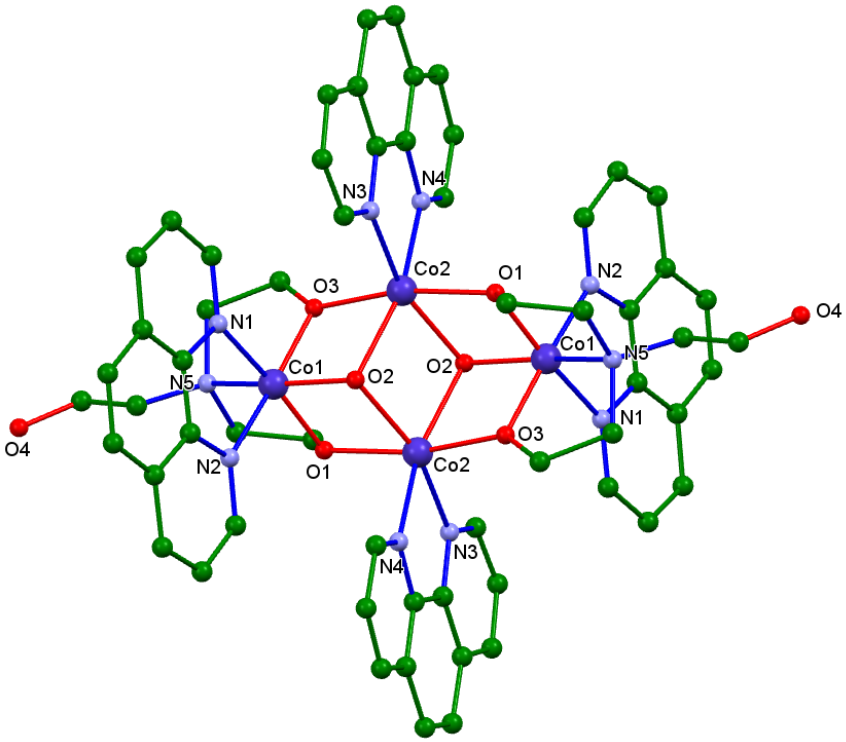

Fig. 1(**a**). Numbering diagram (omitted hydrogen atoms) of **1**.

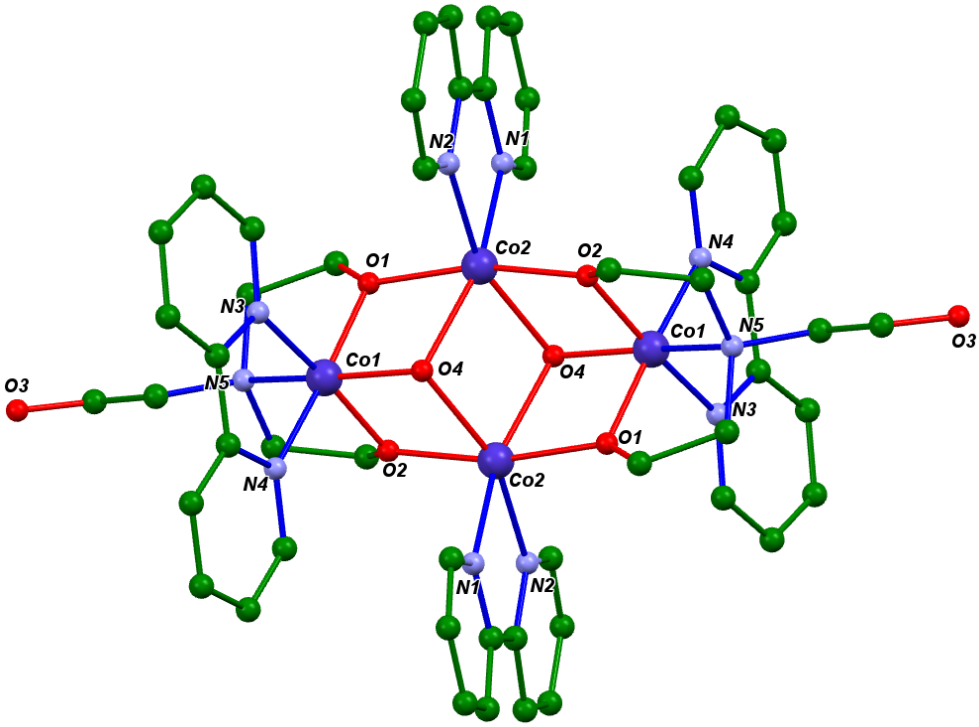

Fig. 1(**b**). Numbering diagram (omitted hydrogen atoms) of **2**.

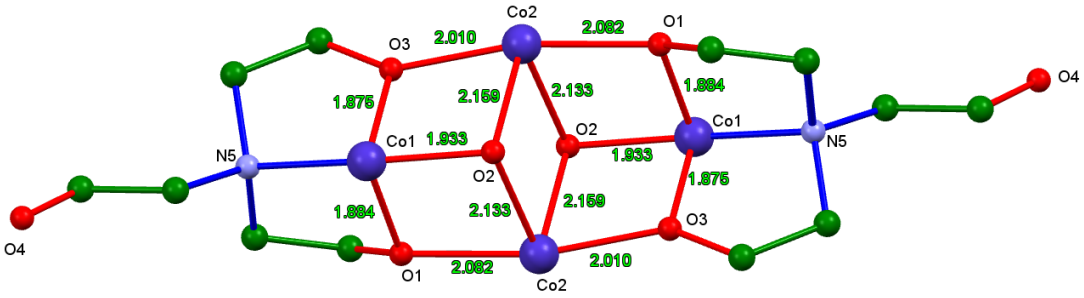

Fig. 2(**a**). The defect dicubane core of **1**.

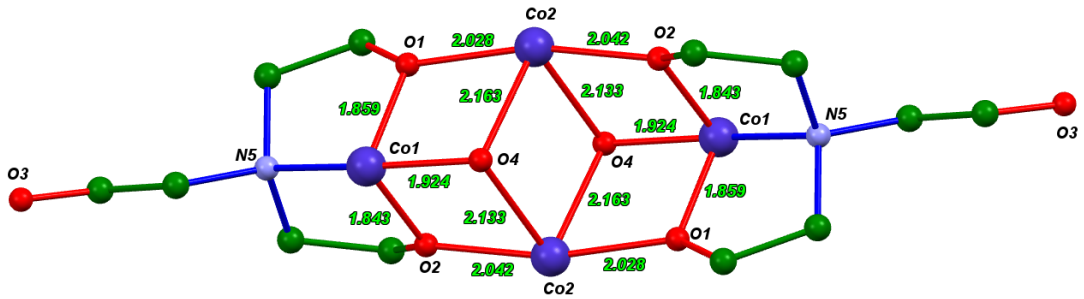

Fig. 2(**b**). The defect dicubane core of **2**.

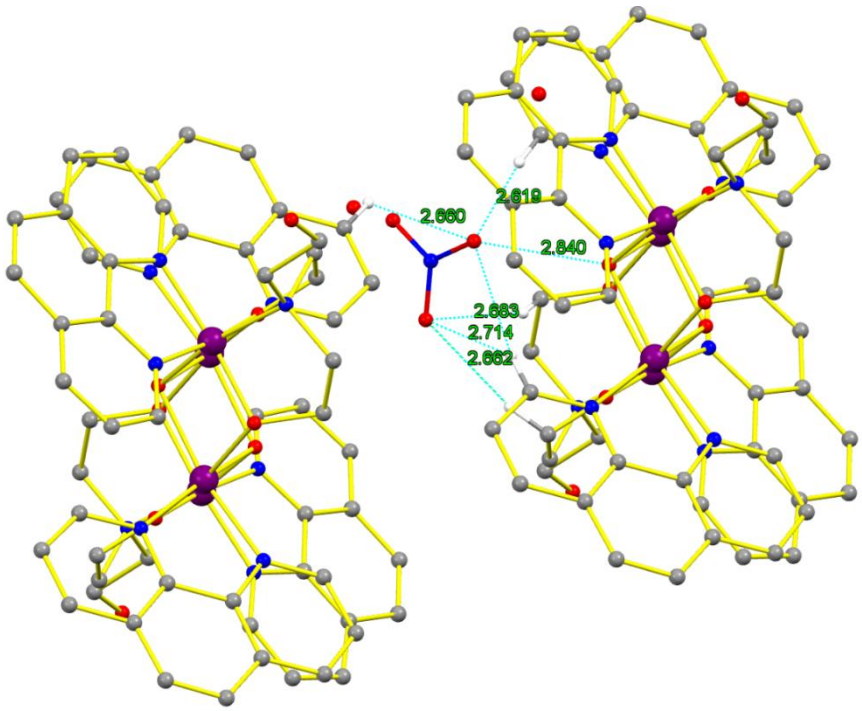

Fig. 3(a). Non-covalent interactions of **1**.

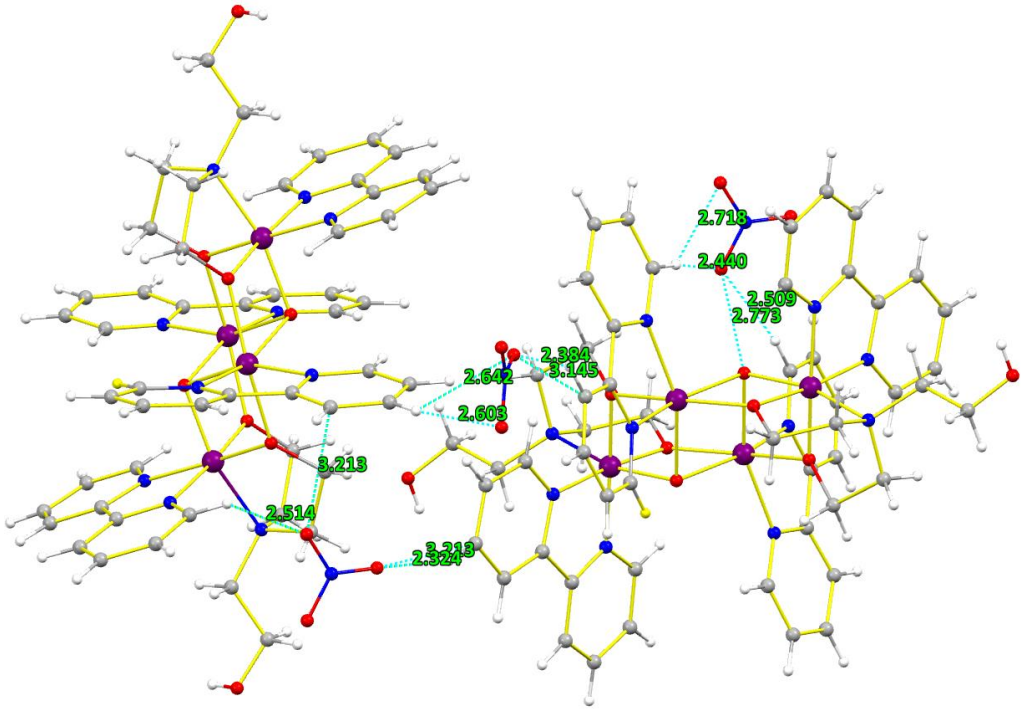

Fig. 3(b). Non-covalent interactions of **2**.

Table 1. Crystal data with refinement parameters for the complexes **1** and **2**.

Parameters	Complex **1**	Complex **2**
Empirical formula	$C_{60}H_{58}Co_4N_{14}O_{28}$	$C_{52}H_{58}Co_4N_{14}O_{20}$
Formula weight	1658.92	1434.84
Temp (K)	100(2)	100(2)
Crystal system	triclinic	monoclinic
Space group	P-1	P $2_1/c$
Unit cell dimensions		
a (Å)	12.014(5)	12.001(5)
b (Å)	12.677(5)	17.204(5)
c (Å)	13.189(5)	13.882(5)
α (°)	65.720(5)	90
β **(°)**	88.957(5)	90.685
γ (°)	66.182(5)	90
V ($Å^3$)	1648.5(11)	2865.9(18)
Z	2	2
ρ (calc) (gcm^{-3})	1.671	1.663
F (000)	848	1472
Crystal size (mm^3)	0.27 × 0.17 × 0.14	0.30 × 0.21 × 0.16
Index ranges	$-12 \le h \le 14$	$-13 \le h \le 14$
	$-9 \le k \le 15$	$-16 \le k \le 20$
	$-14 \le l \le 15$	$-16 \le l \le 9$
No of reflections collected	8997	14463
No. of independent reflection	5986	5040
GOF	1.087	0.996
Final R indices [$I > 2\sigma(I)$]	$R_1 = 0.0712$	$R_1 = 0.1582$
	$wR_2 = 0.1482$	$wR_2 = 0.1225$
R indices all data	$R_2 = 0.0594$	$R_2 = 0.0659$
	$wR_2 = 0.1964$	$wR_2 = 0.1493$

Table 2. Selected bond lengths (Å) and bond angles (°) of the complexes **1** and **2**.

Complex (**1**)		Complex (**2**)	
Bond lengths			
Co1-N1	1.973(4)	Co2-N1	2.123(5)
Co1-N2	1.966(4)	Co2-N2	2.108(5)
Co2-N3	2.138(4)	Co1-N3	1.940(5)
Co2-N4	2.120(4)	Co1-N4	1.935(5)
Co1-N5	1.983(4)	Co1-N5	1.991(4)
Co1-O1	1.884(3)	Co1-O1	1.859(4)
Co2-O1	2.082(3)	Co2-O1	2.028(4)
Co1-O1	1.934(3)	Co1-O2	1.843(4)
Co2-O2	2.133(3)	Co2-O2	2.042(4)
Co2-O2	2.159(3)	Co1-O4	1.924(3)
Co1-O3	1.875(3)	Co2-O4	2.133(3)
Co2-O3	2.010(3)	Co2-O2	2.042(4)
Co2-O3	2.010(3)	Co2-O4	2.163(4)
Co2-O2	2.159(3)	Co2-O4	2.133(4)
Bond angles			
Co1-O1-Co2	102.53(14)	Co1-C15-N3	115.5(4)
Co1-O2-Co2	99.04(14)	Co1-C11-N3	125.2(5)
Co1-O2-Co2	97.88(13)	Co1-C20-N4	125.8(5)
Co2-O2-Co2	94.88(13)	Co1-C16-N4	114.4(4)
Co1-O3-Co2	105.32(15)	Co1-C25-N5	116.2(4)
Co1-C12-N1	112.3(3)	Co1-C23-N5	105.3(3)
Co1-C10-N2	128.5(3)	Co1-C21-N5	104.6(4)
Co1-C11-N2	112.6(3)	Co1-C22-O1	115.3(3)
Co1-C30-N5	113.1(3)	Co1-O2-Co2	104.77(17)
Co1-C25-N5	104.3(3)	Co1-O4-Co2	98.66(15)
Co1-C27-N5	106.0(3)	Co1-O4-Co2	98.02(14)
Co1-C26-O1	109.3(3)	Co1-O2-O1	94.67(17)
Co1-C28-O3	116.6(3)	Co1-O2-O4	82.96(16)
Co1-O3- O1	94.97(14)	Co1-O1-O4	83.12(15)
Co1-O3-O2	82.65(14)	Co1-O2-N4	90.8(2)
Co1-O1-O2	83.90(14)	Co1-O1-N4	174.0(2)
Co1-O3-N2	173.75(14)	Co1-O4-N4	95.17(17)
Co1-O1-N2	90.39(15)	Co1-O2-N3	171.70(19)

Co1-O2-N2	94.77(15)	Co1-O1-N3	92.4(2)
Co1-O3-N1	91.32(16)	Co1-O4-N3	93.56(17)
Co1-O1-N1	173.36(15)	Co1-N4-N3	82.0(2)
Co1-O2-N1	94.83(15)	Co1-O2-N5	87.54(18)
Co1-N2-N1	83.21(16)	Co1-O1-N5	87.02(19)
Co1-O3-N5	85.89(15)	Co1-O4-N5	165.69(19)
Co1-O1-N5	87.28(15)	Co1-N4-N5	95.7(2)
Co1-O2-N5	164.86(15)	Co1-N3-N5	97.20(19)
Co1-N2-N5	97.58(16)	Co1-O1-Co2	105.13(17)
Co1-N1-N5	95.29(16)	Co1-C24-O2	114.5(3)
Co2-C13-N3	129.6(3)	Co2-O4-Co2	94.14(15)
Co2-C24-N3	113.5(3)	Co2-C22-O1	134.5(4)
Co2-C22-N4	128.4(3)	Co2-C24-O2	134.8(3)
Co2-C23-N4	114.1(3)	Co2-C5-N1	115.2(4)
Co2-C26-O1	127.9(3)	Co2-C1-N1	125.4(4)
Co2-C28-O3	138.0(3)	Co2-C10-N2	125.0(5)
Co2-O3-O1	168.97(13)	Co2-C6-N2	115.4(4)
Co2-O3-N4	90.45(14)	Co2 -O1-O2	166.95(15)
Co2-O1-N4	97.71(14)	Co2 -O1-N2	98.76(17)
Co2-O3-O2	96.85(13)	Co2 -O2-N2	88.16(16)
Co2-O1-O2	74.51(12)	Co2 -O1-N1	89.55(17)
Co2-N4-O2	99.82(13	Co2 -O2-N1	102.83(17)
Co2-O3-N3	101.28(14)	Co2 -N2-N1	77.0(2)
Co2-O1-N3	87.67(13)	Co2 -O1-O4	100.98(14)
Co2-N4-N3	78.54(15)	Co2 -O2-O4	73.41(14)
Co2-O2-N3	161.79(14)	Co2 -N2-O4	159.75(16)
Co2-O3-O2	74.12(13)	Co2 -N1-O4	98.54(17)
Co2-O1-O2	97.96(12)	Co2 -O1-O4	73.51(14)
Co2-N4-O2	164.31(14)	Co2 -O2-O4	94.13(14)
Co2-O2-O2	85.12(13)	Co2 -N2-O4	104.18(18)
Co2-N3-O2	101.34(13)	Co2 -N1- O4	163.04(16)

The α-diimine chelators provide two N-sites listed as (N1, N2) or (N3, N4) chelated to each cobalt atom. It is interesting to note (Table 1) that there is an appreciable difference in Co–N bond distances from the α-diimine coordinated to the metal ions [(Co1–N1 or Co1–N2) ~1.96

Å] and [(Co2–N3 or Co2–N4) ~2.12 Å] [22]. The observed shorter bond length of Co1-N1 and Co1–N2 correspond to N-coordination to a trivalent (Co^{III}) ion whereas longer bond lengths Co2–N3 and Co2–N4 (~2.12 Å) are comparable to the corresponding divalent (Co^{II}) oxidation state [23]. This indicates that the dicubane core has two sets (each with two cobalts) in different oxidation states of the metal ions [Co_2^{II}–Co_2^{III}]. The one set with shorter bond length is obviously in higher oxidation state whereas the relatively longer bond distance corresponds to the lower (+2) oxidation state of the metal ion [24,25]. Furthermore, the Co–O bond distances i.e., Co1–O1 (~1.88 Å) is shorter than Co2–O2 (~2.08 Å). Here, it is confirmed that Co1 ion is in (+3) and Co2 ion is in (+2) oxidation state [26].

The tetranuclear discrete molecular unit is, therefore, an example of mixed valence oxo-bridged defect dicubane cluster having the actual stoichiometries as [Co_2^{II}–Co_2^{III}(μ_3-O)$_2$(Htea)$_2$(Phen)$_4$]2NO_3·4H_2O (**1**) and [Co_2^{II}–Co_2^{III}(μ_3–O)$_2$(Htea)$_2$(Bipy)$_4$]2NO_3 (**2**). The dicubane core in the present case contains two high-spin highly paramagnetic Co^{II} ($t_{2g}^5e_g^2$ configuration) centres and the remaining two cobalt atoms in low spin diamagnetic Co^{III} (t_{2g}^6 configuration) as ascertained from magnetic studies.

FTIR, ^{1}H and ^{13}C NMR spectra

FTIR and NMR data for the present complexes and the similar complexes reported in literature has been summarized in **Table 3**. The FTIR spectra of **1** and **2** exhibited characteristic vibrations of C=N due to N chelator groups detected at 1627 cm^{-1} for **1** and 1610 cm^{-1} for **2** (**Fig. 3**) [27]. Bands due to triethanolamine molecules have been investigated in three regions. (a) Medium band 3373 cm^{-1} for **1** and 3270 cm^{-1} for **2** are assigned to the stretching vibrations of OH group (b) 2935 and 2928 cm^{-1} assigned to C–H stretching vibrations in **1** and **2**, respectively, and (c) three bands in the region of 1090 cm^{-1} are attributed to the ν(C–O) stretching for **1** and **2** [28]. A strong band at ~1385 cm^{-1} is assigned to the ionic nitrates [29]. The symmetric stretching vibration [ν(–ONO_2)] are present at 1229 cm^{-1} for **1** and 1318 cm^{-1} for **2** [30]. The bands appearing at 946 and 942 cm^{-1} are characteristic of bridging ν(Co–O–Co) for **1** and **2**, respectively. The bonds observed in the low frequency 430–520 cm^{-1} is characteristics of Co–N and Co–O band stretching vibrations [31].

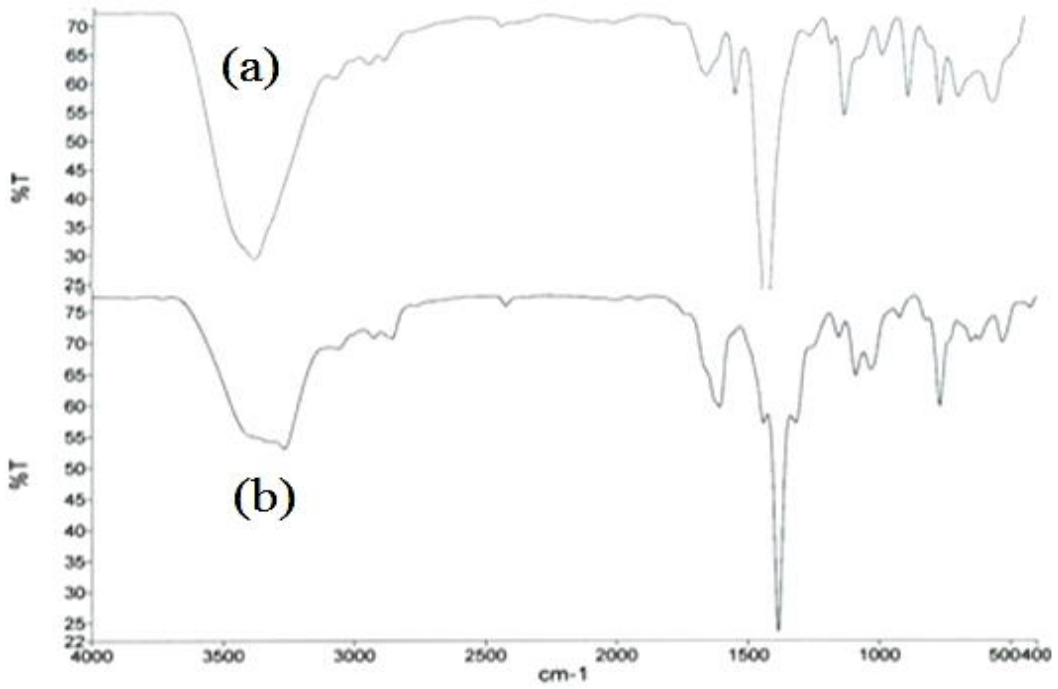

Fig. 3. FTIR spectra of **1**(a) and **2**(b).

The band at ~650 cm^{-1} in both the compounds may be assigned to a Co–O stretching vibration for $Co_3(\mu_3–O)$ group involving a tri-bridging oxo-anion group.

The three bands near 723, 652 and 518 cm^{-1} are due to the "Co4O4" defect dicubane core present in both the complexes [27, 32].

^{1}H NMR spectra of the complexes exhibited resonance signals on the high field side (δ 3.0–3.6 ppm) due to the skeleton CH_2 protons of the ligand (H_3tea). The aromatic protons of the coordinated α-diimine (1,10-phenanthroline and 2,2'-bipyridine) moiety showed multiplets in 7.4–9.0 ppm region. There is a considerable shift in the positions of the various signals compared to that of the uncomplexed ligands and this shift is due to the paramagnetic effect of the metal ion in coordination [33].

The ^{13}C NMR spectra had signals in 38–40 and 124–156 ppm regions corresponding to the methylene (–CH_2–) and α-diimine (1,10-phenanthroline and 2,2'-bipyridine) carbons, respectively [31,34].

Table 3. FTIR and NMR data for the **1** and **2** and the similar reported complexes.

Compound	FTIR data		^{1}H NMR data		^{13}C NMR data		Reference
	ν(cm^{-1})	Assignment	δ (ppm)	Assignment	δ (ppm)	Assignment	
$[Co_4(\mu_3\text{-}O)_2(Htea)_2(Phen)_4]2NO_3{\cdot}4H_2O$ (**1**)	3373	O–H	3.0, 3.2, 3.4	CH_2	38,39	CH_2	This work
	2935	C–H	7.6, 8.3, 8.4,	Phen	128, 134, 144,	Phen	
	1090	C–O	9.0		152		
	1384	NO_3					
	946	Co–O–Co					
	650	$Co_3(\mu_3–O)$					
	430	Co-N					
	520	Co-O					
$[Co_4(\mu_3\text{-}O)_2(Htea)_2(Bipy)_4]2NO_3$ (**2**)	3270	O–H	3.1, 3.3, 3.6	CH_2	38,40	CH_2	This work
	2928	C–H	7.4, 7.9, 8.1,	Bipy	124, 138, 147,	Bipy	
	1090	C–O	8.9		156		
	1385	NO_3					
	942	Co–O–Co					
	645	$Co_3(\mu_3–O)$					
	425	Co-N					
	510	Co-O					
$[Co_4(\mu_3\text{-}OH)_2(\mu_3\text{-}dea)_2(phen)_4]4Cl{\cdot}8H_2O$	3475	O–H	3.4–3.9	CH_2	34–41	CH_2	[31 b]
	2949	C–H	7.5–8.4	Phen	121–150	phen	
	1060	C–O					
	943	Co–O–Co					
	428	Co-N					
$[Co_4(\mu_3\text{-}OH)_2(\mu_3\text{-}dea)_2(bipy)_4]4Cl{\cdot}8H_2O$	3425	O–H	3.4–3.9	CH_2	34–41	CH_2	[31 b]
	2949	C–H	7.5–8.4	Bipy	121–150	bipy	
	1067	C–O					
	945	Co–O–Co					
	427	Co-N					
$[Co_2(dea)_2(Bipy)_2]$	3405	O–H	3.48	CH_2	34	CH_2	[31 c]
	2946	C–H	7.4–8.6	Bipy	124-148	Bipy	
	1145	C–O					
	955	Co–O–Co					
	422	Co-N					
$[Co_2(ea)_2(Phen)_2(O_2)]{\cdot}5.5H_2O{\cdot}2Cl$	3300–	O–H	3.0–3.5	CH_2	35–43	CH_2	[31 d]
and	3350		7.0–8.5	Bipy/Phen	125–155	Bipy/	
$[Co_2(ea)_2(Bipy)_2(O_2)]{\cdot}2H_2O{\cdot}2NO_3$	~1000	Co–O–Co				Phen	
	450–550	Co-N and					
		Co-O					

Electronic and EPR spectral studies

The electronic spectra of **1** and **2** were recorded in 10^{-3} M in methanol. Electronic spectra of the complexes exhibited (**Fig. 4**), two well resolved absorption bands at [(224 nm and 270 nm) (**1**) and (224 nm and 302 nm) (**2**)]. The high energy band assigned to the charge transfer of O→Co ions, whereas low energy band attributed to $\pi \rightarrow \pi^*$ transition. Brown methanolic solution showed a broad low intensity band at 527 nm (**1**) and 505 nm (**2**), which

can be assigned to d-d transitions of low spin d^6 (Co^{3+}) and high spin d^7 (Co^{2+}) ions in accordance with the Co^{II}/Co^{III} state in octahedral geometry in the polynuclear cluster complexes [35].

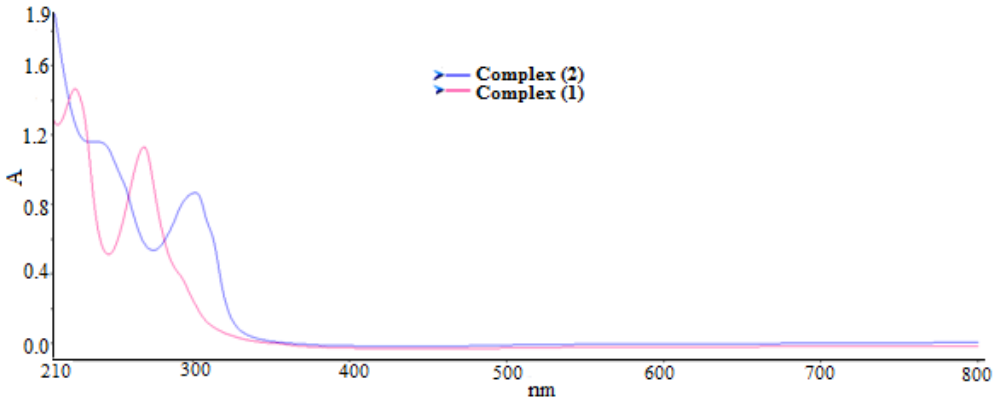

Fig. 4. Absorption spectra of the **1** and **2**.

The polycrystalline powder X-band EPR spectrum measurement of the **1** and **2**, was performed at room temperature (**Fig. 5**). The g value obtained from the EPR spectra display large variation in the range 22–1.4 for **1** and **2** which is an indication of an exchange interaction between the paramagnetic Co(II) ions. The dominant broadening effect emerges when the g strain is converted into B strain through the Equation:

$$\Delta B = -(h\nu/\mu_B)(\Delta g/g^2)$$

The parameters in above equation have their usual meaning. Thus, the largest and smallest g values of the sample spectra have field widths that differ by an order of magnitude and, thereby, rationalize the broad high-field features of the spectrum [36].

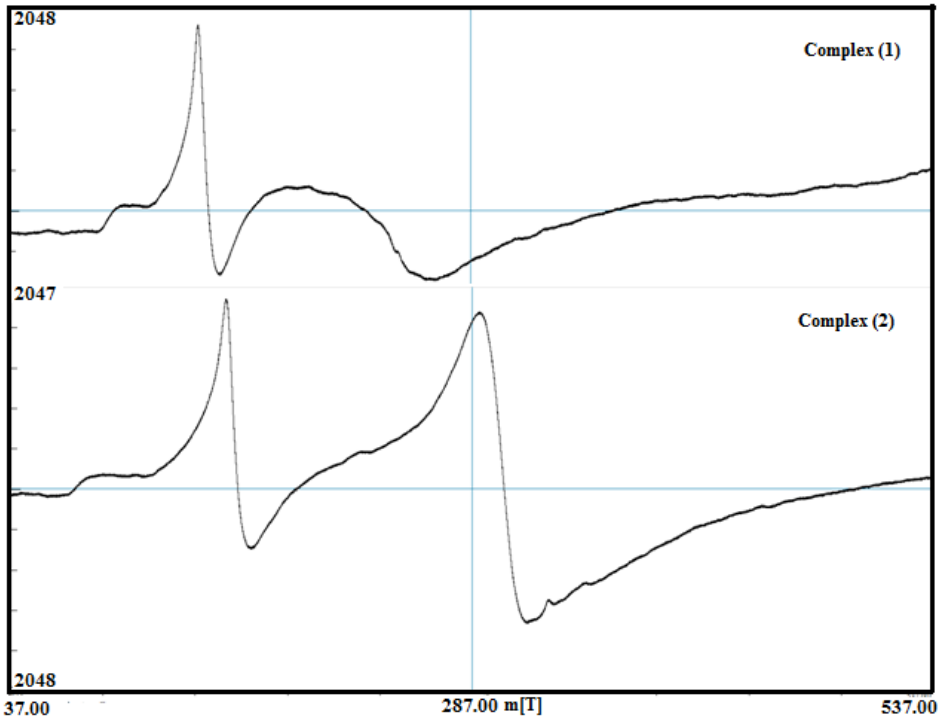

Fig. 5. Scanned EPR spectra of **1** and **2**.

Thermogravimetric analysis (TGA)

Thermal stability of **1** and **2** was examined using TGA in a nitrogen atmosphere at the rate of 5 °C per minute. The thermal fragmentation of **1** showed a weight loss ~12% in 25–170 °C temperature range corresponding to elimination of four lattice water molecules [37] and two nitrate ions, in **1**. In this range 25–170 °C, **2** exhibited weight loss of 8.5% due to the elimination of two NO_3 ions. On further increasing the temperature up to (~300 °C), further weight loss of ~26.83% and 35.36% suggests elimination of the α-diimine (Phen or Bipy) of **1** and **2**, respectively (**Fig. 6**) [38].

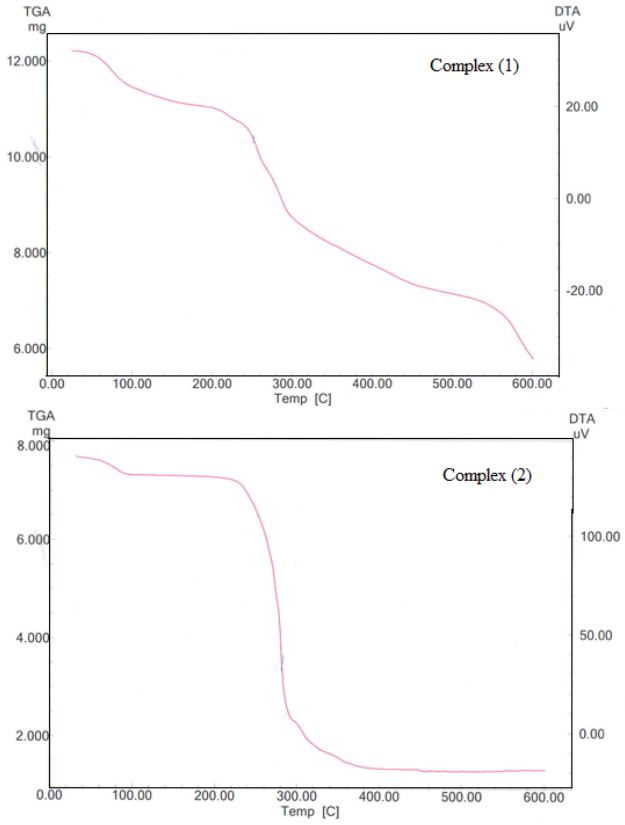

Fig. 6. Thermogravimetric analysis (TGA) of **1** and **2**.

Cyclic Voltammetric studies

The cyclic voltammograms of **1** and **2** in the potential range +1.0 to –1.0 V with the reference to Ag/AgCl electrode at room temperature in the presence of $[^{n}Bu_4N]ClO_4$ were recorded to investigate the changes in oxidation states of metal ions in solution. The electrochemical redox properties **1** and **2** are given as (**Fig. 7**) at different scan rate (100,150, 200, 250, 300 Vs^{-1}).

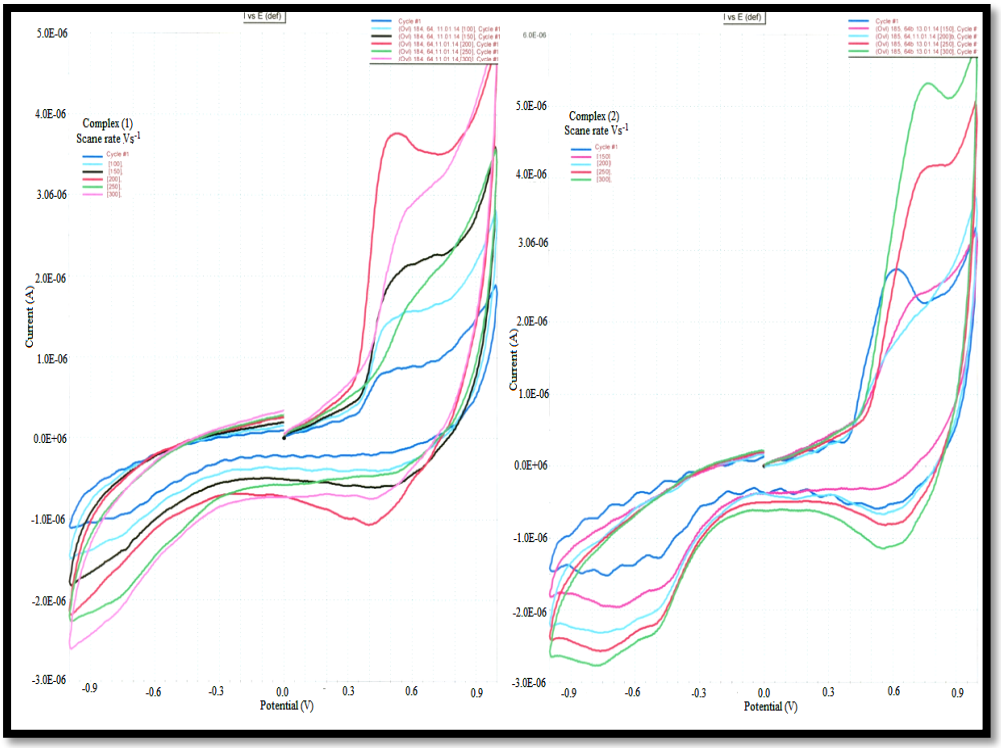

Fig. 7. Scanned voltammograms of **1** and **2**.

The nature of the peaks is almost similar at all scan rates indicating the stability of the complexes in the solution. The voltammogram for the complexes shows cathodic peak [E_P^c = 0.52 V (**1**), E_P^c = 0.75 V (**2**)] in the forward direction, which is coupled with the anodic peak [E_P^a = 0.43 (**1**), E_P^a = 0.55 (**2**)] in the reverse direction, forming a quasi-reversible redox couple [$E^0_{1/2}$ = 0.04 V for (**1**) and –0.10 V for (**2**)]. The CV data indicated that there is formation of quasi-reversible redox couple in both the complex solutions as following [39–41].

$$[Co^{II} - L - Co^{II}] \rightleftharpoons^{2e^-} [Co^{III} - L - Co^{III}]$$

Magnetic studies

Magnetic studies were performed to investigate the paramagnetic behaviour the complexes. Magnetic susceptibility is measured using very sensitive instrument known as a magnetic susceptibility balance. The balance contains a pair of magnets mounted at opposite ends of a beam, initially in equilibrium, when sample is introduced into the balance, a disruption of the magnetic field results. A current through a coil located between the poles of

a second pair of magnets returns the beam to equilibrium. The current through the coil is measured and transformed into a numerical reading. Diamagnetic materials are weakly repelled by an external magnetic field, resulting in a negative reading. Paramagnetic materials are attracted to an external magnetic field and give a positive reading.

The magnetic analysis supported the mixed valence states of the cobalt ions in the clusters. The magnetic moment of the complexes was calculated using by the formula as follows:

$$\chi_{g=} \frac{LC_{bal}(R-Ro)}{10^9(m)}$$

l = height of sample in tube in units of centimetres

m = mass of the sample in units of grams

R = reading for tube plus sample

R_o = reading for the empty tube

C_{bal} = balance calibration constant = 1.0

The molar magnetic susceptibility is then calculated from the gram magnetic susceptibility using the following equation

$\chi_m = \chi_g$.(molar mass),

$\chi_A = \chi_m$ – diamagnetic correction

The magnetic susceptibility for a particular substance is not particularly useful in itself. However, the effective magnetic moment for a particular substance can be calculated from the gram magnetic susceptibility using the following equation.

$$\mu_{eff} = 2.283\sqrt{\chi_A.T}$$

{χ_g magnetic susceptibility erg.G^{-2}.gm^{-1}, χ_m molar susceptibility erg.G^{-2}.mol^{-1}, and μ_{eff} effective magnetic moment B. M.}.

Magnetic data indicates that μ_{eff} for the complexes **1** and **2** are 6.6 and 6.3 BM, respectively, which is suggestive of highly paramagnetic behaviour of the complexes. It is clear from magnetic studies that each complex contains six unpaired electrons. It is further confirmed that two cobalt ions (Co^{2+}) are high spin (paramagnetic, $t_{2g}^5e_g^2$) and remaining two cobalt ions (Co^{3+}) are low spin (diamagnetic, t_{2g}^6) [42-44].

Conclusions

Two tetranuclear cobalt clusters of tetradentate [N,O,O,O] ligand i.e. triethanolamine and α-diimine (1.10-phenanthrolin or 2,2'-bipyridine) have been synthesized and characterized. X-ray data indicated a tetranuclear mixed valent defect dicubane core. Tetranuclearity is obtained by checking further polymerization using α-diimine chelator. Spectral and TGA data are consistent with the purposed structure of the complexes. CV studies indicated formation of a quasi-reversible redox couple in solution.

References

[1] E.G. Mednikov, L.F. Dahl, Small, 4 (2008) 534.

[2] G. Schmid, Nanoparticles—From Theory to Application, Wiley-VCH, Weinheim, 19 (2005) 7.

[3] G. Aromi, E.K. Brechin, Struct. Bonding, 122 (2006) 1.

[4] R.E.P. Winpenny, Chem. Soc. Rev., 27 (1998) 447.

[5] S. Mukhopadhyay, S.K. Mandal, S. Bhaduri, W.H. Armstrong, Chem. Rev., 104 (2004) 3981.

[6] S. Shit, G. Rosair, S. Mitra, J. Mol. Struct., 991 (2011) 79.

[7] V.K. Yachandra, K. Sauer, M.P. Klein, Chem. Rev., 96 (1996) 2927.

[8] P. Giastas, N. Pinotsis, G. Efthymiou, M. Wilmanns, P. Kyritsis, J.M. Moulis, I.M. Mavridis, J. Biol. Inorg. Chem., 11 (2006) 445.

[9] B. Schmid, H.J. Chiu, V. Ramakrishnan, J.B. Howard, D.C. Rees, in Handbook of Metalloproteins, ed. A. Messerschmidt, R. Huber, T. Poulos, K. Wieghardt, Chichester, New York, Weinheim, Brisbane, Singapore, Toronto. 1025 (2001).

[10] R.H. Holm, Adv. Inorg. Chem., 38 (1992) 1.

[11] G.E. Kostakis, S.P. Perlepes, V.A. Blatov, D.M. Proserpio, A.K. Powell, Coord. Chem. Rev., 256 (2012) 1246.

[12] O.V. Nesterova, M.V. Kirillova, M. Fátima C.G. da Silva, R. Bočacd, A.J.L. Pombeiro, CrystEngComm, 16 (2014) 775.

[13] S.K. Langley, K.J. Berry, B. Moubaraki, K.S. Murray, Dalton Trans. 973 (2009).

[14] International Tables for X-ray Crystallography, Kynoch Press, Birmingham, England IV (1974).

[15] SMART & SAINT Software Reference manuals, Version 6.45, Bruker Analytical X-ray Systems, Inc., Madison, WI. (2003).

[16] G.M. Sheldrick, SADABS, software for empirical absorption correction, Ver. 2.05, University of Göttingen, Göttingen, Germany (2002).

[17] XPREP, 5.1 ed., Siemens Industrial Automation Inc. Madison, WI. (1995).

[18] G.M. Sheldrick, SHELXL97, Program for Crystal Structure Refinement, University of Göttingen, Göttingen, Germany. (2008).

[19] A. Altomare, M.C. Burla, M. Camalli, G.L. Cascarano, C. Giacovazzo, A. Guagliardi, A.G.G. Moliterni, G. Polidori, R.J. Spagna, J. Appl. Crystallogr., 32 115 (1999).

[20] O. Roubeau, R. Clérac, Eur. J. Inorg. Chem., 28 (2008) 4325.

[21] P. King, R. Clérac, W. Wernsdorfer, C.E. Anson, A.K. Powell, Dalton Trans. (2004) 2670.

[22] Y.A. Mikhailenko, E.V. Peresypkina, A.V. Virovets, T.G. Cherkasova, Russ. J. Inorg. Chem., 54 (2009) 568.

[23] A. Baysal, M. Aydemir, F. Durap, S. Ozkar, L.T. Yildirim, Inorg. Chim. Acta, 371 (2011) 107.

[24] I.D. Brown, K.W. Wu, Acta Crystallogr. Sect. B: Struct, Crystallogr. Cryst. Chem., 32 (1976) 1957.

[25] H.H. Thorp, Inorg. Chem., 31 1585 (1992).

[26] H. Brintinger, B. Hesse, Z. Anorg, Allg. Chem., 248 (1941).

[27] K. Nakamoto, Infrared, Raman Spectra of Inorganic and Coordination Compounds, Wiley-Interscience, New York. (1986).

[28] R.P. Sharma, A. Saini, P. Venugopalan, V. Ferretti, F. Spizzo, C. Angeli, C.J. Calzado, New J. Chem., 38 (2014) 274.

[29] (a) Z.G. Li, J.W. Xu, H.Q. Jia, N.H. Hu, Inorg. Chem. Commun. 9 (2006) 969.

(b) Z. Boulsourani, V. Tangoulis, C.P. Raptopoulou, V. Psycharis, C.D. Samara, Dalton Trans., 40 (2011) 7946.

[30] N.T. Madhu, P.K. Radhakrishnan, Transition Met. Chem., 25 (2000) 287.

[31](a) B.F. Hoskins, R. Robson, G.A. Williams, Inorg. Chim. Acta, 16 (1976) 121.

(b) Z.A. Siddiqi, A. Siddique, M. Shahid, P.K. Sharma, M. Khalid, Anjuli, J. Mol. Struct., 1036 (2013) 209.

(c) Z.A. Siddiqi, A. Siddique, M. Shahid, M. Khalid, P.K. Sharma, Anjuli, M. Ahmad, S. Kumar, Y. Lan, A.K. Powell, Dalton Trans., 42 (2013) 9513.

(d) M. Shahid, A. Siddique, I.A. Ansari, F. Sama, S. Chibber, M. Khalid, Z.A. Siddiqi, M.S.H. Faizi, J. Coord Chem., 68 (2015) 848.

[32] R. Chakrabarty, S.J. Bora, B.K. Das, Inorg. Chem., 46 (2007) 9450.

[33] D. Russels, Physical Methods in Inorganic Chemistry, Reinhold Pub. Corp (1965).

[34] F. Lions, I.G. Dance, J. Lewis, J. Chem. Soc. A., 565 (1967).

[35] A.B.P. Lever, Inorganic Electronic Spectroscopy, Elsevier, Amsterdam. (1984).

[36] A. Abragam, B. Bleaney, Electron Paramagnetic Resonance of Transition Ions, Clarendon Press, Oxford, U. K. (1970).

[37] J.S. Kwag, M.H. Jeong, A.J. Laugh, J.C. Kim, Bull. Korean Chem. Soc., 31 (2010) 2069.

[38] Z.A. Siddiqi, P.K. Sharma, M. Shahid, M. Khalid, J. Photochem. Photobio. B: Biology, 125 (2013) 171.

[39] Z.A. Siddiqi, V.J. Mathew, Polyhedron, 13 (1994) 799.

[40] Z.A. Siddiqi, M. Shahid, M. Khalid, S. Noor, S. Kumar, Spectrochim. Acta Part A., 74 (2009) 391.

[41] C.D. Samara, P.D. Janakoudakis, D.P. Kessissaglou, G.E. Manoyussakis, D. Mentzapfos, A. Terzis, Dalton Trans. (1992) 3259.

[42] B.N. Figgis, J. Lewis j. In Lewis, R.G. Wilkins, Eds.; Modern Coordination Chemistry; Interscience Publishers Inc.: New York, 400 (1960).

[43] R.J. Angelici, In Synthesis and technique in inorganic chemistry, W.B. Saunders. 198 (1977).

[44] C.E. Housecroft, A.G. Sharpe. Pearson Education Limited, 3. In Inorg. Chem. (2008).